1996

The development of fiber optic strain and vibration sensors for control of smart structures

David J. Holden
Lehigh University

Holden, David J.

The Development of Fiber Optic Strain and Vibration Sensors for Control of Smart Structures

June 2, 1996

The Development of Fiber Optic Strain and Vibration Sensors for Control of Smart Structures

by

David J. Holden

A Thesis

Presented to the Graduate and Research Committee

of Lehigh University

in Candidacy for the Degree of

Master of Science

in

Mechanical Engineering

Lehigh University

Bethlehem, Pennsylvania

May 1996

CERTIFICATE OF APPROVAL

This thesis is accepted and approved in partial fulfillment of the requirements for the degree of Master of Science in Mechanical Engineering.

May 1, 1996
Date

Thesis Advisor
Dr. John P. Coulter

Chairperson
Dr. Robert P. Wei

Acknowledgments

I would like to thank my parents for their support during the time I have spent here at Lehigh, and for their support throughout my life. Without their continued financial and emotional support, and their never ending ability to point out the good, I don't think I would be where I am. Thanks also to my brother, Jeff, for answering all of the questions I had about composite panels with fibers embedded, and giving me the visual tour of his own lab, and for being a lighthouse on the shores of reality. You have helped a lot. And to my uncle, without whose corrupting influence I wouldn't have pursued engineering in the first place, thanks. To all of my family, thank you for letting me live this gypsy lifestyle for the past several years and still setting me a place at the table.

I would like to extend a very special thanks to my friend and roommate, Todd Holbert, for putting up with me for so long and for letting me be crazy when I needed to be, making me think all the time, and generally keeping me honest and on the straight and narrow. To say he is fortunate to have met me is absurd, it is *I* who was fortunate. Thanks also to his family for adopting me as their own, and to all my friends who have adopted me over the years, you have been a cushion for me to fall upon during hard times. Thanks to Mike Wessner for invaluable knowledge and helping me to develop a global perspective, and for teaching me to make stuff. To my friend Kristi, for letting me get here in the first place, and humoring me when I needed it, thanks Kid; to Kristin for maintaining my sanity and listening to me babble at all hours, and coming up with sane answers to crazy questions, thank you so much (Remember why you are there). Thanks to Jack for dragging me out at the wrong times and letting me "live" at his house; to L.T. for being a crazy guy and making me laugh; to Super Don, als6, and jara for making me think kaleidoscopic thoughts; to everyone that dragged me into more administrative things and letting me see what that's like. To the rest of the cast of characters that I have seen and met and had good times with and learned from (and with): Rieth, Hoddinott, Mike, Strieffler, Ms. Reilly, The Star Lady, Shack, Babek, and Mo; good luck and best wishes and my sincerest thanks to you all. To La Gata Negra, my fondest thoughts and best wishes will always be with you. Thanks to Dave C. the EMT and his family for being so generous and kind and making things fun. Thank you also to Bruce Smackey for showing me the world outside of Packard Lab, and for indulging my creative tendencies. My check is on the way. Thank you to all of the professors, deans, and everyone else who asked me to do this tour or that tour; seeing those people benefited me more than years of experience could. It just took a lot of time. It just goes to prove that NGAFL.

Thank you to the Mechanical Engineering Machine Shop Staff, for doing jobs faster and better than I might have, and for doing it without all the red tape. Dick, Jim, and Bob, you have been more help (and humor) than you will ever know. Thanks to Tim Nixon for making the electrical stuff at least seem not so terrible, and for talking racing. Thanks to Emerson and Frank for teaching me about machining way back when, to Chris Muir (the wizard) for teaching me about the NC and helping me get through ME240, (Scott, Good Luck next year!), to Gayle, Donna, Dorothy, Jennifer, and Kathy for always having the right forms and taking care of all the little things. Thanks to Dr. Ochs and Fred for letting me learn, not without a lot of ribbing mind you, about the intricacies of running ME240 on the fly.

Finally, I would like to acknowledge the support of the Dr. Gary Anderson at the ARO for his support, and for the funding which supported my research, Grant no. DAAL03-92-0388. I also would like to thank Dr. John. P. Coulter for his support during this study and directing my learning, and Dr. Arkady Voloshin for getting me started in the field of fiber optics. Thank you to Melek Yalcintas, Seth Flanders, Andy Shiang for assisting in transferring their acquired knowledge and experiences to help me as well. I also need to thank Drs. Sergei Egorov and Anatoly Mamaev for teaching me more about the practical matters of optics in a day than I could have learned in 5 years. I would also like to thank the Lord Corporation for providing the ER materials used in this study. Lastly, thanks to the Johns Hopkins Applied Physics Laboratory for preparing the large plate and beam specimens.

Table of Contents

Chapter 7

LIST OF FIGURES

Chapter 1

Strain Measurement

In the various fields of engineering and applied science it is necessary to precisely measure the amount of strain being endured by a material. The capability to measure the properties of strain allows material scientists and engineers to determine numerous physical quantities about that material. From measurements of the strain in a material, resulting from the force applied to a simple tensile test specimen, the modulus of elasticity and Poisson's ratio can be determined for a specific material. These properties are compiled into tables, which are used by engineers and product designers to design an infinite number of highly stressed, and often critical components.

For example, measuring the amount of strain in pressure vessels allows us to compute the fluid pressure inside the vessel. We can determine temperature changes in a material or a system by measuring the strain which that system undergoes. By incorporating a programmed monitor to the method of strain measurement, we can measure and record the number of times that the system reached or exceeded a preset level of strain, and use this as an indicator that the structure may have been damaged. We can also use this method to indicate that the system has reached its normal operating status. Further additions to the system of measurement can incorporate methods of measuring the rate at which the strain is changing, and the magnitude of that rate, to determine the operating frequency of the system. Knowing this frequency provides

insight into the operating regime and condition of the system, and whether or not it is operating at a known harmonic. With this information, appropriate action can be taken to maximize the life of the structure.

Currently there are several options for strain measurement. Often a product engineer would like these options to fulfill requirements of very high sensitivity and accuracy, at an affordable price. Consideration is given by the engineer to the operating range of the gauges as well as other situation specific conditions. Many applications also require careful selection to minimize the risk of fire or explosion associated with a sensor. Durability of the sensor and the performance in the intended environment are also important considerations that must be taken into account. Once the importance of these features have been determined, and their worth evaluated on an appropriate scale, the engineer will select the gauge that meets his or her needs.

1.1 Electrical-Resistance Strain Gauges

The most common type of strain gauge in use today is the electrical resistance strain gauge, a schematic of which is shown in **Figure 1.1.** These gauges are sold by Omega Corporation and a host of other companies, and are based on the simple principle that, when stretched, the electrical resistance of an electrical wire will change in a linear fashion, for small ranges of strain. An electrical resistance strain gauge is an array of wires which, when subjected to a strain, changes its resistance. This change in resistance

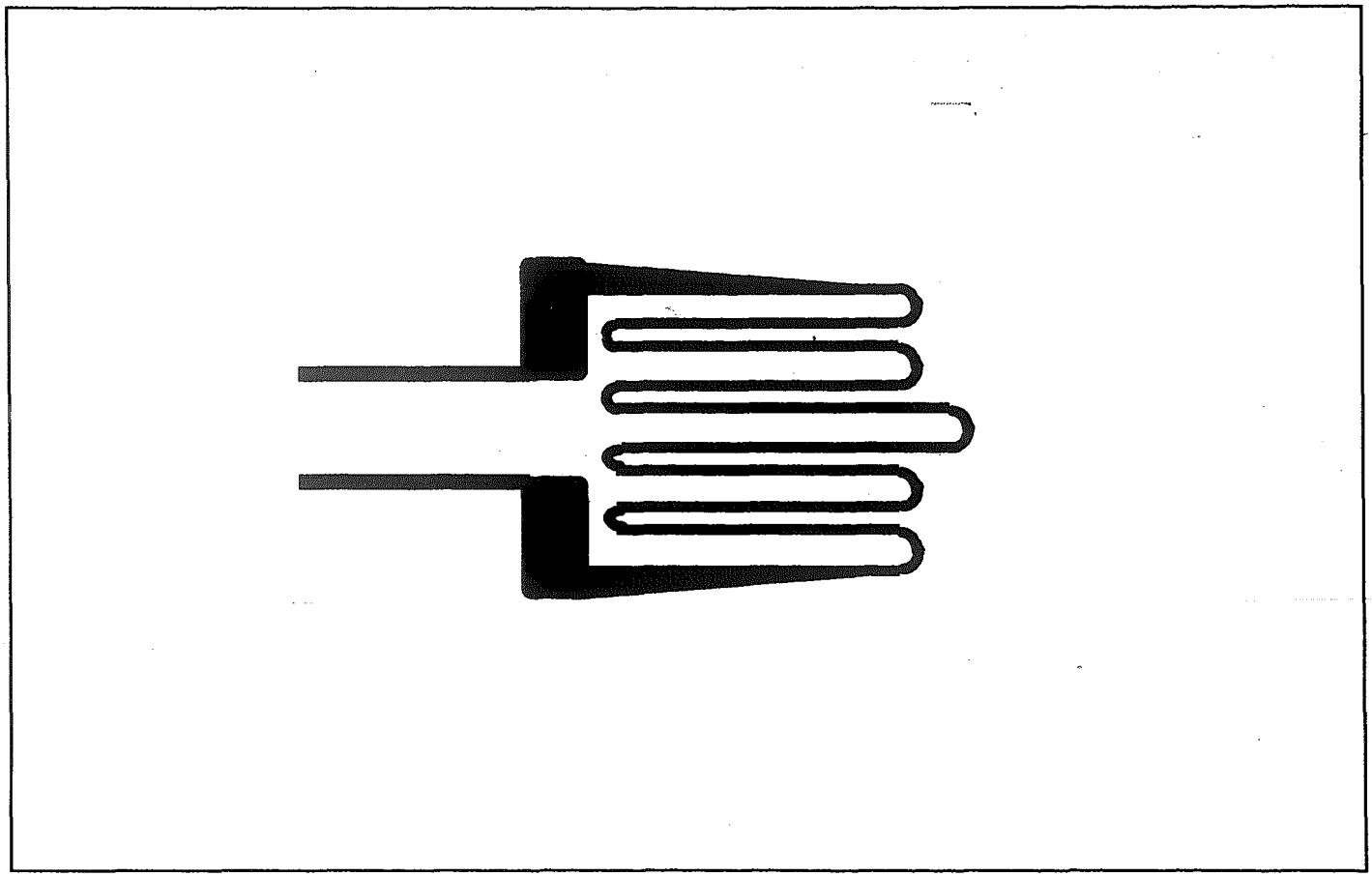

Figure 1.1. Schematic of an Electrical Resistance-Type Strain Gauge

will lead to a change in voltage over a Wheatstone bridge circuit, as shown in **Figure 1.2**, and this change in voltage can be measured using a common multimeter. When plotted, the change in voltage will be linearly proportional to the strain experienced by the sample.

An electrical-resistance based strain gauge is typically the most inexpensive gauge in common use, and is relatively easy to prepare for experimental use. Since the gauge can be ordered in numerous configurations, linear or rosette with various rosette angles for example, exact gauge geometry can vary from experiment to experiment, and can be tailored to part geometry and experimental set-up and the equipment available at the site. Similarly, gauge materials vary somewhat depending on their intended application, generally ferrous or non-ferrous. All gauges however are connected to the specimen using an adhesive tailored to the application, and lead wires are connected from the gauges to a power source. These wires are used to measure the change in voltage due to any strain experienced by the gauge.

Electrical resistance-type strain gauges are the most readily available type of strain gauge on the market and can be found in a myriad of testing applications. They can be used as easily to measure the strain on a pressure vessel as to measure the strain in a tensile specimen , and they can be used in thermal experiments. Typical accuracies for these electrical-resistance strain gauges vary depending on the electronic measuring and conditioning circuitry used. However, some insight into the comparative performance of

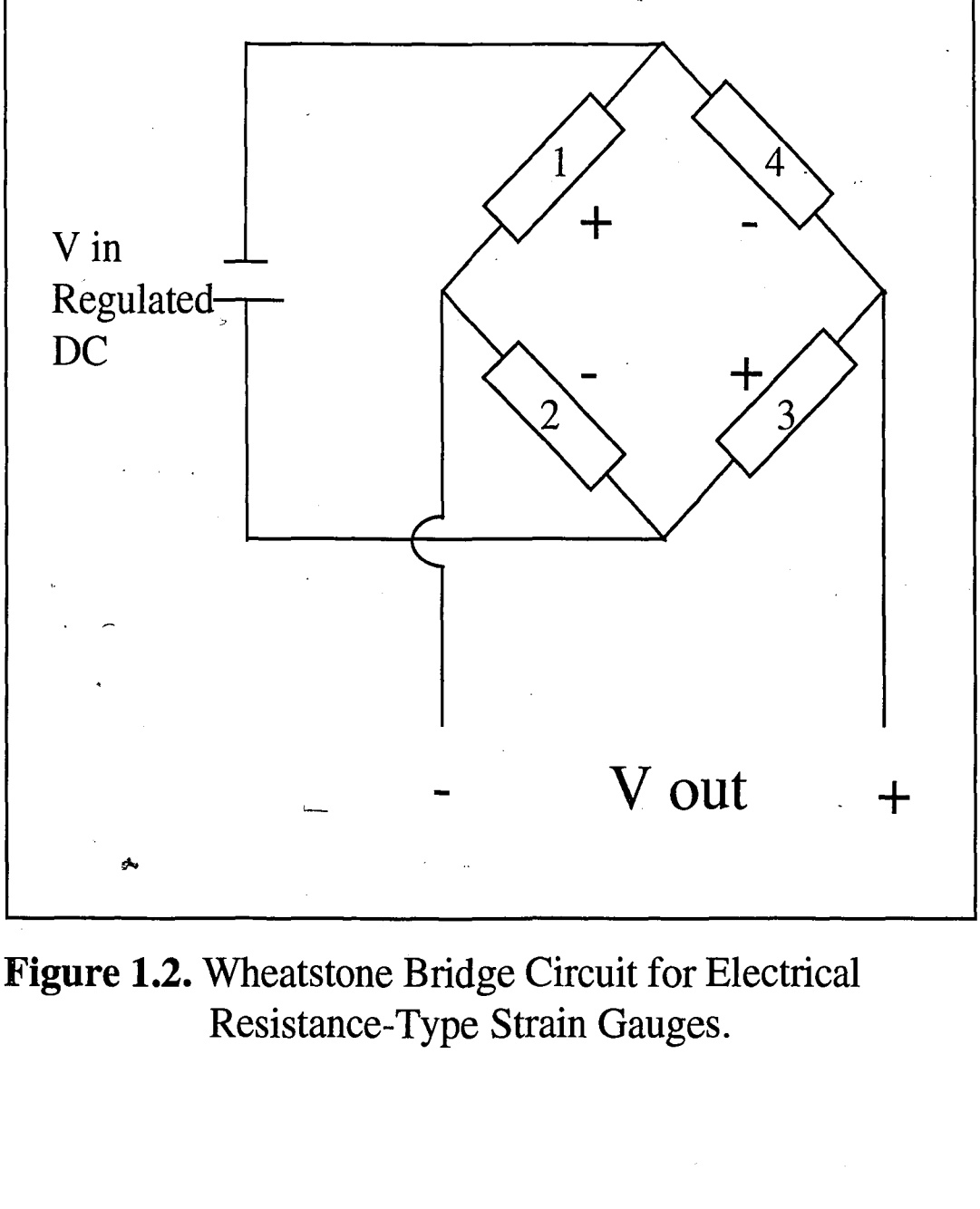

Figure 1.2. Wheatstone Bridge Circuit for Electrical Resistance-Type Strain Gauges.

individual gauges can be gained by examining the output of the strain gauges in terms of mV/V at a pre-specified level of strain input, some gauges have sensitivities of 2 mV/V at 1000 microstrain ($\mu\varepsilon$). These gauges typically offer reliable performance in the range of strain up to 2%, with their maximum strain ratings given as 3% to 5%, depending on gauge material and configuration (Omega, 1992).

As these gauges do require electrical power and there are changes in the electrical fields every time the gauge undergoes a strain, there exists a potential for these gauges to be a fire and explosion hazard. As well, the gauges are subject to breakage if mishandled or not applied in accordance with the manufacturers instructions. As mentioned above, it is necessary to be certain that the type of gauge that is being purchased matches the type of material that is being tested. These gauges do exhibit characteristics which differ from their designed properties if they are attached to a specimen for which they were not designed.

Another drawback of electrical resistance type gauges, a drawback which is shared with many other strain gauges, is their reliance on the adhesive which bonds the gauge to the surface of the specimen. In the ideal case there would be no slip between the surface of the specimen and the strain gauge, however this is not the case. The adhesives that are used are typically cyanoacrylate based, and are formulated to minimize any slippage loss at the interface of the gauge, though this loss can never truly be eliminated. Save for some of the optical schemes which rigidly mount the device to the system,

through mechanical fasteners, one must always prepare the gauges and the specimens very carefully to ensure an optimum bond between the gauge and the specimen. The issue of specimen preparation shall be further discussed in Chapter 5 when we consider the preparation of a sample strain gauge using optical fiber techniques.

Finally, and most importantly, electrical resistance strain gauges are extremely sensitive to electro-magnetic radiation, of the type commonly found in smart structures. Electrical fields used to energize smart structures tend to generate electro-magnetic fields (EMF) which would make electrical resistance strain gauges useless as a means of sensing strain and vibration on any smart structure. As we will discuss later, fiber optic sensors do not display this sensitivity to EMF and are largely the reason that optical fibers show such potential for sensing applications on smart structures.

1.2 Piezoelectric Force and Strain Measurement

Another type of device that can be used in strain measurement is the piezo-electric strain gauge. These gauges are usually used in load cells, but they can be configured for strain measurement. A piezo-electric material is one that has the property of expanding and contracting under an applied voltage field. Conversely, when they are forcibly expanded and contracted, they emit a measurable change in output voltage, which is measured against a calibrated curve for the material, and the output voltage is converted into a displacement, thus a strain. Attachment to the specimen is usually accomplished

by bonding the piezo-electric material to mounting plates, and then attaching these plates between rigid fixtures and the specimen.

These gauges are not very common in application due to the specific set-up that is required and the fact that their use provides no real improvement in sensitivity unless more sophisticated, and more expensive, multimeters and signal processing software is used in conjunction with the system. In typical applications, as in load cells, the sensitivity of the piezo-electrics is similar to electrical resistance-type strain gauges. Like electrical resistance-type strain gauges, these devices can be considered a fire and explosion hazard, as they too produce electrical charges when they undergo strains, and these charges are located in the immediate vicinity of the experiment or test apparatus.

1.3 Optical Distance Measurement Techniques

When much greater accuracy and sensitivity are required, on the order of nanometers, light or laser based strain gauges are used. These devices are extremely application-specific, and require specialized hardware and software. Consequently, they are among the most expensive type of strain measurement devices currently available. Their extreme precision, and potential for very large displacement measurements, permits them to be used in such diverse applications such as tightly toleranced machining operations in the military and aerospace industry, and in mirror preparation for telescopes and objective lenses. Though not necessarily a strain gauge in the traditional sense, these

gauges nevertheless perform the distance and change in distance calculations inherent in any strain measuring device.

In order to measure distance using a lightsource, the frequency and wavelength of the lightsource and the refractive index of the medium which is acting as the carrier need to be known. Then, by using precise timers to determine the time between the two locations, the distance between the locations can be determined. Carrier media can range from air, to glass fiber, to an evacuated chamber.

Optically based strain gauges as described above rely on precise timing of light as it travels an unknown distance. Once the duration of time taken by the light to travel that unknown distance is measured, assuming the speed of the light and the properties of the working medium are known, the unknown distance can be calculated. Performing these calculations thousands of times per second allow a machine to know exactly at what rate it is moving in any one direction, and enables it to perform motion commands much faster than other means of distance and position measurement. These devices are used in complex machining centers, as shown in **Figure 1.3**. This machining center uses known distances and geometric calculations to accurately determine the location of the tool, and thus perform extremely accurate (+/- 0.002 mm) machining operations.

In addition to the potential for measuring with extreme precision, optically based gauges as described above permit measurement between two objects spaced at great

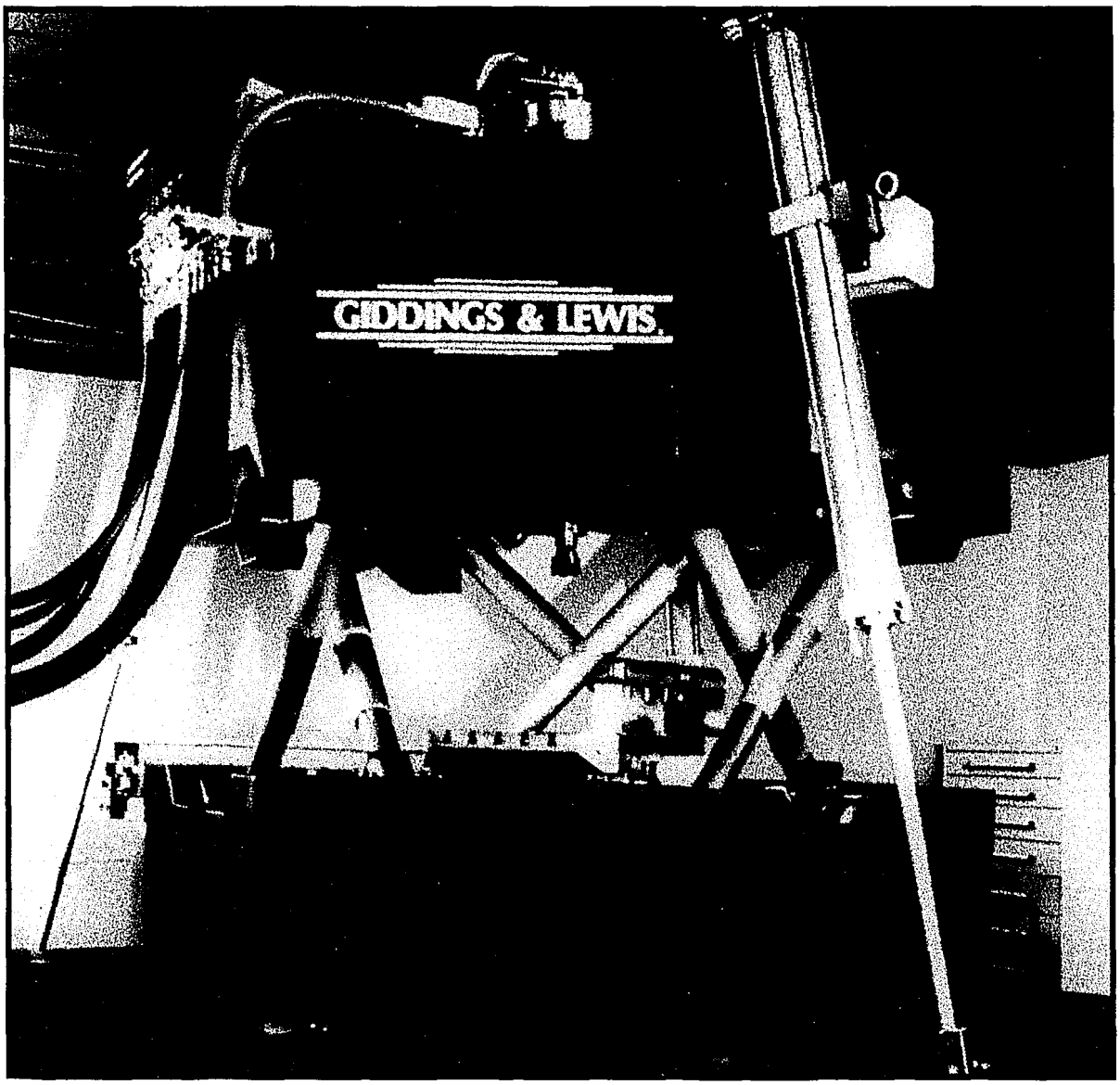

Figure 1.3. Giddings & Lewis Variax® Machining Center which uses optical distance measuring techniques to determine the position of the machine spindle to perform precision machining. (Giddings & Lewis Machine Tool Co.)

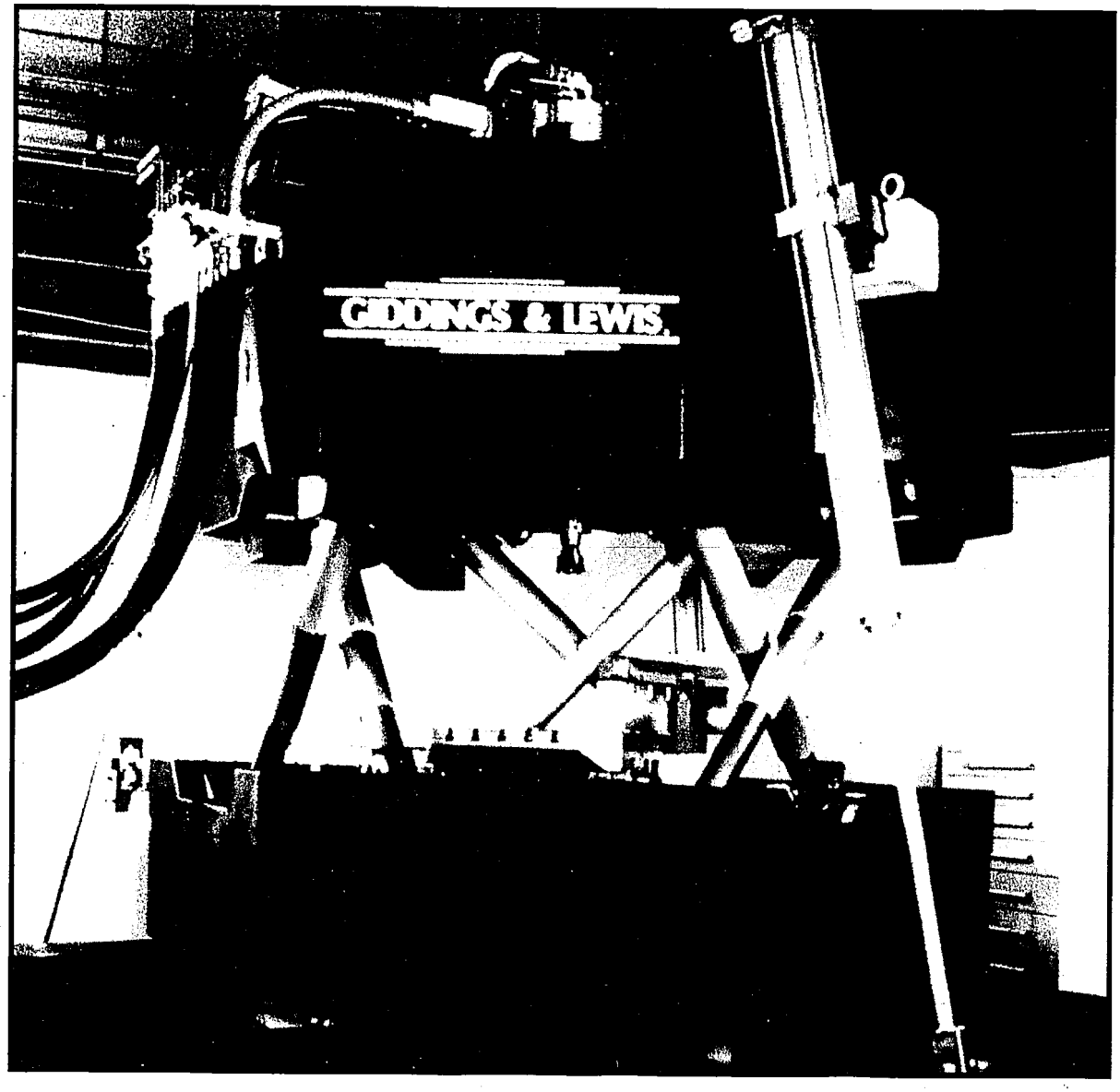

Figure 1.3. Giddings & Lewis Variax® Machining Center which uses optical distance measuring techniques to determine the position of the machine spindle to perform precision machining. (Giddings & Lewis Machine Tool Co.)

distance. To this end, scientists have used optical measuring techniques to compute the movement of two locations on the surface of the earth, many miles apart, to determine the direction and speed at which the locations are traveling, essentially measuring the strain occurring in the tectonic plates at the surface of the Earth.

The potential for the type of strain measurement using optical schemes seems unlimited. There are numerous situations that might benefit from the type of strain measurement, as well as the precision and accuracy, permitted by optical techniques. These gauges have the benefit that, usually, they are not a fire or explosion hazard. Also, depending on the specification of the hardware, they can be used in most common environments. Usually however, best performance is obtained when the laser or light source has a clear line of sight through a still, clean medium, such as air, or other light transmitting material. As contaminants build up in the air, the performance and accuracy deteriorate unless compensation software has been incorporated into the system. With the exception of a few special cases, these systems are designed to operate as sealed devices. These types of systems tend to be very expensive, as currently configured, due to the unique hardware and software that is often required. Also, for some measurements where space is a consideration, it is impractical to attach a signal and reflector to the specimen when the desired strain might be taking place on a very small portion of the surface of the specimen.

Calibration of all of the aforementioned gauges can be accomplished by using the initial signal as a reference signal, and computing all changes in the output signal, be it a voltage or a time which is converted into distance by calculation, based on that signal. Since the only desired variable is the change in the output variable, in most cases a distance, scientists need not be concerned with the raw value of that variable, either a light intensity or a time, as these values are manipulated to produce the output strain or distance.

1.4 Fiber Optic Strain Measurement

When downsizing the aforementioned large scale light-based techniques of measuring distance and the change in distance to a size useful for a laboratory setting, some modifications must be made to the measurement methods. Where the optical distance measurement methods in large machining cells measure the time taken by a light beam to travel a certain distance, using a simple mirror set-up returning the signal to the source point, fiber optic sensors (FOS) typically do not return the signal to the source point. Instead, the signal is sent through the fiber optic cable to an electronics package that includes a photodetector which is connected to a sophisticated multimeter, this multimeter often taking the form of an analog-to-digital (A/D) board based voltage converter used in conjunction with a personal computer.

Fiber optic strain measurements are generally based on the principles of interferometry in one form or another. Using the wave theory of light and principles of constructive and destructive interference, a fiber optic sensor superimposes two or more signals of light to produce a single signal of light. The intensity of this single signal will vary as the two signals of light which are superimposed constructively and destructively interfere. A simple representation of the superposition of two signals is shown in **Figure 1.4**.

When applied to interferometric fiber optic strain measurement, these principles can be very effective tools for measuring micro-strains on the surface of test specimens, and more relevant to the present study, on the surfaces of smart structures experiencing vibrations. The source of the uniform light wave is usually a laser, nominally operating at a single, known wavelength. Using various means, the input signal is usually divided using optical hardware, and the resulting two signals are used for measurement. One signal is treated as the reference signal, while the other signal is taken as the measurand. The measurand is exposed to the disturbance, in this case a strain, and then re-combined with the reference signal. The two recombined signals are exposed to a photodiode, which effectively measures the amplitude of the combined signals, and outputs a voltage proportional to this amplitude. By monitoring the change in the voltage output by the photodiode it is possible to measure the phase shift of the two signals, reference and measurand. There are many advantages to the use of these sensors in experimental lab work as well as in field applications. Since the fibers that are used in these sensors

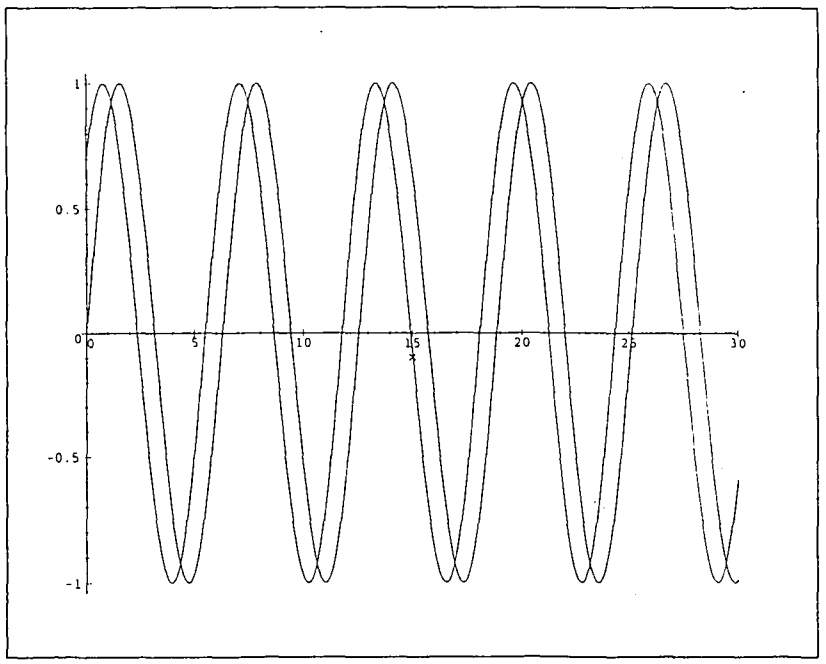

a)

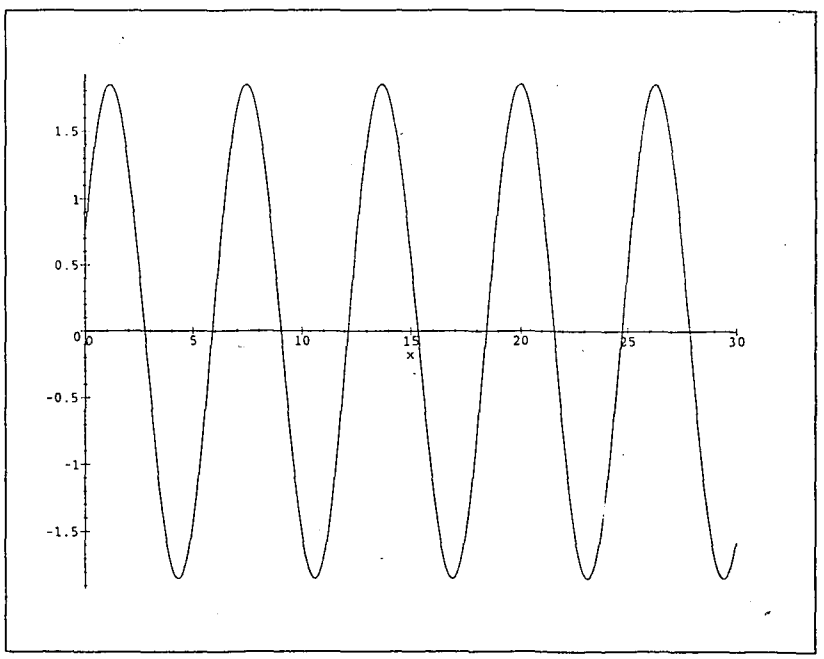

b)

Figure 1.4. a) Two Wave Signals Incident on a Photodetector b) The Combination of those Two Signals

typically are lightweight and very small in diameter (less than 500 μm), their effect and interference on the experiment is minimal. The signals from these fibers are not affected by electro-magnetic interference fields generated when subjecting a set-up to the high voltage fields often used with smart materials and smart structures. As the photodiode is usually located remotely from the set-up, the only energy being applied at the set-up is in the form of light, and the risk of explosion is greatly minimized. Multiplexing a large number of sensors into an A/D board and into a computer is also possible, permitting data from many sensors to be recorded using a single array of measuring equipment.

Fiber optic strain sensors share some of the drawbacks associated with other strain gauges, in addition to having some drawbacks uniquely their own. As these gauges are bonded to the structure using an adhesive, it is possible that there will be some mechanical motion mismatch losses between the surface being sensed and the sensor. The light source for this type of sensor is typically a scientific laser, which is considerably more expensive than a simple multimeter and a voltage supply used with electrical resistance-type gauges. Optical couplers, objective lenses, and surface mirroring operations also have an associated higher cost than any of the equipment used for alternate strain measurements. A multiplexed system as described would require greater light input than a single sensor system, due to the losses associated with the optical couplers and objectives, and thus requires more laser power. Stepping to higher and higher values of laser power invariably increases the cost and type of laser required. For example, small laboratory lasers costing around $1,000.00 have an output power of

around 1.5 mW. These lasers operate within a suitably narrow wavelength range to make measurements accurate and repeatable. If it is desired to add more sensors to the system, considerably more power will be required. Lasers with more power are considered specialized units, and are considerably more expensive, costing $5,000.00 and up. Finally, due to the fact that common fiber optic sensors are based on silica-glass, the typical values for maximum strain are usually in the range of 1-2%. Though the resolution of the sensor is often quite good, given a properly chosen light source wavelength, this limited strain capability does limit the applicability of the sensors.

1.5 Purpose of This Investigation

This investigation was primarily concerned with the testing and development of suitable fiber optic means for measuring the vibration and strain of smart structures. Due to the harsh environmental conditions often present in these structures conventional means for measuring vibration and strain were incompatible with most of the devices tested. In order to effect some level of controllability, and to fully exploit the potential of intelligent materials, and specifically here, the potential of electro-rheological fluids, high performance fiber optic sensors needed to be developed. Additional consideration was given to economic factors, and minimizing those factors, in order that the sensor package be appealing to potential users. Finally, work was done to increase the robustness of the sensor, minimizing the chance that accidental handling or misuse would damage the sensor, thereby increasing the service-life of the sensor.

It will be shown that fiber optic sensors represent the most efficient and most promising means to measure the vibrations and strains which take place in intelligent structures, specifically in light of the high electro-magnetic fields present which often interfere with the operation of conventional sensors. By nature, most ER-structures have a controller or many controllers associated with them and the described fiber optic strain and vibration sensors have been experimentally evaluated for their performance and integrity on an ER-fluid smart structure, both under manual control and under automatic control, using a neural network controller. These neural network controllers were used to effect instantaneous and autonomous control of the test structures and results from these tests are presented here. Several engineering applications of ER-fluids are presented in Chapter 2. The integration or ER material adaptive structures and fiber optic strain and vibration sensors is covered in later chapters, along with recent developments and evolutionary enhancements to improve both sensor and smart structure controller performance.

Chapter Two

Electrorheological Materials and Their Applications

As we have discussed, electrorheological fluids have the ability to vary their viscosity in the presence of an applied electric field. The unique properties of ER fluids, and the analogous properties exhibited by magneto-rheological fluids, can make the design and control of numerous mechanical devices much simpler. When incorporating a fiber optic sensor (FOS) with these devices, it is possible to to create a device with complete sensing and adapting capabilities. That is, the device has the capability to change its performance in response to changing operating conditions.

In this chapter, we will discuss the properties and the composition of ER fluids and obtain a deeper understanding of the microscopic mechanisms which permit these materials to exhibit such unique macroscopic properties. Important considerations when designing an ER device will also be presented to help differentiate between successful and unsuccessful designs. Examples of ER devices that have been designed and built in the past shall be discussed, and the devices themselves will be described in detail. Finally, details regarding the specific application of fiber optic strain and vibration sensors, and the ways in which these sensors can be used to improve the performance of each device, shall be presented.

One of the most exciting elements of ER-fluids in their application to a variety of engineering problems is the simplicity of design that can be exploited by using these fluids. Where once a complex and sometimes inefficient mechanism performed the task of metering fluid flow through a valve, a redesign of the valve using ER fluid can produce a similar pressure differential across the valve with no moving parts (Winfield, 1989).

Similar performance enhancements could be made in numerous subsystems and components in the automotive and aerospace industries, as well as in other niche markets that have not been given much consideration. These applications for ER fluids include shock absorbers for automobiles and other vehicles, vibration dampers for machinery, fluid film bearings, variable stiffness mounts for vehicle seats. and hydraulic proportioning valves (Tolu-Honary and Court, 1994). In addition, engine mounts for cars, dampers for wings on aircraft, and viscous coupling clutches with variable torque transmission characteristics have been built. These devices have been designed and tested for real world applications, with limited success. Other devices still very early in the development stage include structural applications to allow bridges and buildings to have variable stiffnesses, permitting a greater factor of safety in the face of Mother Nature, devices to help the vision impaired (Garner, 1994), suspension systems for Maglev mass transit systems (Pennisi, 1992), and tension controllers for wire drawing in the microelectronics industry (Stangroom, 1989).

2.1 Fundamentals of ER Fluids

One of the most important properties of ER devices derived from their performance makes them an attractive proposition in engineering design. Their ability to exhibit variable performance over a broad range, a property known as the controllability, is but one. Controllability is typically evaluated by examining the controllability factor, which is expressed as the ratio of the force, displacement, or other measured parameter, experienced under a voltage field, divided by the appropriate parameter under no voltage field. It is desireable to have a large controllability factor to permit device operation over the broadest performance range.

$$C_f = \frac{F_{\text{Max E-field}}}{F_{\text{0 E-field}}} \qquad (2.1)$$

Because of their low power consumption, the very low level of complexity, smoothness and quick response make these fluids attractive in many areas, particularly the automotive, aerospace, and manufacturing sectors. ER mounts have been proposed for machinery, in order to improve the performance of the machines to which they are coupled, by allowing higher operating speeds, reduced scrap production, and improved surface finish. ER automobile dampers have been tested with good results for performance and durability (Petek, 1992). Actively controlled frame stiffeners are being investigated to reduce noise levels in the cabins of airliners (Korane, 199).

ER fluids exhibit the ability to change their apparent viscosity when exposed to an applied electric field. This field is generally applied through a positive and negative electrode set-up. A generic sketch of this set up appears in **Figure 2.1**. The manner in which this fluid's viscosity changes involves the formation of particle chains within the fluid, chains which are made up of the dielectric particles. It is thought that, under the applied electric field, the poles of the dielectric particles align in a positive-to-negative fashion, as shown in **Figure 2.2.**

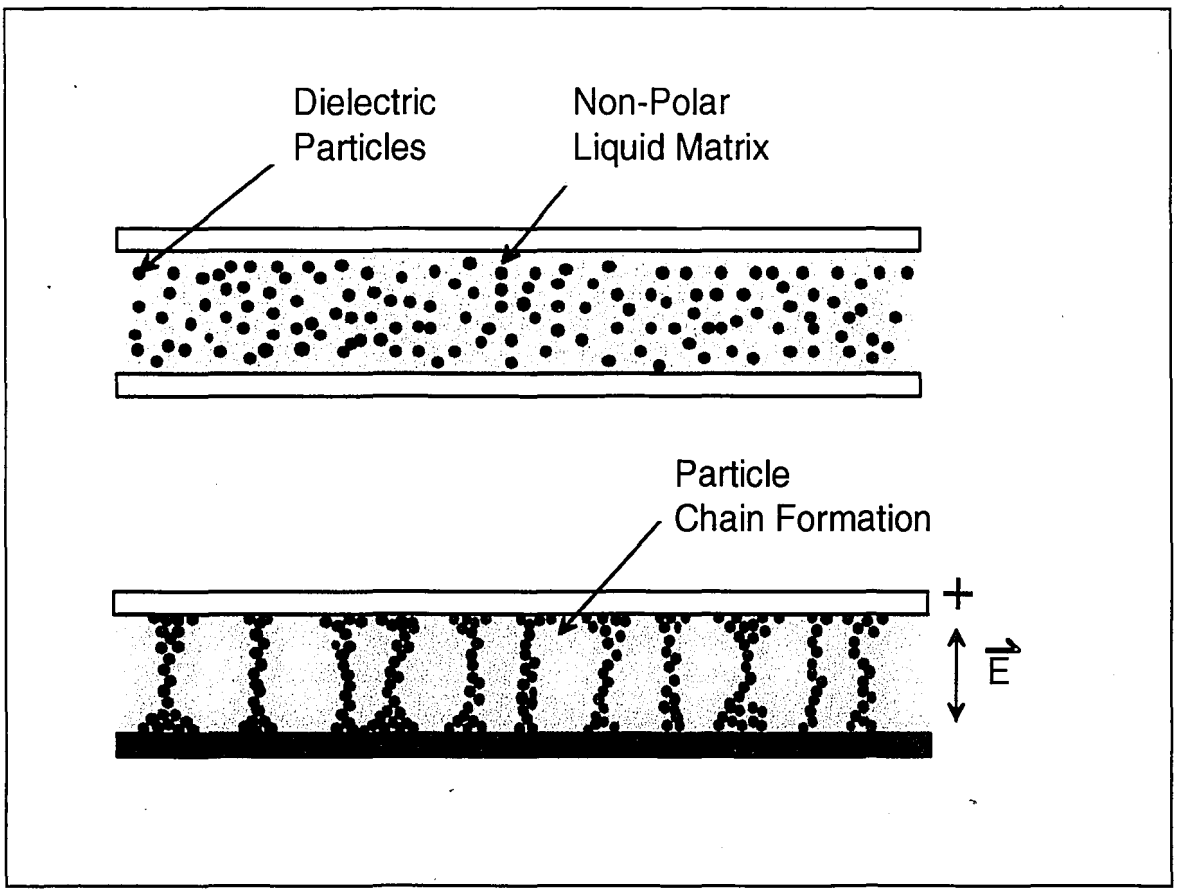

Figure 2.1. ER Phenomenon a)no electric field b)with electric field applied.

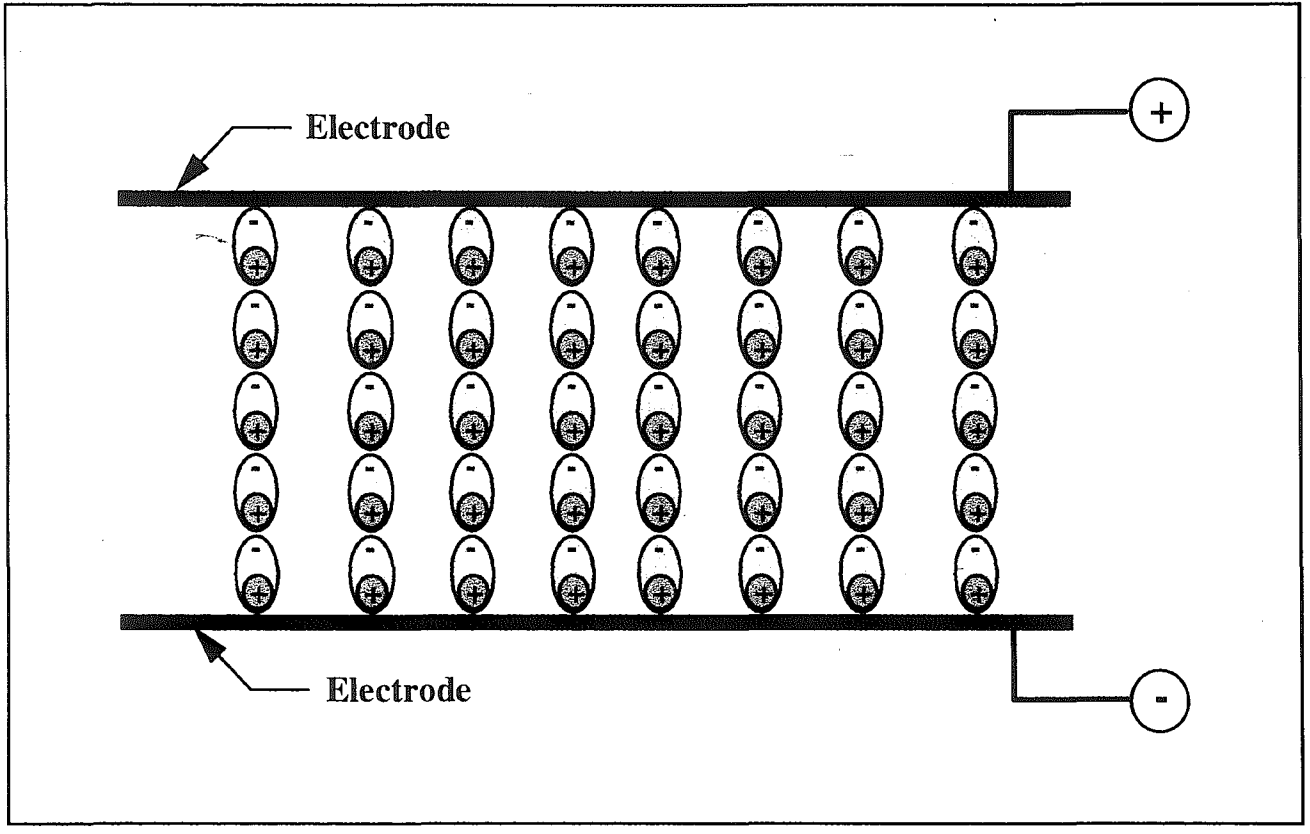

Figure 2.2. Dielectric Particles Aligned Under Electrical Field. Note how the particles form chains which attach to the electrode plates.

As the fluid between these two electrodes is exposed to the electric field, the fluid's apparent viscosity increases. It typically takes only a few milliseconds for the ER-effect, that is the change in the behavior of the structure due to the viscosity change of the fluid, to be observed. The viscosity change of ER fluids with respect to applied voltage fields is often considered to be purely linear, though from rheological studies it has been shown that the the fluid behaves with two apparent rheological regimes, depending on the magnitude of the strain and rate-of-strain being applied to the fluid. This effectively divides the fluid behavior into two regimes, pre-yield and post-yield. The behavior of ER materials in these two regimes can be clearly seen in **Figure 2.3**. When designing a device it is important to consider the rate of strain and whether the device will be in the pre-yield or post-yield ranges of the material behavior.

2.2 Fixed Plate Versus Sliding Plate Configurations

In order to classify ER devices, it is useful to classify them as fixed plate or sliding plate devices. In fixed plate devices the ER material is typically forced through a gap between the electrodes, and the corresponding pressure drop across this gap, as the fluid in the electric field applied by the electrodes has increased its viscosity, provides the resistance force for the device. In sliding plate devices, the typical resistance is provided by the viscous drag on the electrodes, as one slides past another. These devices can utilize one or more sets of electrodes in order to tailor the performance of the device to the particular application. A schematic of a simple fixed plate and a simple sliding plate electrode configuration appear in **Figure 2.4**.

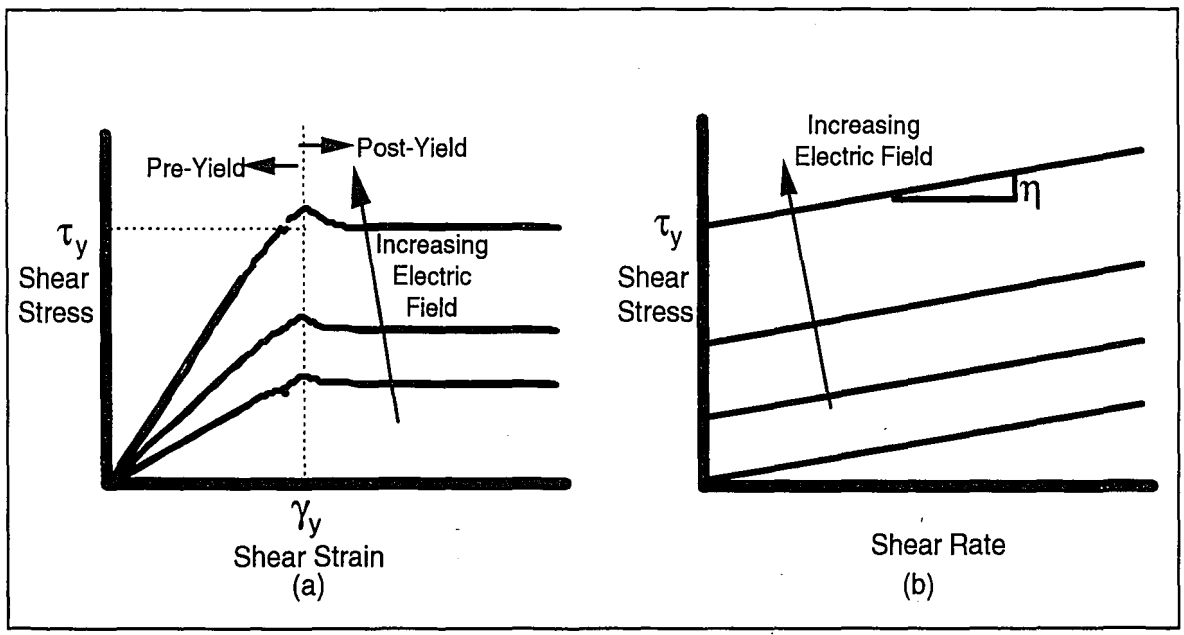

Figure 2.3. ER Material Behavior as a function of a) shear strain and b) shear rate.

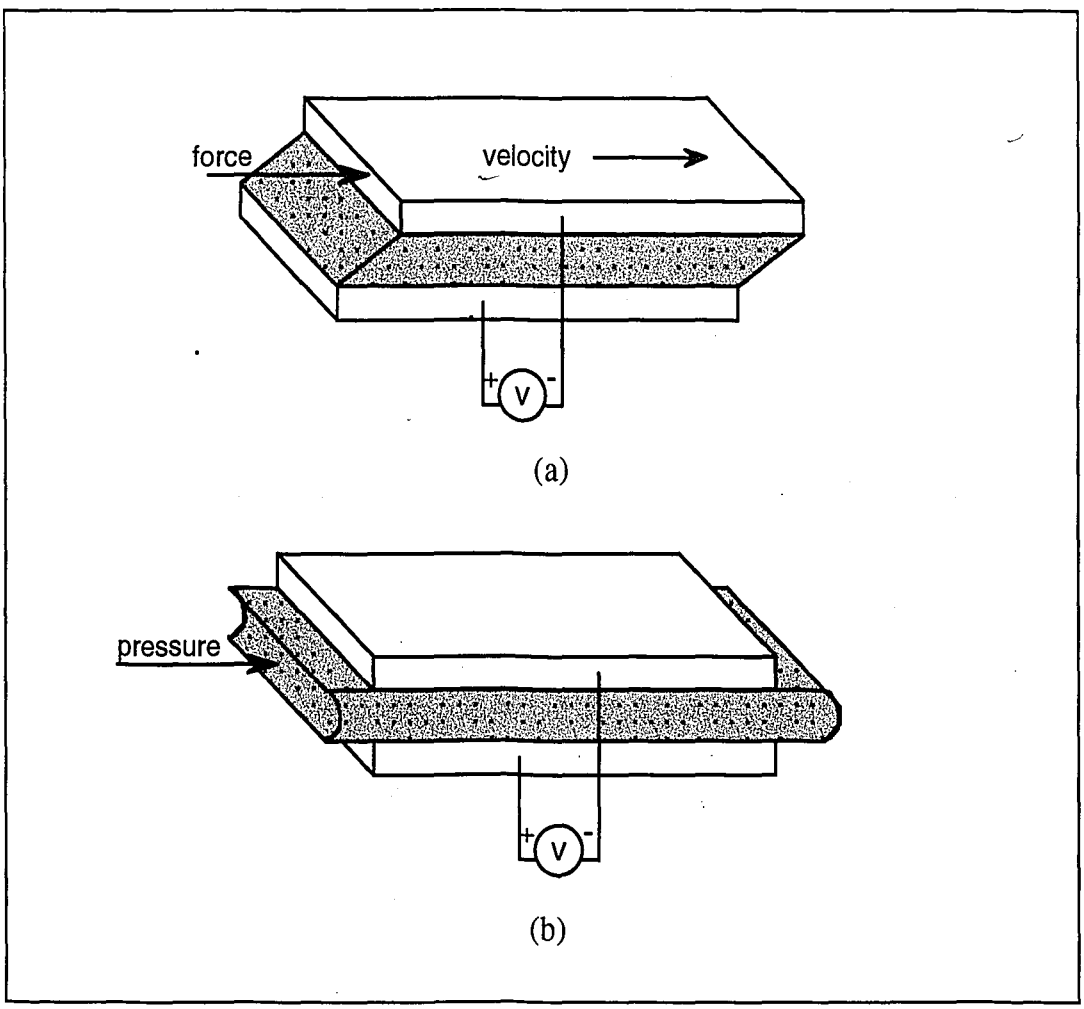

Figure 2.4. a) Sliding Electrode Mode b) Fixed Electrode Configuration or Flow Mode.

2.3 Design Constraints and Considerations

Though numerous ER devices have been proposed, and many have been built and tested, several engineering challenges in the field of ER fluids remain. Due to fact that these fluids are typically suspensions of particles in a carrier fluid, some particle settling within the fluid is inevitable, no matter how closely the specific gravities of the carrier oil and the particles are matched. Once some of the dielectric particles have separated out of the original mixture, the fluid will not behave as it originally did under electric field, the most noticeable performance change will be that the controllability factor will begin to decline. If the fluid is not mixed or is left inactive for a period of time, even more fluid particles will separate out of the matrix, until most of the particles have settled out of the fluid. This typically results in a failure of the device, and it must be refilled and cleaned, or even entirely replaced. And, as these fluids currently cost hundreds of dollars per gallon, replacement is a very expensive proposition.

As with most hydraulic systems, some fluid should be expected to weep past the seals due to inexact fits between parts and sealing materials, normal wear, or damage to the device. In conventional hydraulic systems this is usually not a problem, an operator simply adds more hydraulic fluid to the reservoir of the system. However, in ER systems, the material that leaks past the seals during use or which weeps out slowly is more likely to be the carrier oil, rather than the dielectric particles, as the fluid molecules are smaller than the dielectric particles. Some leakage of ER particles past seals has been seen, but this problem is considered to be uncommon given careful attention to design and the fit of parts. In any case, this leakage results in a particle-carrier oil ratio that might vary from the nominal volume fraction. ER fluid mixtures can be up to 25% by volume dielectric particles (Conrad, et. al., 1989). When carrier oil is lost, this ratio increases, resulting in

the ER material in the device having an even higher volume fraction. A higher volume fraction usually causes the fluid to be thicker under no voltage field. Under an applied voltage field, the fluid might behave as if it were under a higher voltage field than that to which it is being subjected. Another common problem associated with ER fluids is their incompatibility with some sealing materials. This is most likely due to the incompatibility of the carrier material with the seals, and is often overcome with proper material selection for sealing the device. A final caveat for leaking systems comes from the aeration of the fluid. Once fluid has leaked past the seals, air often replaces the fluid in the device, increasing the liklihood of arcing within the device, an occurrence detrimental to the performance and the durability of the device.

If air is present in the device, through leaking or fluid frothing, the opportunity exists for arcing of the electric field within these newly released air bubbles in the fluid. Fluid arcing is important to avoid in order to assure the durability and reliability of the device. Essentially, when arcing occurs within the fluid, the polarized particles and the electrodes themselves are damaged. Electrode damage can be considered a minor reduction in the electrode area, or a permanent short circuit as the electrodes often permanently weld themselves together due to the small gap (typically 1mm or less) between the positive and negative electrodes. It is possible to break these welded spots with manual movement of the electrodes in theory, but in some devices this is difficult to do, for example in fixed plate devices. The areas on the electrode where arcing occurred are blemished with a buildup of carbon, and unless cleaned these small areas, on the order of a few millimeters square, will be prone to arcing in the future, forming more carbon and potentially wleding the electrodes together. These spots where welds once existed are now surface high spots, and are more prone to arcing due to the reduced distance between them, under an applied electric field. In the case of the electrodes permanently

welding together, the device will not be able to sustain any voltage field, and all performance will be lost. In the case of a reduction in the area of the electrode, less fluid will be subject to the viscosity change due to the applied electric field. This pocket of unaffected fluid will be located in the region of the electrode, and will result in irregular and erratic performance of the device. Over time, this damaged region in the electrode can potentially short circuit under electric fields with magnitudes much less than the designed field, which will then permanently damage the electrodes and cause the device to fail. Also, as there is a reduction in the shear stress in the damaged region on the electrode, fluid particles are thought to migrate there to "escape" the shear stresses occurring at the healthy electrodes. This is an example of shear stress diffusion process, and will be discussed along with design consideration for ER devices (Leighton, 1985).

2.4 Current Design Practices

When designing a device to utilize the unique properties of ER, and to an extent MR fluids, it is important to keep in mind the causes of poor fluid performance and device failure discussed above. By designing a device that takes into account fluid leakage, particle settling, and temperature effects, the designer and user can be assured that the device will provide reliable service with minimal maintenance. Several novel solutions to the aforementioned problems with ER fluids have shown promise for reducing or eliminating the problem of fluid settling and consequent loss of performance that practical ER devices face.

There are two courses of action which seem to be the predominant means to reduce or eliminate particle settling. These two means are through fluid agitation and through optimization of the initial device design. This does not include matching the

specific gravities of the fluid and the particles. By matching the specific gravities of the particles to that of the carrier fluid, one can minimize the tendency of the particles to settle out of the suspension. However, one should never expect that particles and carrier oils will be perfectly matched and that no settling will occur. Also, as extensive financial and human resources must be committed in order to perform the chemical research necessary to "design and build" carrier materials with higher specific gravities, it is often preferred to use off the shelf components as carrier materials rather than formulate specific materials, some of which can cost upwards of $250 per gallon. Additionally, it may not be chemically possible due to elemental limits in the periodic table. Currently, it is also difficult to formulate a custom carrier material that meets device specifications, with a specific gravity above 1.8. This is due to the fact that, during formulation, adding heavier molecules to the molecular chains of the carrier result in the formation of members of the chlorinated fluorocarbon (CFC) families. These CFC based carrier materials are neither practical nor safe for ER device applications.

2.4.1 Agitation Mechanisms

In order to ensure that the particles stay mixed, and that the mixture remain homogeneous, some designers have incorporated agitation mechanisms in their devices to keep the particles and the carrier material properly mixed. These agitation mechanisms typically supply very small amplitude mixing impulses to maintain fluid homogeneity. Some utilize the mechanical energy of the device to perform the agitation, while others employ an external source and mechanism to achieve fluid mixing. Examples of these mechanisms range from small rotary blades which stir the fluid constantly and more complex mechanical designs, to a reliance on the vibration of the device to keep the fluid agitated. In the case of an automotive shock absorber, the constant action of the shock

absorber is often used to mix the fluid in the device. Advantages of this system are that the fluids are constantly stirred and have a greater chance of maintaining the optimal fluid mixture. Disadvantages associated with this method of fluid mixing are that some of the mechanical complexity that was removed from the device by switching to ER fluid is re-introduced through a mechanical mixing mechanism. In addition, this mixing might cause frothing and the addition of air bubbles to the fluid, eventually leading to a performance degradation. In the event that this mixing device were to fail, the ER device could still function, though with a less than ideal fluid mixture, the device's performance would be expected to deteriorate (Oppermman et al., 1989).

2.4.2 Optimizing the Initial Design

Another possible solution to the problem of fluid settling is to initially design the device so as to minimize the shear stress differential within the device. It has been shown in the shear stress diffusion theory that particle suspensions will tend to separate in the presence of a variation in the shear stress. This variation in shear stress was originally observed during rheometer testing on common fluid suspensions, and at first was believed to be responsible for the separation of some foods during packaging and processing (Leighton, 1985). However, similar conditions also exist in ER devices. That is, a differential in the shear stress exists where the electrode area does not encompass the entire volume of the fluid, or where the fluid in the device is subject to different electric field strengths. Different electric field strengths could occur in regions where internal dimensions change to accommodate radiused locations, allow part clearances, or in locations such as fluid reservoirs and accumulators, plumbing and miscellaneous fluid lines.

By designing the device so that the shear stress experienced by the fluid is uniform, it is thought that there will be no tendency for the particles to migrate to regions of lower shear stress. The reliability of the device should be greatly improved. In addition to preventing fluid problems, a design placing all of the ER fluid under the electric field can be considered optimal in that all of the fluid is being put to work. Given that ER materials once commercialized are expected to be expensive (Lord Corp, 1994), minimizing the amount of fluid in any device is always a concern.

Important consideration must be given to the problems associated with the performance of ER fluids when the fluids undergo a temperature change. Commercial ER fluid formulations are tested and have their engineering properties classified by the manufacturer, and these properties are usually given in a narrow temperature range. Their engineering properties, such as current density and the shear stress, often vary with temperature. This behavior is expected, as these fluids are often mineral oil based, and these mineral oils usually tend to vary their properties with temperature. These conventional mineral oils typically will sustain lower values of shear stress as the temperature increases, and might froth under heavy use or at elevated temperatures. However, this behavior also contributes to an increase in the conductivity of the fluid. This important change in the fluid property requires much higher current supply requirements to maintain the same performance of the device, and thus more power is consumed by the device. In one case, it was experimentally observed that the required current for an ER device *almost **doubles*** with every 10-12°F rise in operating temperature. (Lord Corporation , 1993) This current increase results in a direct increase in the power consumed by the device, as seen by the general power equation below:

$$\text{Power} = VI \tag{2.2}$$

Where P is power consumed by the device, V is the applied voltage field, and I is the current that must be supplied.

2.5 ER Fluid Clutches and Torque Coupling Devices

The potential applications for electrorheological fluid-based clutches and torque coupling devices has driven research and piqued commercial interest in those same devices. Potential applications for these devices abound in the automotive industry, particularly in high-speed robotic assembly operations. These operations require that robots assemble and tighten numerous fasteners in a vehicle assembly before it is installed in the vehicle, or while the assembly is in the car on the assembly line. An ER-fluid device that is capable of high-speed switching from different torque settings, in the interest of allowing a single robot to perform several different assembly tasks, is highly desirable. This can potentially speed up the assembly process, shorten an assembly line, reduce the total number of robots required, and reduce capital expenditures on heavy equipment (Coulter et. al., 1992)

Typical ER-fluid clutch and torque couplers are configured in one of two ways, either a concentric drum type or a multi-plate clutch pack type. In the concentric drum type, a rotating drum spins inside of a stationary outer cylinder. The stationary cylinder acts as the negative or ground electrode, while the center rotating drum acts as the positive electrode. When there is an applied electric field, the fluid between the inner and outer drum undergoes a viscosity change, and applies a moment to the central drum. In

this way, the device can maintain a level of force to transmit power, for example when tightening a bolt in an assembly. When the level of torque on the bolt reaches the level to break the force transmitted by the ER-drum, the drum freely rotates and no further torque can be transmitted. By varying the electric field applied to the drum, the amount of torque transmitted to the bolt can be varied. For concentric cylinder configurations, it is difficult to manufacture a device with two or more concentric cylinders using conventional machining techniques. And, as the device is limited by the amount of electrode surface area and the ER fluid under the voltage field from those electrodes, to provide suitable torque transmission capabilities the device must be inordinately long, or of a very large diameter. A simple sketch of a concentric cylinder ER-fluid clutch appears in **Figure 2.5a**.

In a clutch-pack type configuration, multiple plates are stacked, with a small gap between them. By adding more and more plates to the configuration, the amount of torque transmitted by the device can be increased or decreased. This design offers greater potential for commercial applications in that the stacked plate configuration is more compact than the concentric drum configuration, and offers more torque transmission for a given amount of device volume. However, as the fluid at the center of the device experiences lower shear stress than the fluid at the outer edges of the stacked plate, the potential exists for the fluid particles to migrate to this region. A basic schematic of the clutch-pack type torque coupler appears in **Figure 2.5b.**

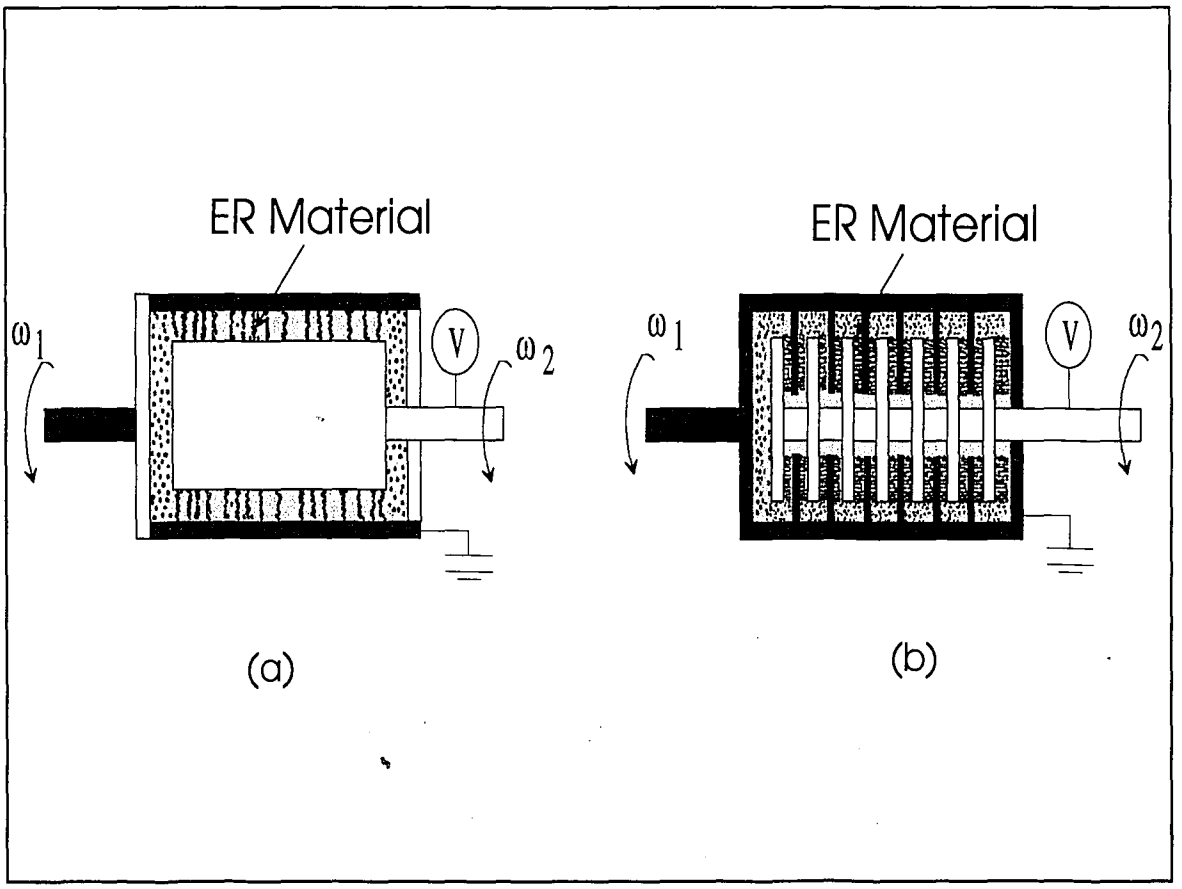

Figure 2.5. ER Clutch and/or Brake (a) concentric cylinder configuration (b) parallel plate configuration.

In order to determine the torque that can be transmitted by an ER-fluid clutch, one must consider the total electrode area of the device and the yield strength of the fluid under a specified electric field. This can be computed with the following equation:

$$T_{ER} = \frac{2}{3} N\pi\tau_y(R_o^3 - R_i^3) \tag{2.3}$$

Where τ_y is the yield strength of the ER material under the applied voltage field, N is the number of clutch packs or sections, R_o is the outer radius of the clutch, and R_i is the inner radius of the clutch.

The viscous torque, that is the torque that could be transmitted by the device under zero field, can be computed with the following equation:

$$T_o = \frac{N\pi\eta f(R_o^3 - R_i^3)}{g} \tag{2.4}$$

Where η is the zero field viscosity of the fluid, g is the electrode spacing, and f is the rotational speed.

From these two equations, the control factor of the device can be derived. Recall that the control factor is given in this case by the amount of torque transmitted under the maximum applied electric field, divided by the torque transmitted with zero applied electric field, with the result:

$$C_f = \frac{2\tau_y}{\eta f} \tag{2.5}$$

In addition, an important consideration for these devices is the amount of power consumed. The power consumption for any ER device can be computed by multiplying the total electrode area by the required current density of the fluid at the maximum transmitted torque, multiplied by the voltage field applied. The result is:

$$\text{Power} = AJV \tag{2.6}$$

Where A is the total electrode area, J is the current density of the fluid, and V is the applied voltage level.

The issue of current requirements and power consumption are crucial to any application, as high voltage amplifiers are typically specified by the amount of current that they can provide at a given voltage. When designing for automotive applications, a designer must pay careful attention to the desired levels of torque that the customer might want to transmit, the amount of power they are willing to devote to these devices, their voltage supply network, and most importantly, the maximum permissible dimensions of the device. For automated applications, the latter issue will likely determine if the device is capable of reaching confined areas for installation, and thus whether or not it will exact the advantage that ER fluid torque couplers can provide.

An additional, rather unique variation on ER fluid torque couplers is an ER fluid brake. This device provides a constant resistance to an input force, such as rotary motion over a pulley, and has been investigated for potential use in several applications, including controlling the descent of objects, as well as providing a means to accurately control tension in wire drawing operations of precious metals in the electronics industry.

The ER material is ideal for the tensioning application due to the immediacy of its response. In addition, the smoothness with which it changes its response resists breaking fine strands of gold wire, typically 0.025 mm (0.001") in diameter or less (Korane, 1991). The equations governing the resistance of a drawing pulley are the same as those for ER clutches, and the entire process is often monitored by computer to account for variations that might occur between batches or other anomalies in production.

2.6 ER Fluid Engine Mounts

In many vehicle applications, it is important to isolate occupants and parts of the automotive structure from engine vibrations, both for passenger comfort and also to increase the durability of the vehicle and component subsystems. To this end, automobile manufacturers have developed engine mounts which are tuned to absorb the vibrations of the engine and drivetrain components. However, as these mounts are passive, and can not vary their performance, designers and engineers must select dampers to isolate certain frequencies that will most likely be encountered under normal operating conditions. In order to assure passenger comfort and vehicle durability, this frequency range is chosen as the range where the vehicle will be in steady state, i.e. cruising at highway speeds. It is at this constant and prolonged operating speed that any harsh vibrations are likely to present the greatest threat to components of the vehicle. These constant speeds also present a threat to the driver in terms of induced fatigue, reduced alertness, and general passenger discomfort.

Thus, some of the earliest experiments with ER fluids in practical devices involved the testing of ER-based engine mounts. A typical engine mount configuration and an ER engine mount configuration appear **Figure 2.6**. As can be seen, a passive

automotive engine mount consists of a rubber spring element, and the manufacturer relies on the natural damping properties of this rubber to isolate engine and drivetrain vibration from the rest of the vehicle. More sophisticated passive engine and drivetrain mounts incorporate different types of elastomeric material in the mount in order to offer damping properties that can be tailored to minimize vibrations in axial or radial directions. However, these mounts must still be tailored to a narrow vibration range, albeit now in more than one direction. ER engine mounts offer the possibility to suppress vibrations over a much wider range than has previously been possible with conventional dampers, by utilizing the variable viscosity of the ER fluid in the mount.

By incorporating a positive and negative electrode into an engine mount, and filling it with ER fluid, it is possible to stiffen or soften the engine mount depending on engine operating speed. In the configuration seen in **Figure 2.6b**, the electrodes can be seen in the middle of the device, between two chambers of fluid. The lower chamber acts as an accumulator, to allow for a change in volume between the top and bottom cavities of the device as the mount proceeds through its stroke. As the voltage is increased, the fluid in the region between the electrodes undergoes a viscosity change, and the shear stress in the region between the electrodes increases. Thus, it requires more force to move the engine mount and displace fluid into the lower chamber. As the fluid passes through the electrode gap, its viscosity changes once again and it fills the lower compliance region. Since the voltage can be manipulated according to vibrational conditions, the viscosity of the fluid passing in the electrode region can be manipulated as well. The shear stress in the region can be controlled, and the damping constant of the device can be varied depending on engine operating speed, or other vibrational considerations.

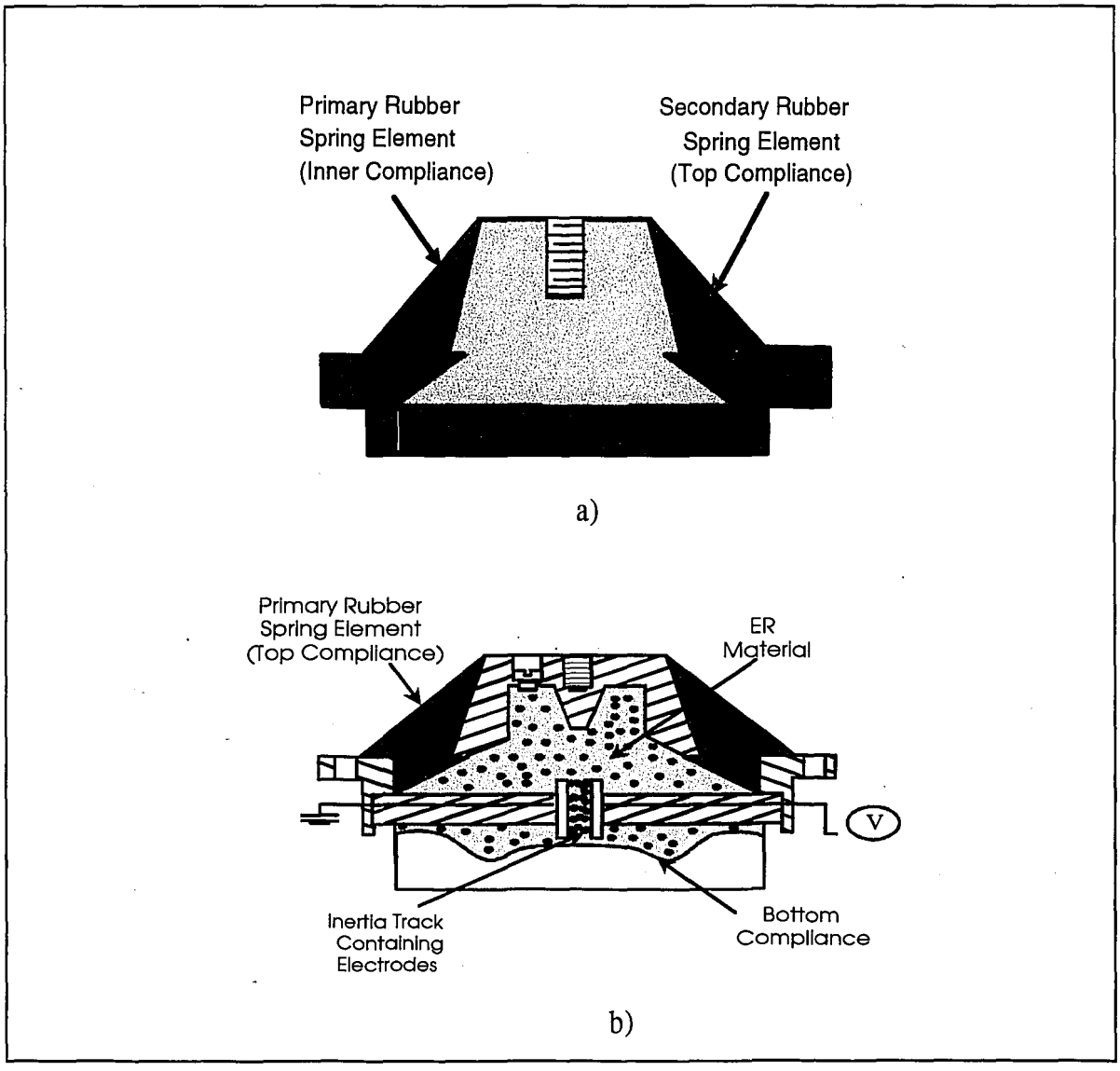

Figure 2.6. a) Passive engine mount and b) ER fluid filled engine mount.

It can also be seen from **Figure 2.6b** that the device does not place the entire volume of the fluid under the same field of shear stress. This mount contains only a small electrode area in the center of the device, while the rest of the ER fluid is not directly subject to an electric field. This could present problems with ER fluid migration to the regions of lowest shear stress, according to the Shear Stress Diffusion Theory. In this case, the regions of lowest shear stress are outside of the direct electrode areas. Over time, this might result in the ER-fluid particles migrating to the corners of the device and the only damping action would result from the motion of the carrier oil, unaffected by the electric field applied at the center of the device, as the fluid is forced through the orifice between the upper and lower regions of the device. Endurance studies performed on ER-fluid enginemounts have proved very promising, with prototypes functioning well for millions of loading cycles and hundreds of hours at temperatures likely to be found in the engine compartment of automobiles and other vehicles (Opperman et al., 1989)

Results of testing and the benefits from these devices have been reported in the technical literature, though conclusive results for or against these devices are more difficult to obtain. Some studies have tested the devices in conditions that test device behavior when going from cold to room temperature conditions, while others have tested the devices for 200 hours at temperatures simulating those that might be seen in an engine compartment of an automobile. Some studies report good results, but fail to report, or do not consider, any fluid settling experienced by the device, while others conclude that results could have been improved with better or more stable formulations of ER fluids.

2.7 ER Fluid Dampers for Vehicle Applications

Great interest has been shown in ER fluids by the automotive industry. The immediate response of ER fluids, the smoothness with which these fluids change viscosity, and their potential to offer a wide range of damping properties has led the automotive industry to extensively examine ER fluids for suspension applications. Adaptive shock absorbers, or semi-active shock absorbers, potentially offer vehicle engineers and designers the capability to provide a car that delivers a supple ride, capable of isolating road irregularities from the passengers and the vehicle, while at the same time permitting the suspension to be firm when necessary. Such a device would allow engineers to offer suspensions which can be comfortable and also high-performing.

To that end, ER fluid dampers have been developed to take advantage of the unique rheological properties of ER materials. Dampers based on the conventional linear design have been developed, in which fluid is displaced by a piston, and the fluid flows through the electrode region, undergoing a viscosity change, thereby changing the damping force of the device. The aforementioned configuration is called fixed plate, as the piston of the device is not part of the electrode system of the device. A schematic of this design appears in **Figure 2.7a**. In a design where the piston is either ground or high voltage, this configuration is known as sliding plate, since the piston is typically coupled directly to the wheel movement. A schematic of a sliding plate configuration ER damper appears in **Figure 2.7b**.

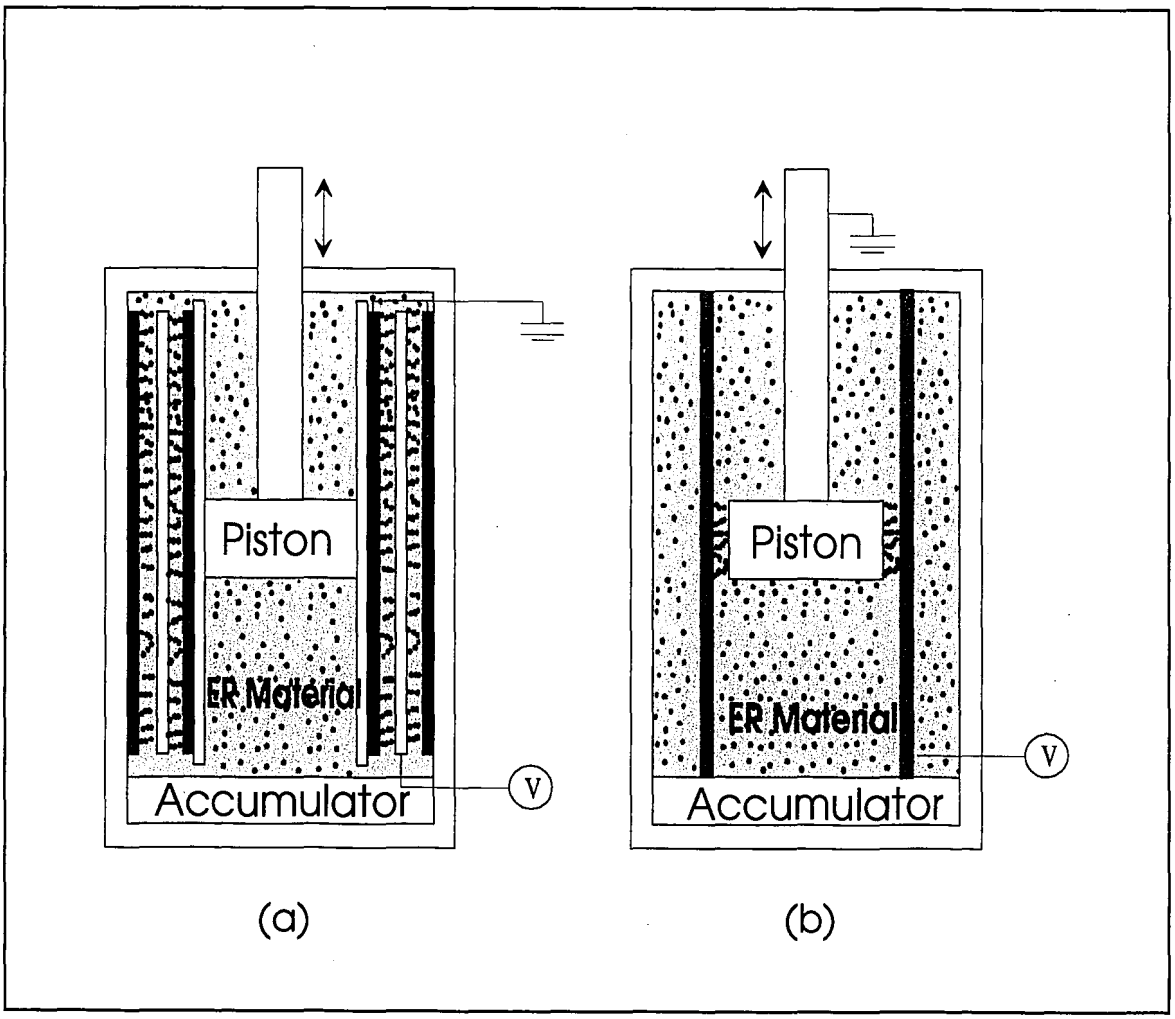

Figure 2.7. ER controllable damper (a) fixed plate configuration and (b) sliding plate configuration.

Another novel configuration for dampers involves the conversion of linear motion to rotary motion, which permits the device to be configured like an ER clutch or brake device. This directional conversion is accomplished through the use of a linear ball screw mechanism. As the lead screw travels in linear fashion, the lead of the screw converts the linear motion to rotary motion, and this motion is transferred to the device through the bearing collar which rides on the lead screw, commonly called the ball nut. This ball nut can be coupled either to a concentric cylinder or to a parallel plate configuration as described elsewhere in this chapter. A schematic of both concentric drum and parallel plate configuration dampers utilizing ball screw directional energy conversion appear in **Figure 2.8**.

The apparent benefits of this configuration are the potential space savings compared to other ER fluid damper designs, and a high degree of fluid utilization in that most of the fluid is placed under a voltage field. The disadvantages to the device are that the ball screw is not 100% efficient at converting the motion of the device. There is also an introduction of bearing friction and lost energy in the thrust bearings that must be incorporated in the design to account for the linear to rotary motion energy conversion. The bearing forces that are introduced and the lack of a 100% energy conversion result in a higher than optimal zero-field performance of the damper, in that more force will be required to move the damper and ball screw mechanism. This negates the possibility of using this directional-conversion type damper in applications where very low field-off performance and very high field-on damper force is required (Coulter, 1993).

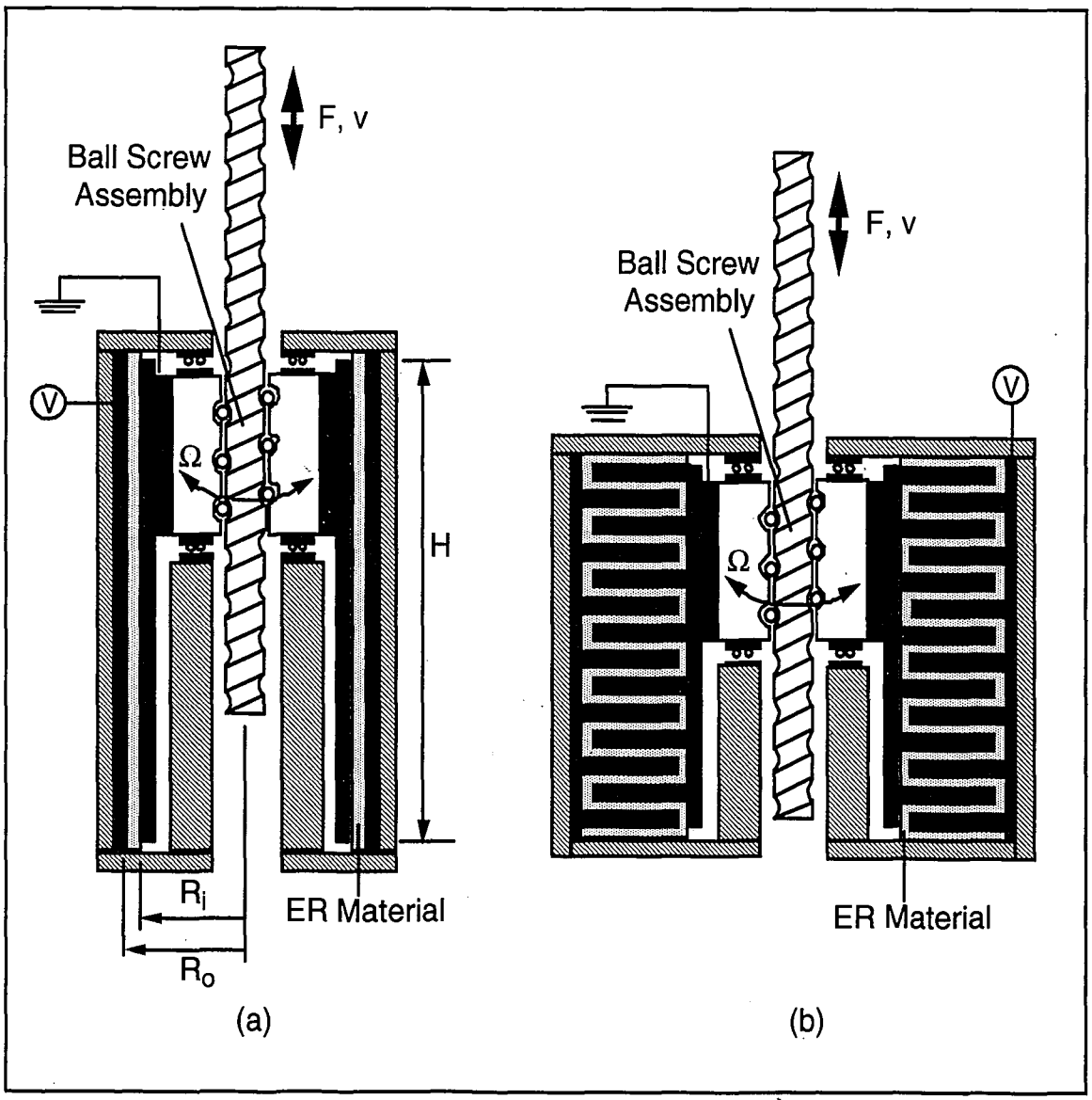

Figure 2.8. Directional Damper a) Concentric cylinder configuration and b) parallel plate configuration.

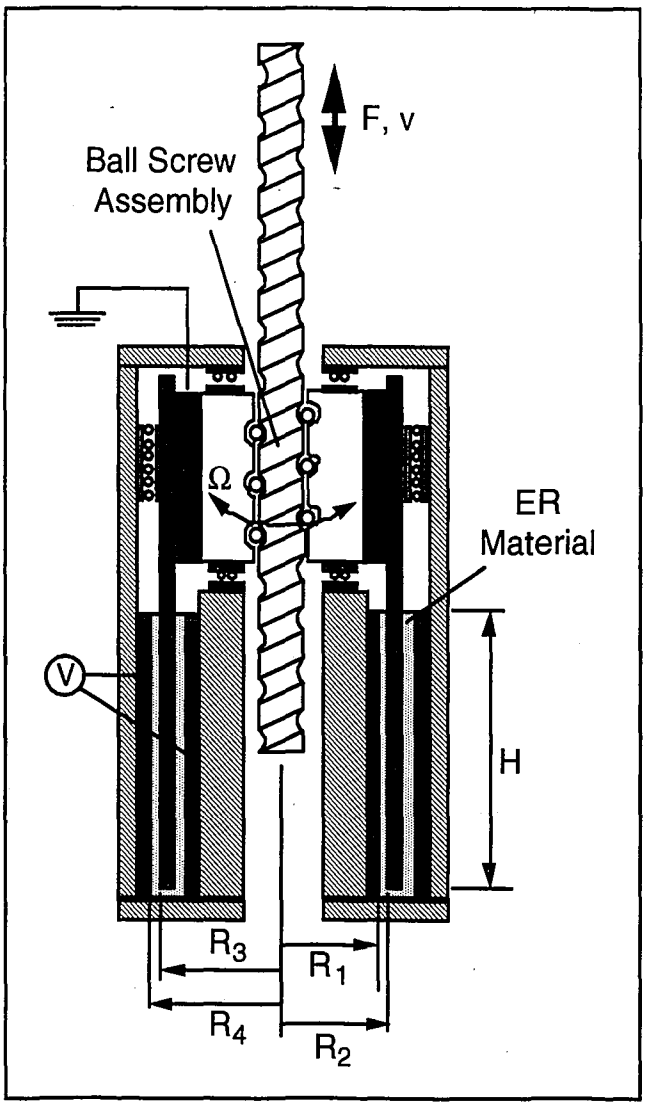

Figure 2.9. Generic Ball Screw Damper.

Directional energy conversion dampers can be characterized and their performance analyzed by relating the axial force on the lead screw to the rotational torque for the device. From the dimensions of a generic ball screw damper in **Figure 2.9**, the torque relation is:

$$F = \frac{2\pi eT}{L} \tag{2.7}$$

where e is the efficiency of the ball screw and L is the lead length of the ball screw.

The total torque that can be maintained by the device can be characterized the sum of the torque of the fluid and also the torque of the bearings:

$$T = T_{fluid} + T_{bearing} \tag{2.8}$$

If we are to assume that a concentric cylinder configuration is used, then the torque of the fluid on the drum can be characterized as:

$$T_{fluid} = \frac{4\pi\mu H(R_i^2 R_o^2)\Omega}{(R_o^2 - R_i^2)} \tag{2.9}$$

Where,

$$\Omega = \frac{2\pi V}{L} \tag{2.10}$$

Thus, the torque on the drum of a concentric device is then described by,

$$T_{fluid} = \frac{4\pi H(R_i^2 R_o^2)}{(R_o^2 - R_i^2)} \left\{ \eta\Omega - \tau_y \ln \frac{(R_i)}{(R_o)} \right\} \qquad (2.11)$$

Where η is the Bingham plastic viscosity.

Currently, several damper manufacturers are offering suspension systems incorporating dampers that feature multi-mode performance, or switchable performance (Winfield, 1995). These dampers are designed with electro-mechanical devices incorporated into the damper body, which varies one of the damper parameters in response to an input, often from the driver selecting the desired damper performance. These dampers usually offer three to five different damping positions. More sophisticated, and more expensive, systems use inputs such as the rate of change of steering, vertical wheel velocity, vehicle speed and rate of acceleration. These systems react within a hundredth of a second to alter the damping properties of the suspension. Currently, only luxury and high-performance automakers can offer such systems on their more expensive models.

The aforementioned systems differ from fully active suspension systems in that they react to inputs from the systems or devices they are controlling, and change the damping characteristics of the system, the spring force in the system, or the effective mass of the system. Fully active systems are capable of applying mechanical energy to

the system, in the form of movement or positioning of the suspension element. An actiove suspension is generally effected through a system of hydraulic pumps, servovalve, and actuators (Bamsey, 1993). These actuators replace the conventional hydraulic dampers and springs that are specified on normal production vehicles. This actuator is typically an electro-hydraulic device, and reaction times are typically 3-5 milliseconds (Bamsey, 1993). However, these systems have been seen on only a few research vehicles and racecars. One car sold for road use, the Infiniti Q45, offered as an option a hybrid version of an active suspension and a conventional suspension. Unfortunately, this option was discontinued due to a lack of sales stemming from the high cost associated with the hydraulically actuated suspension system. It is expected that these fully active systems will never see mass production due to their complexity and high manufacturing costs. Instead, semi-active suspension systems capable of very quick reaction times will replace conventional suspensions offering improved suspension response and better passenger comfort.

Because ER fluids offer a very simple method of altering the performance of a vehicle damper, as quickly as an active suspension system reacts with far less complexity, vehicle manufacturers have tested several configurations dampers for automotive use. Both conventional linear dampers as well as rotary dampers have been tested, with good preliminary results. However, these dampers are still undergoing rigorous testing for cold weather performance, transient temperature performance, and durability. Additional research into MR fluid suspensions is also continuing as a possible competitor to ER suspension systems.

2.8 ER Material Adaptive Structures

The same engineering properties of ER fluids which make them so attractive for devices such as automobile dampers and engine mounts also makes them very attractive for use in adaptive structures. Adaptive structures are structures which are constructed using ER or other materials which are capable of affecting the overall properties of the structure. Beams or plates which are made of ER material have been shown to have significant potential to reduce the amplitude of vibration over a broad range of frequencies, reducing the vibrations which are tranferred to any device mounted to these structures (Yalcintas et. al., 1994). In addition, as the ampltiude of vibration is generally reduced, the acoustic disturbance created by the beam can also be considered to be reduced.

In the scope of this investigation, fiber optic sensors were developed for adaptive structures made from ER materials. These structures were configured as beams and plates, with single or multiple electrode regions, which premitted the electrical field to be discretized to each electrode region. The construction of these adaptive structures will be discussed later in this report.

It is not difficult to envision numerous applications for smart structures. Structural elements such as beams in bridges, variable stiffness panels which would reduce the vibrations transferred to a compartment of an aircraft, and apparatus for isolating vibrations from critical hardware on maritime vessels have all been proposed. It is also not unforseen that devices to capable of providing earthquake protection could be developed and tested. ER adaptive structures have potential applications in such diverse

fields as the building and structural industries, automotive and aircraft industries, to specialty applications in the military and space exploration. The focus of this investigation was the development of a fiber optic device capable of measuring the frequencies of vibration of beam and plate structures. These structures might be used in panels in aircraft, as rotor blades for helicopters, and numerous other specialty structural applications.

2.9 Additional Unique ER Fluid Applications

As we have seen, several applications for ER fluid devices have shown considerable potential to replace conventional mechanical designs, and extensive research and development has gone into proving out designs in these and other fields. However, potential applications for ER fluid devices exist that are just being reported. The National Aeronautic and Space Administration has patent and licensing rights to a tactile display using ER fluids (Garner, 1994). This device utilizes numerous small electrode dots and ER fluid to produce surface topography changes, and can effectively reproduce the Braille raised dot characters. Using a computer to control the switching of these dots, it is possible to scroll text on a small pad for the reader. This device could lead to simplified storage and retrieval of text for persons with vision impairments.

Another potentially beneficial application of ER fluid technology is being investigated by aeronautical researchers and helicopter manufacturers. It has been discovered that by changing the twist and stiffness of a helicopter blade, the vibration, and thereby noise, generated by that blade can be controlled or reduced (Wereley, 1994). In addition, actively controlling the aerodynamic profile of the blade provides an added measure of adjustment and performance advantage in terms of increased lift and reduced

drag (Boggs, 1991). Other mechanisms are also being investigated to achieve this level of control and quick response time.

2.10 Sensing Issues and How to Utilize FOS to Make an Intelligent Structure

In all of the previously mentioned applications, it is necessary to have the information about the frequency and amplitude of vibration of the ER-material-based system. Some of the devices involve very large amplitudes of motion that would be inappropriate for strain gauge use, they would be better monitored by an LVDT device. However, some applications such as helicopter rotor blades, vehicle skins, beam structures in buildings, and fiber reinforced composite panels present unique problems that fiber optic strain sensors can solve. Sample implementation of fiber optic sensors on the aforementioned systems will briefly be presented here in order to assist in our further understanding of the implementation of fiber optic strain and vibration sensors for intelligent structures.

In order to properly and efficiently effect control over an adaptive system, it is necessary to know as much information about the system as possible. The primary variables from a mechanical system that need to be known for use in a control algorithm, either a straightforward control program or a neural-network-based controller, are the amplitude of vibration and the frequency of vibration. Additional variables such as the rate of change of frequency and amplitude, assuming the changing is cyclic and can be predicted, can also be used to further refine the response of the adaptive system.

Once it has been determined that a fiber-optic strain gauge is to be used, the location and placement of these gauges must then be considered. In some mechanical

systems the choice for the location of the sensor is obvious, it is attached to a crossmember or a straight link, in a manner similar to electrical-resistance strain gauges. In some cases care must be given to the selection of the location of the sensor. Lead-in and lead-out lengths can sometimes interfere with the proper operation of the device, or the lengths can be damaged. To ensure that the sensors operate for a prolonged period of time and that they are able to provide reliable data, proper location selection for mechanical systems is of utmost importance.

Some ER-structures that have been tested, beams and plates, permit the sensors to be placed on the surface of the structures. The frequency and amplitude of vibration are read from the location on the surface of the beam and then input into the controller, which determines the opitmum voltage that must be applied to the structure. The optimum voltage is defined as that voltage which must be applied to minimize the amplitude of vibration of the structure. This voltage is applied through a high-voltage amplifier to electrodes in the structure, which effect the viscosity changes in the fluid. This change in the fluid viscosity chages the stiffness of the structure, shifting the natural frequencies of the structure to higher frequencies, and reducing the amplitude of vibration. This process of sampling the frequency and amplitude, inputting to the controller, and outputting to the structure is repeated numerous times per second, in order to minimize the vibrational amplitudes of the structure.

Some systems provide unique opportunities for the placement of sensors. These structures are primarily in the field of fiber reinforced composites, where the fiber optic sensor can be sandwiched in between layers of the fibers in the structure. Because of the comparative size between the diameters of fiber optic cable and the tows of graphite

fibers used in many composite structures, the structural integrity of a composite panel is not considered to be compromised with the inter-laminar insertion of a fiber optic sensor.

In the manufacture of a composite panel, for example, several plies of fiber reinforcement are usually layered together, with panels often being made up of more than 10 plies of fibers. In between these layers, typically mid-section, a fiber optic strain gauge and the appropriate lead-in and lead-out lengths are inserted. The lead-in and lead-out lengths are then routed as unobtrusively as possible, to locations where the light source and montioring software and hardware will be attached after all manufacturing has been completed and the panel is ready for service. Panels which have been fully built-up with the specified number of fiber plies are then placed in an autoclave, where a prescribed cycle of temperature and are used to cure the resins which bond the plies together, providing strength in the composite. Once the composite has been cured, the fiber optic sensor is usually put through a series of status tests to ensure that it has not been damaged in the manufacturing process. If the sensor has not been damaged during manufacture, and all finishing processes have been completed, the panel is ready for service.

Once in service, the fiber optic sensor in the panel can perform several functions. As long as a signal is being received from the sensor, it can be assumed that the region immediately surrounding the sensor has not been damaged, either through accident, artillery strike, or other unintended occurrence. Additionally, the magnitude of the strain from the sensor can be compared with the known mechanical and aerodynamic loadings in order to evaluate the nature of fatigue in the panel. If it was found that under a certain set of steady state conditions the strain from the sensor was increasing, it could be concluded that some hysteresis was occuring in the panel and the original ultimate

loadings would not be supported by the panel, and the ultimate loading before failure would be less than designed. Designers and operators could use this information to schedule routine maintenance and replacement of parts to ensure optimum performance and reliability.

Common to all of these applications of fiber optic sensors is the requirement that the strain and frequency of vibration of the system be known. By performing a Fourier analysis on the signal from the fiber optic sensor, it is possible to know the frequency of vibration of the system, including several modes, and this information can be processed by the adaptive controller. Once the controller has the information on the frequency and amplitude of vibration, the proper control sequence that must be applied can be implemented, and control of the system can be effected.

Chapter Three

Fiber Optic Strain Sensors

As was previously discussed in Chapter 1, this investigation focused on the development of fiber optic sensors for use in smart structures. It is possible to configure these sensors in numerous ways to measure frequencies of vibration and to measure strain. Fiber optic sensors have also been used to measure numerous structural properties and to perform sensing tasks which have typically been performed by more conventional sensors. In the case of smart structures, conventional sensors are not appropriate or would perform poorly, and thus the use of a fiber optic sensor capable of performing well under the corresponding conditions is appropriate. Tachometers, thermocouples, and distance measurement calculations have been accomplished using various configurations of fiber optic sensors. In this study a fiber optic sensor was tested on a beam in pure bending, with clamped-clamped end conditions.

Traditional vibration monitoring techniques have involved the use of accelerometers or resistance-type strain gauges which were attached to the structure. The output from these sensors, in the form of a voltage signal, would be sent to a processor to determine the amplitude and frequency of vibration. These sensors typically perform passively, interfacing with a converting processor which interprets the voltage signals in terms of displacements or frequencies. Some newer applications of these strain gauges, used to determine bridge loading by measuring the strain on structural fasteners, are

attempting to integrate the strain gauges with a controller to predict a safe loading for the bridge, permitting optimum traffic flow on the bridge. Should the loading approach critical values, the engineers can implement a staggered traffic pattern or close the bridge altogether (Severson, 1995).

Using data from a fiber optic sensor, monitoring the vibration of a smart structure, the characteristics of the beam can be altered to offer optimum structural properties. This ability far exceeds the aforementioned approach of shutting down the bridge. Utilizing these sensors in conjunction with a neural network controller, the properties of the smart structure can be tailored to optimize the beam performance under most every vibration condition. This allows fully active control of the structure, as the properties can almost instantaneously, within 3 ms, be varied in response to changing vibrational input.

3.1 Principles of Fiber Optics

Fiber optic cables used to transmit light are based on the premise that a difference between indices of refraction will cause light to be internally reflected inside of a fiber optic cable, rather than escaping out of the fiber and being dissipated. A diagram of a typical optical fiber construction is shown in **Figure 3.1** (Newport, 1995). To achieve the condition of internal reflection, the core of an optical fiber is coated with a polymeric material, called the cladding, whose refractive index is higher than that of the actual core itself. Providing the angularity condition for internal reflection is fulfilled, that is that the

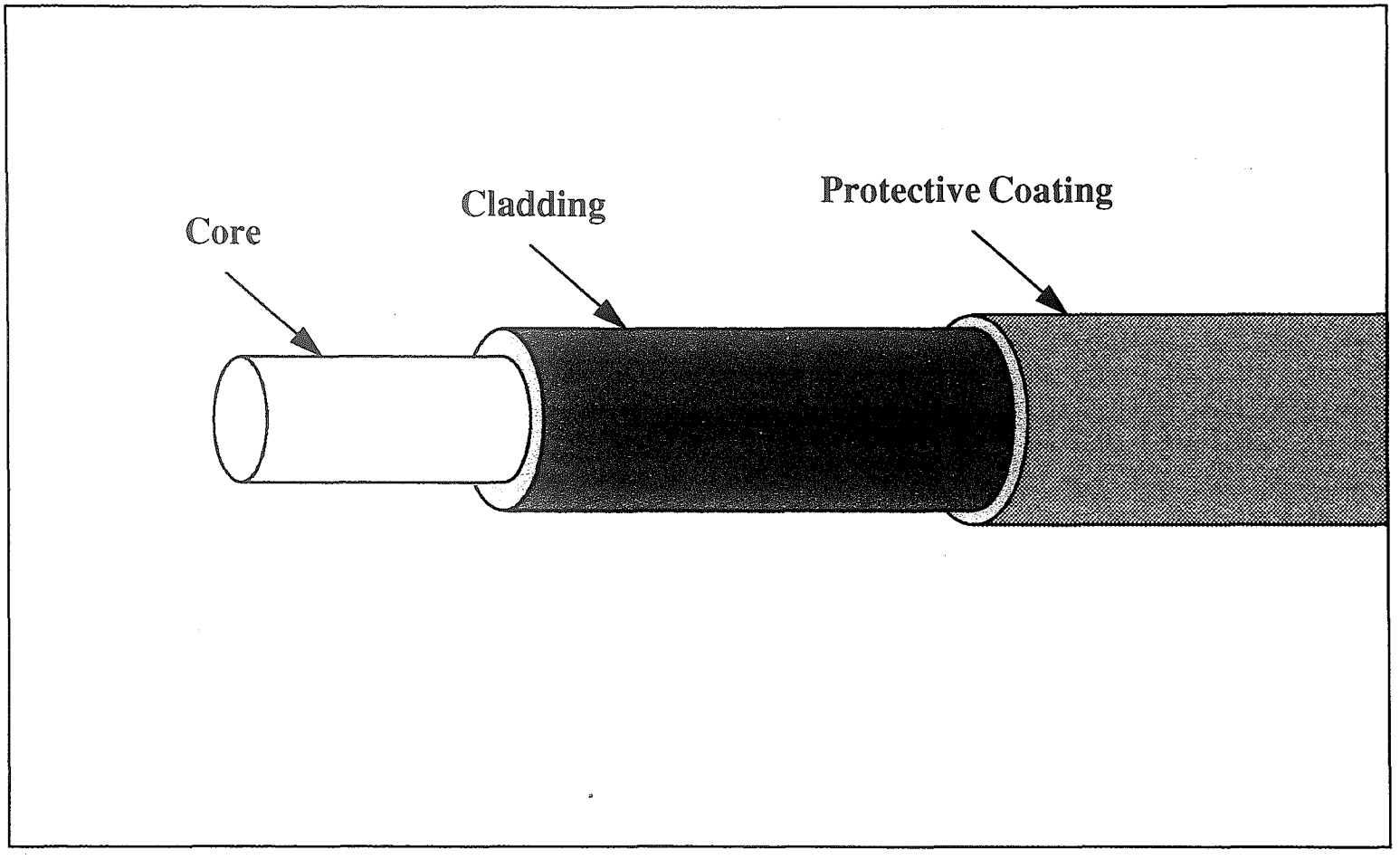

Figure 3.1. Typical Fiber Optic Cable Construction

light is not incident at such a high angle as to directly be transmitted to the cladding, any light striking the core-cladding interface will be perfectly reflected back towards to longitudinal axis of the core.

Fibers can be manufactured from many materials, such as fused silica glass, fused quartz, optical glass, and sapphire. Sapphire fibers are used for high temperature applications, where the high cost of the fibers can be justified by the performance required of the fiber. Optical glass is used for general purpose applications and most experimental work where thermal gradients are generally not a problem. By and large, the three most common types of fibers used are optical glass, fused silica and fused quartz.

Fused quartz can be used in place of fused silica as a conventional fiber material. The difference between these two types of fiber lies in their method of manufacture. Fused quartz is produced by melting and re-fusing of silica sand and natural quartz. This process requires that the raw materials be of high purity, otherwise the impurities will be present in the final material matrix, resulting in absorption of energy at certain wavelengths, generally the ultraviolet spectrum. Fused silica is produced by flame hydrolysis of silica halide. The final product is of higher purity than fused quartz, and does not exhibit the tendency to absorb energy in the ultraviolet regime. Both fibers are used for high power applications, and are more resistant to thermal shocks than optical glass, from which the fibers in this investigation were manufactured (Ealing, 1995).

Optical fibers used for interferometric experiments are single mode type, while polarimetric experiments generally use a high-birefringence fiber. Single mode fibers permit the light to propagate in the fiber without regard to a longitudinal fiber axis. High-birefringence fibers, on the other hand, are manufactured with induced axes along which the light will travel most efficiently. These axes are commonly called the fast and slow axes, and are created when the fiber is manufactured using any process which imparts residual stresses in the fiber. These axes are oriented ninety-degrees from each other, and any light traveling off these axes will be rapidly dissipated. **Figure 3.2** illustrates a high-birefringence fiber.

In order to launch light into a fiber optic cable, the light is usually focused in a lens objective onto the end of the fiber optic cable. The focal length of the lens must be known, and the fiber is positioned using a micro-positioning stand. This arrangement ensures that the maximum amount of light is launched into the fiber. It is important to ensure that the fiber optic cable has been cut, or cleaved, very cleanly , and perpendicular to the axis of transmission. If the end is not cleaved cleanly, the light striking the face of the fiber optic cable will be dispersed, resulting in less light in the cable, and a correspondingly weaker signal. Similarly, at the output end of the fiber, the preparation and finish will affect the strength of the signal being output to the photodetector.

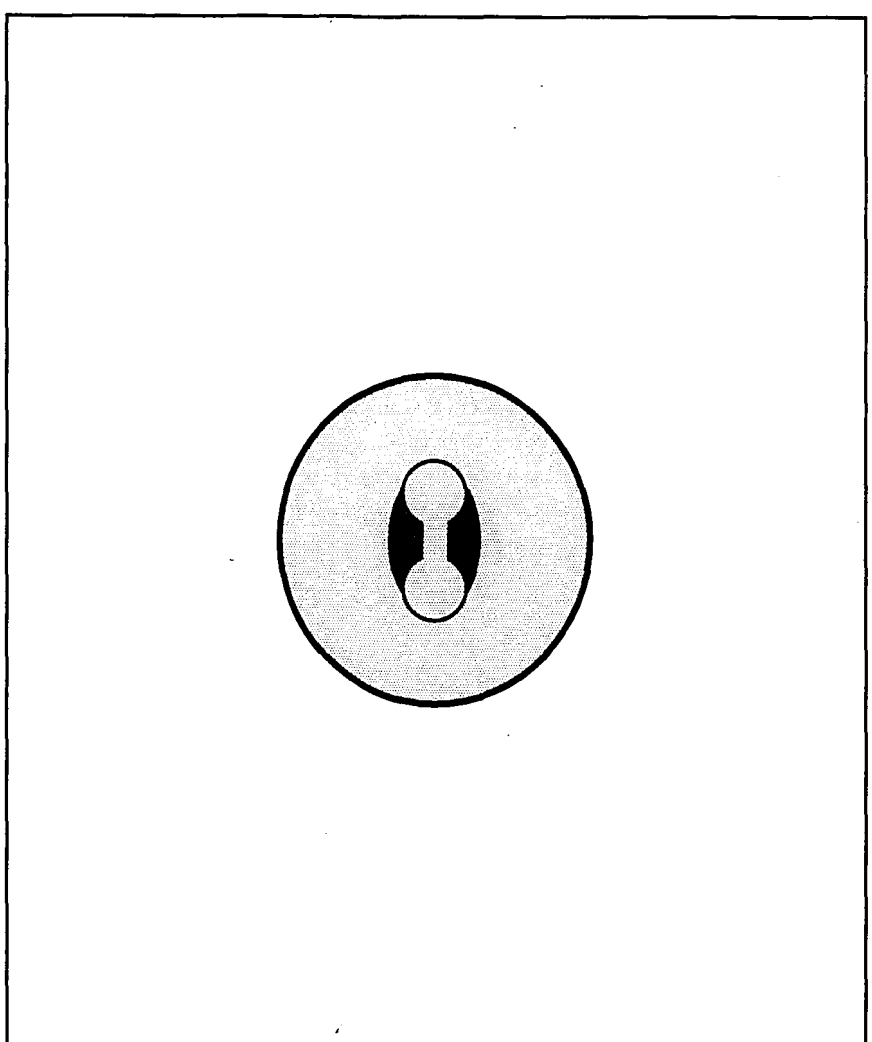

Figure 3.2. A High-Birefringence fiber used for polarimetric fiber optic sensors. The fast axis is oriented vertically, the slow axis horizontally. (Newport, 1995)

Light can be transmitted along a fiber optic cable through the mechanism of internal reflection. The fiber optic cable typically will have an index of refraction which differs from the surroundings, usually air. When a light wave propagates along the length of the cable, the light wave will reflect from the top and bottom of the cable, when viewed in cross section, and the wave continues to propagate along the length of the cable. There will be a critical angle of incidence at which the light will not reflect from the surfaces of the cable, but will instead escape from the fiber optic cable. This angle is dependent on the amplitude and wavelength of the light wave. Once the light signal has been launched into the fiber optic cable, it is possible to use this light signal for strain measurement. Strain measurement can occur in a number of different ways, but it is primarily accomplished by superimposing two light signals, one exposed to a strain and one not exposed to the strain. These two signals are then manipulated to determine the strain applied to the fiber. The proceeding is a detailed discussion of the mechanisms involved in the use of polarimetric fiber optic strain sensors.

3.2 The Development of Fiber Optic Strain Measurement

In the field of strain measurement, fiber optic sensors are generally classified as one of two types, either interferometric or polarimetric. The two sensors rely on different types of fibers and minor changes in the optical hardware to accomplish the superposition of two light waves. However, from this superposition of light waves a phase difference, and thus a strain, is calculated. In effect, the two sensors differ very little, and the

argument could be made that a polarimetric fiber optic sensor is actually an interferometric sensor. The two fiber optic sensors will be treated here as unique measuring techniques, and are thus discussed separately.

3.2.1 Polarimetric Fiber Optic Sensors

Light for a polarimetric fiber optic sensor is launched into a polarimetric fiber after having been decomposed into orthogonal components. The light is decomposed into orthogonal components by launching the He-Ne laser into a polarizing and a quarter-wave plate. The light then enters the fiber and travels along the orthogonal axes of the fiber. A polarimetric fiber preserves light launched down the fiber along two orthogonal axes, these axes having an induced difference in their respective refractive indices. This difference in the refractive indices results in what is commonly known as a "fast" and a "slow" axis, and two light components traveling along these axes will have different velocities.

In order to ultimately detect the strain of the fiber, and thus that of the system to which the fiber is attached, we desire to detect the phase difference between the two signals. This can be done using a linear polariscope. We will define ϕ as the phase shift between the two orthogonal components of the fiber. Letting θ_1 equal the angle between the first direction of the quarter wave plate Q_1 and the fast axis of the lead-in fiber, we can then define the components of the lightwave velocity along the fast and slow axes.

These components are defined as

$$U_{1f} = a_o \cos\theta_1 \, e^{j\omega t} \tag{3.1}$$

on the fast axis, where the speed is $v_1=c/n_1$, a_0 is the amplitude of the incident light phaser, and

$$U_{1s} = a_o \sin\theta_1 \, e^{j\omega t} \tag{3.2}$$

on the slow axis, where the speed is $v_2=c/n_2$. The indices n_1 and n_2 are the refractive indices along the fast and slow axes, respectively, and c is the speed of light. The resulting light wave that is transmitted along the fiber is a combination of these two components

$$U_{2f} = U_{1f} \cos\theta_2 = a_o \cos\theta_1 \cos\theta_2 \, e^{j\omega t} \tag{3.3}$$

on the fast axis, where θ_2 is given as the angle between the first direction of the quarter wave plate Q_2 and the fast axis of the lead-out fiber. Along the slow axis the component is

$$U_{2s} = U_{1s}\cos\theta_2 = a_o \sin\theta_1 \sin\theta_2 e^{j(\omega t - \phi)} \quad (3.4)$$

In order to determine the intensity of the light transmitted in a linear polariscopic arrangement, we must compute the product of the sums U_{2f} and U_{2s} and its complex conjugate. Once computed, we have the intensity of light as

$$I = a_o^2(\sin^2\theta_1\sin^2\theta_2+\cos^2\theta_1\cos^2\theta_2)[1 + \frac{2\sin\theta_1 \sin\theta_2 \cos\theta_1 \cos\theta_2}{\sin^2\theta_1 \sin^2\theta_2 + \cos^2\theta_1 \cos^2\theta_2}\cos\phi] \quad (3.5)$$

taking a_o as the amplitude of the incident phaser. In some situations, when θ_1 or θ_2 is equal to 0°, 90°, the light intensity will not be a function of the phase shift ϕ, and thus ϕ can not be detected using a photodetector.

A circular polariscopic arrangement utilizes two circular polarizers to reduce and hopefully eliminate the effects of the isoclinics, or dark bands where the principle stress directions are parallel to the transmission axes of the polarizer, caused by the existence of θ_1 and θ_2 (Sirohi and Kothiyal, 1991). As shown in **Figure 3.3**, the light phaser becomes

$$U = \frac{a_o}{2} e^{j\omega t}[e^{j(\theta_1+\theta_2)} - e^{j(\theta_1+\theta_2+\phi)}] \quad (3.6)$$

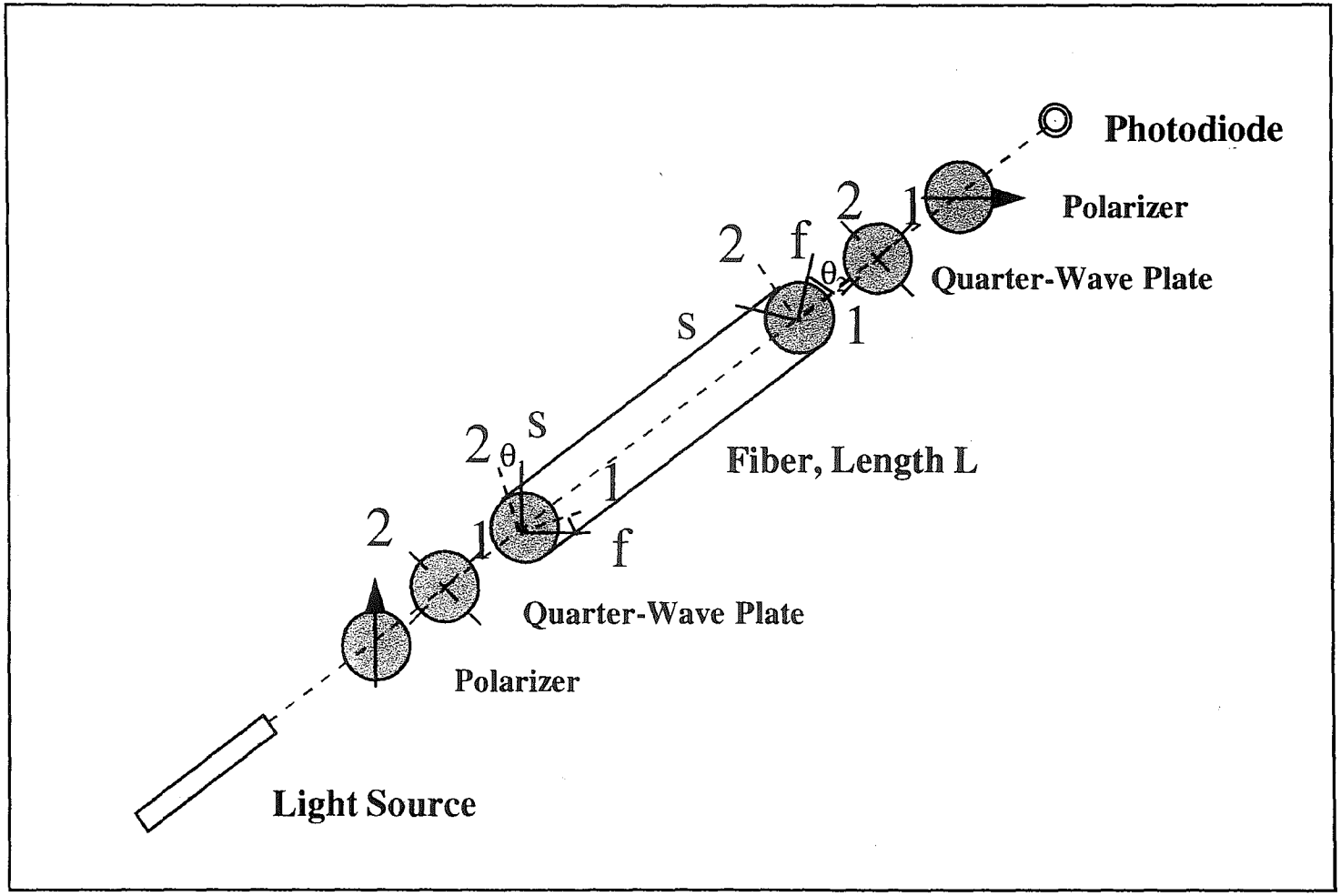

Figure 3.3. Schematic Arrangement of a Polarimetric Fiber Optic Vibration and Strain Sensor

Where θ_1 is the angle between the first direction of the first quarter wave plate, Q1, and the fast axis of the lead-in fiber, and θ_2 is the angle between the first direction of the second quarter wave plate, Q2, and the fast axis of the lead-out fiber.

As it is unlikely that the fiber will be installed torsion-free, it is impossible to state the relationship between the θ_1 and θ_2. The intensity of the transmitted light will then be equal to the product of the phaser U and its complex conjugate, as shown below.

$$I = U^*U = \frac{a_o^2}{2}[1-\cos\phi] \tag{3.7}$$

where ϕ is expressed as

$$\phi = (2n\pi+\phi_o) + \Delta\phi = bL + bL\varepsilon \tag{3.8}$$

where ϕ_o is defined as the static phase change in the fiber under zero applied strain. The expression for the intensity of the phaser can be rewritten into the form

$$I = \frac{a_o^2}{2}(1 - \cos\phi_o\cos\Delta\phi+\sin\phi_o\sin\Delta\phi) \tag{3.9}$$

where $(2n\pi + \phi_o)$ is the static phase change in a fiber which is not loaded. $\Delta\phi$ is a term relating to the dynamic longitudinal strain, ε, b is the propagation constant and L is the total length of the fiber.

For cases when the term $\Delta\phi$ is significantly less than π, the change in light intensity ΔI can be written as

$$\Delta I = (\frac{a_o^2}{2} \sin\phi_o)\, \Delta\phi \tag{3.10}$$

Substituting the relation for $\Delta\phi$ from (3.8) into (3.10), we obtain that the change in intensity of the light at the photodetector is proportional to the longitudinal strains that are induced in the fiber, ε.

For larger values of $\Delta\phi$, there will be a sinusoidal non-linearity between the strain in the fiber and the corresponding light intensity output from the fiber. Since we are most often concerned only with characteristics of the power spectrum, the problem is relatively simple. In order to satisfy the signal-to-noise (S/N) requirement, it can be seen that $\Delta\phi$ should be not less than 0.1 and not more than π

$$0.1 \leq \Delta\phi \leq \pi \tag{3.11}$$

3.2.2 Interferometric Fiber Optic Sensors

In contrast to polarimetric fiber optic sensors, interferometric fiber optic sensors do not need to utilize quarter wave plates, polarizing lenses, and the associated polarimetric fibers with induced polarization preserving axes. The fibers are single mode fibers, as opposed to high-birefringence fibers used in polarimetric experiments, and are 125μm in diameter for He-Ne lasers. The light is launched directly into the end of the fiber through a focusing objective. As the name implies, the interferometric sensor relies on the interference of the light waves to produce a corresponding change in the output intensity of the phaser. This intensity striking the photodiode will be detected and output as a voltage signal, which can be processed by the experimenter manually or integrated with an A/D computer program to automatically measure this voltage change and convert it directly to a strain.

Interferometric fiber optic sensors can take several forms when configured for strain measurement. These can be Mach Zehnder, Michelson, and Extrinsic or Intrinsic Fabry-Perot type interferometers. All of these fiber optic sensors utilize the interference pattern of two light signals to determine the strain being applied to the sensor. In order to compute a strain from the light signals it is necessary to obtain a reference signal and a measuring signal. Typically, a beam splitter is used to obtain the reference signal, wherein the incoming light source is partially reflected and directed to the measuring

photodiode. The remainder of the light signal is sent to the sensing region for measuring purposes.

If we consider the general form of an interferometric sensor, the field intensities of the two beams being used in the sensors can be represented by

$$\psi_1 = A_1 e^{j(\omega t+\phi_1+\phi)} \tag{3.12}$$

and

$$\psi_2 = A_2 e^{j(\omega t+\phi_2)} \tag{3.13}$$

A_1 and A_2 are the amplitudes of the initial light phasers, ϕ is the phase difference between the two signals, and ϕ_1 and ϕ_2 are the static phase differences. The output of the photodetector is then known to be proportional to the product of the sum of the two intensities and the complex conjugate, shown by

$$I = (\psi_1 + \psi_2)^* (\psi_1 + \psi_2) = A_1^2+A_2^2 + 2A_1A_2\cos[\phi(1+\frac{\phi_1 - \phi_2}{\phi})] \tag{3.14}$$

An important factor to consider when examining the intensity of the signal is the visibility of the signal. The visibility is effectively a measure of the strength of the signal.

The lower the visibility, the more difficult it is to determine the strain from the signal. The visibility can be mathematically defined as:

$$V = \frac{I_{max} - I_{min}}{I_{max} + I_{min}} = \frac{2(\frac{A_1}{A_2})}{(\frac{A_1}{A_2})^2 + 1} \tag{3.15}$$

When A_1 is equal to A_2, the maximum visibility is reached. The output from an interferometric fiber optic sensor will be periodic in the phase difference. In order to overcome this problem, it is either necessary to count the number of periods, a task which is not readily performed. Generally, strains of one-half a wavelength are measured in the classical configuration of fiber optic interferometer.

In general, interferometric fiber optic sensors are more sensitive than polarimetric sensors. The phase shift due to any applied strain can be related by

$$\phi = KL\varepsilon \tag{3.16}$$

where K is the phase sensitivity factor of the fiber optic strain sensor, L is the sensing length, and ε is the average applied strain. For a polarimetric fiber optic sensor K is typically $0.44\text{-}8.5 \times 10^{-4}/\mu\varepsilon \cdot cm$. Typical values of K for an interferometric sensor are in the range of $1.98 \times 10^{-1}/\mu\varepsilon \bullet cm$. This constant for fiber optic sensor can be represented

as a phase change of 2π corresponding to the deformation of $\lambda/2$, with the elongation of the fiber being ΔL. To obtain K analytically, we use the relation

$$2\pi = KL\frac{\Delta L}{L} \quad KL \quad \frac{\lambda/2}{L} \tag{3.17}$$

where the wavelength, λ,is equal to 0.6328 μm for the He-Ne laser used to in this experiment. Therefore, the shorter the sensing length, the more suitable it is for use as a pointwise vibration sensor.

3.3 Experimental Preparation of Polarimetric Fiber Optic Strain Sensors

In order to adequately evaluate the performance a fiber optic sensor for smart structures, and the ensure that the best configuration of sensor was developed, both polarimetric and interferometric fiber optic sensors were tested. From the aforementioned description of both polarimetric and interferometric sensors, it is necessary to discuss the preparation of the types of sensors used in the present investigation.

Polarimetric sensors are perhaps the easiest type of fiber optic sensor to manufacture. In order to manufacture a polarimetric FOS, one must decide which type of sensor is going to be manufactured, lengthwise or pointwise. In order to manufacture a

lengthwise sensor, the experimenter must properly cleave a length of fiber of suitable length to attach along the length of the structure while also reaching the light source and the photodetector. To make a pointwise sensor is nearly as easy, with a length of fiber being cleaved and wrapped in a small bow-tie shape, which will be attached at the point on the structure which we desire to sense. Additional fiber length is required to connect to the light source and to the photodetector.

Once the fiber has been cleaved to the correct length, it can be attached to the surface using a cyanoacrylate adhesive. The fibers were generally held in place with cellophane tape while the glue cured. After the glue had cured to permit handling of the fiber and beam structure, the lead-in length of the fiber was positioned in an optical mount. The quarter wave plate and the polarizer were positioned between the end of the lead-in length and the lead-out length. The lead-out length was positioned in the photodetector mount, with a second polarizer and quarter wave plate placed between the end of the fiber and the photodetector.

After the fibers have been assembled and placed in the experimental set-up, it is necessary to rotate the polarizers and quarter wave plates such that the axes of transmission of the polarizers a coincide with the axes of transmission of the fiber. This is readily achieved by either monitoring the strength of the output signal using an oscilloscope, or by watching the intensity of the signal from the end of the fiber as it is

aimed at a white screen. Once the intensity of this output signal has been maximized, experiments with this polarimetric sensor can take place.

3.4 Experimental Preparation of Interferometric Fiber Optic Strain Sensors

Over the course of the investigation, several interferometric Fabry-Perot fiber optic sensors were prepared and tested. These sensors were evaluated in terms of the signal strength and the operating range, as well as visibility of the signal. Because of their ease of assembly, extrinsic Fabry-Perot sensors were chosen as the means to measure the strain and frequency of vibration. A generic schematic of the Fabry-Perot sensor used in this experiment is shown in **Figure 3.4**. In addition, the overall experimental set-up of the experiments is shown in **Figure 3.5.**

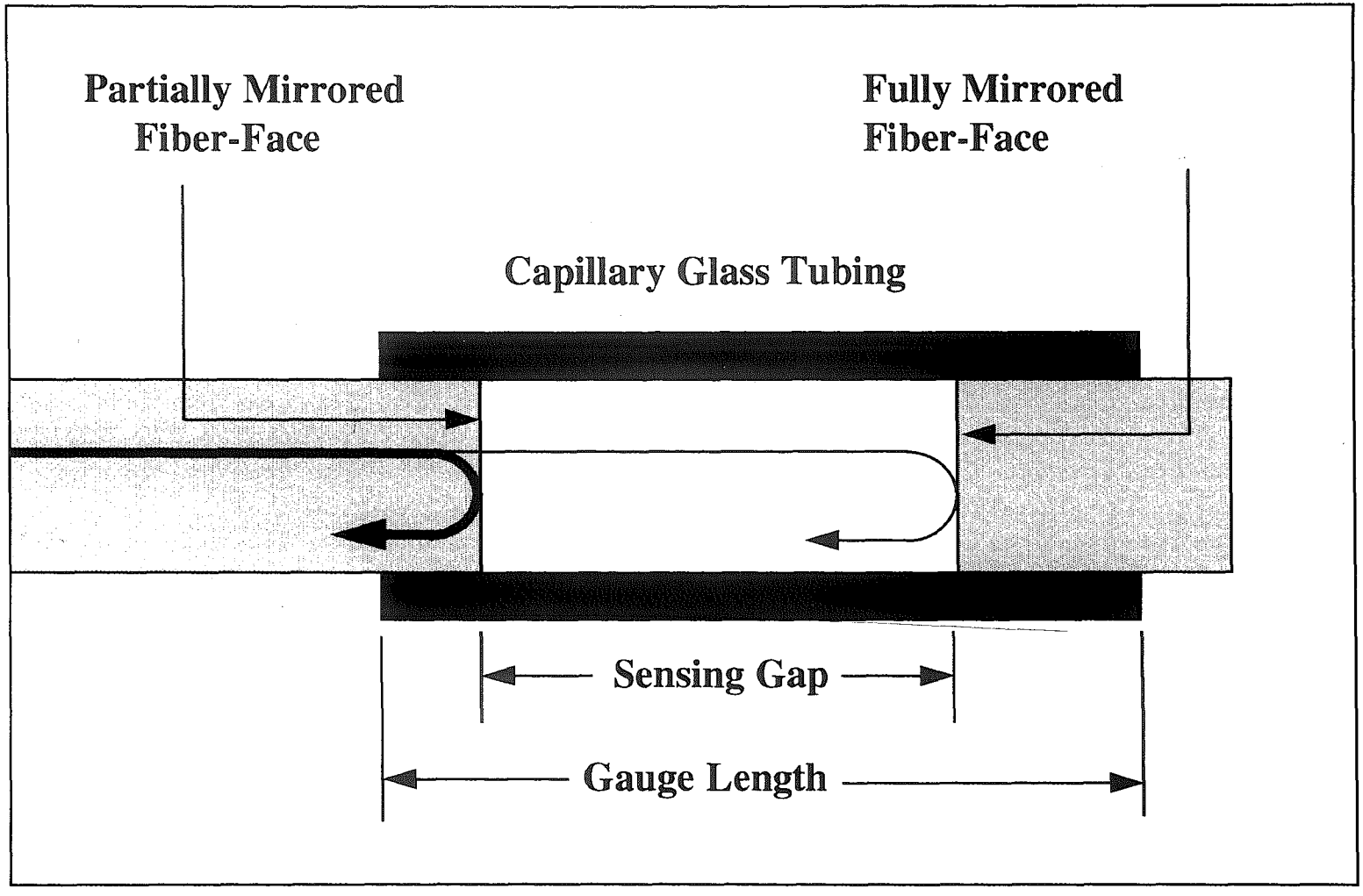

Figure 3.4. Generic Extrinsic-Fabry Perot Sensor

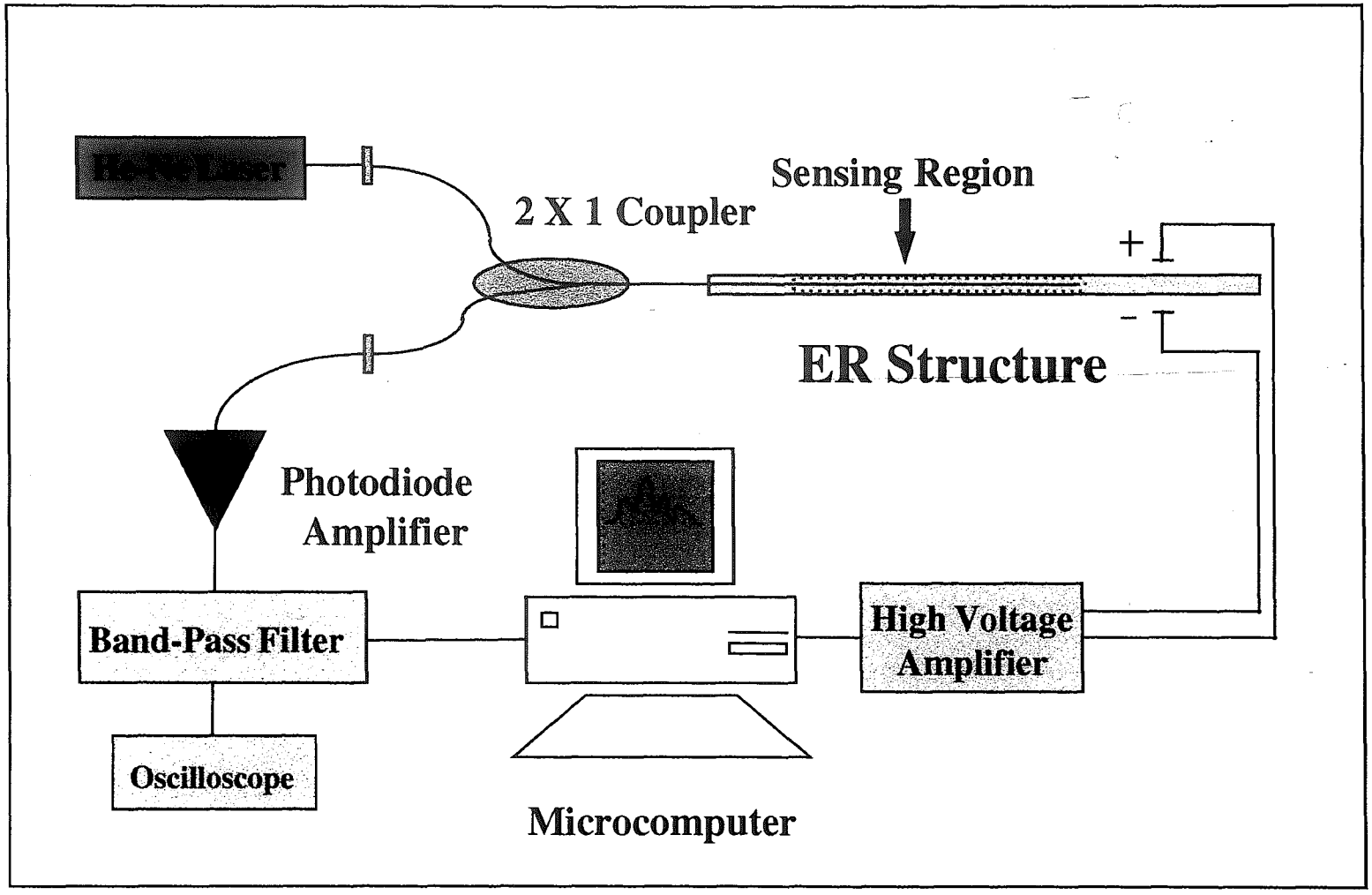

Figure 3.5. Typical Experimental Set-Up for Fabry-Perot Fiber Optic Strain and Vibration Sensing

As can be seen from **Figure 3.5**, the ends of the fiber coupler are mirrored in order to reflect a portion of the light signal back towards the coupler. Within the coupler, the light beam is split and transmitted along the lengths of the coupler, eventually reaching the photodiode. In order to produce this mirroring, one leg of the fiber optic coupler was spliced and examined to ensure that it had a satisfactory end finish. Once the finish was determined to be sufficient, aluminum was evaporated onto the end of the fiber, until the thickness of the coating permitted approximately 60% of the light to be transmitted. This would prove to be one of the most crucial variables which affected the performance of the sensor. A coating too thick would not allow enough light into the measuring cavity, resulting in only the reference signal being reflected back to the photodiodes. A deposition too thin would result in a weak reference signal, and thus the only signal that would be measured is the signal entering the cavity. As suitable equipment for measuring the thickness of the coating was unavailable, the trial-and-error method was used to determine the evaporating conditions which would provide suitable results.

In order to prepare the fully mirrored ends of the measuring cavity that would be used to reflect the signal back into the length of fiber from the fiber optic coupler, short lengths of fiber were cleaved, cleaned and prepared for mirroring. Using a fixture made to position the fibers vertically, several short lengths of fibers were prepared for mirroring. This fixture was placed in the evaporator and aluminum was mirrored onto the ends of the fibers. The evaporation time was approximately 45 seconds to ensure full

mirroring of the ends of the fibers. To further judge the reflectivity of the fibers, and to have a record for each sensor which was made, a glass slide was placed inside the evaporating chamber for every evaporation procedure.

In order to present a reasonable measuring cavity, hollow glass tubing was purchased that had an inside diameter of 155 μm. This tubing was purchased because of the apparent ease of modifying it for use as a sensing cavity, and the fact that the cost per sensor of the tubing was less than $0.50. To prepare the cavity, a length slightly less than 2 cm was cut from the spool of capillary tubing and cleaned. It is worth noting that all elements of the tubing and the fibers after cleaning were handled with forceps to minimize the build-up of skin oils on the optical elements of the sensor. The tubing was then placed under the microscope to ensure that it was cleaved cleanly and that it was not visibly damaged in any other way.

Once the evaporation process had been completed, and the ends of the fiber had been cleaved and cleaned to permit the maximum amount of light to be launched into, and transmitted out of, the ends of the fiber, assembly of the Fabry-Perot sensor could begin. Taking the partially mirrored end of the coupler, the capillary tubing was placed over the partially mirrored end. Carefully placing the two parts on the work surface under the microscope, a discarded piece of fiber optic cable was used to apply the cyanoacrylate-based adhesive to the two pieces. Capillary action was observed under the microscope to draw in the adhesive toward the partially mirrored end of the fiber, and the

fiber was adjusted if necessary to prevent the adhesive from covering over the partially mirrored end of the fiber. After sufficient setting time, a fully mirrored end was placed into the other end of the capillary tube, and bonded in similar fashion. It was critical to measure the sensing gap as precisely as possible, as light losses due to conical dispersion, shown in **Figure 3.6,** reduce the effectiveness of the sensor. It was also very important at this stage to apply the correct amount of adhesive to prevent fouling of the fiber end with adhesive, and to maintain the sensing gap. A smaller sensing gap resulted in a stronger reflected signal from the measuring cavity, thus higher frequencies could be measured.

After the ends were prepared and the sensor had been fabricated, and the adhesive allowed to cure, the sensor was attached to the structure. The sensor was attached using the same adhesive used to fabricate the sensor itself, and the laser was aligned with the lead-in length of the fiber optic cable. The lead-out length of the cable was aligned with the photodiode, and some calibration tests were made to ensure that the sensor was operating. At this point the sensor is ready for vibration and strain measurement. In the scope of this experiment, it was necessary to develop a sensor that was robust and self-contained, that could be attached in a number of locations on a smart structure, and that would make efficient use of the light launched into the fiber. During the course of the project, several variations on the previously described Fabry-Perot fabrication technique have been made. A new method of software processing was evaluated incorporating spectral processing techniques, which will be discussed in Chapter 4.

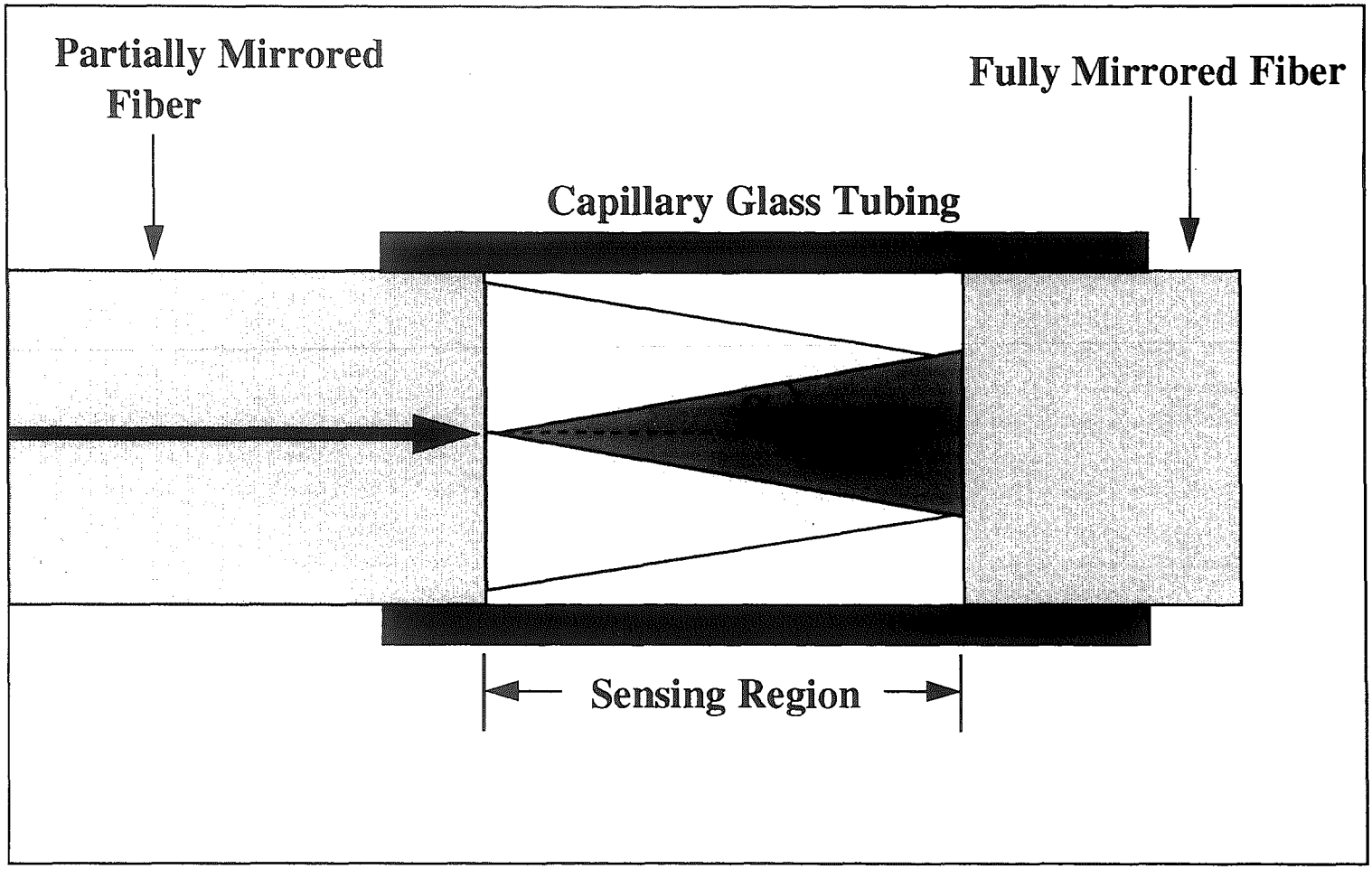

Figure 3.6. Conical Dispersion Effect as Light Exits and Re-Enters a Fiber Optic Cable. α is the conical dispersion angle.

Chapter Four

Advanced Fiber Optic Techniques

With the advent of fiber optic measurement and sensing schemes capable of making simple strain measurements, it has become desirable to integrate the fiber optic sensors with the available programming codes to produce an autonomous sensing capability with a very high degree of sensitivity. Additionally, it has also become necessary, in order to increase the use of fiber optic systems for measurement, that any sensing system be generic enough that it may be easily adapted to a host of sensing situations. Such sensing situations might entail the strain measurement of a rocket case on ignition, strain measurement of various bridge structures, or pressure vessel measurement.

The work of several scientists at SVET Ltd. in Russia can be cited as being one of the major innovations in the field of fiber optic displacement measurement. SVET, Ltd. is a private research concern in Moscow which, working closely with the University of Moscow, has been attempting to commercialize various fiber optic sensor configurations. SVET has developed a rather unique signal processing technique for white light interferometric measurement and has recently offered their first commercial product. This product is a complete fiber optic measuring system and processing algorithm incorporating the broadband illuminating light source, optical connectors, and necessary hardware. The signal processing algorithm is capable of displaying the strain from the

sensor in real-time, and which allows the user to alter the parameters of the sensor in-situ. The response time of this system is said to be 100 ms using a 486/66 IBM personal computer (SVET, 1995).

In the fall of 1995, two scientists from SVET visited Lehigh University, and the author was able to observe their methods. These two scientists were able to share their experiences with extrinsic Fabry-Perot sensors and contributed new methods to fiber processing techniques subsequently used during this investigation. The principles of white light interferometry will be discussed in the next section as an advanced method for strain measurement. Additional development will be given to the potential application of the technique in sensing of smart structures. In conventional structures, where control of the structure might not necessarily be possible, the advanced sensing systems could be implemented to perform warning and other sensory tasks of vital importance.

4.1 White Light Interferometry-An Introduction

White-light interferometry operates on the principle of illuminating the sensing region, in this case an interferometric sensor, with a broadband light source, to introduce numerous discrete frequencies for strain measurement. In theory, this technique permits the experimenter to obtain the output interference pattern and intensity, I_p, over the entire spectral range of the light source. If it is not possible to measure the intensity as it is distributed over the entire range of the signal, it is desired to measure over at least several

distinct frequencies . Using the method of white light interferometry, one can extend the range of unambiguous strain measurements when compared to a conventional strain measurement using a single wavelength fiber optic sensor.

Several techniques for the use of white light interferometry can be implemented. Initially, two or more distinct wavelengths can be introduced into an interferometer. In the most basic layout these two distinct wavelengths can be supplied by two lasers, provided that there is a useful difference between the wavelengths of the two lasers. A red and a green He-Ne laser could be used, for example, to approximate the two distinct wavelengths of light. Experimental issues sometimes make the introduction of these two light sources a challenge. Such a set-up using two light sources must utilize more optical connectors and beam splitters, which has the adverse effect of reducing the power which ultimately reaches the sensing region, and the power that is reflected back to the photodetectors as well. When trying to implement such a set-up it is important that the experimenter carefully optimize the optical set-up, in terms of fiber preparation and alignment, in order to ensure that the maximum light is available for signal processing.

A more practical solution to the problem of introducing many wavelengths of light into a fiber is the use of a light emitting diode which has a broad bandwidth, thereby introducing several wavelengths into the system at one point and reducing the number of optical connectors and beam splitters that are required. These broadband LED's are commercially available and have been utilized by several experimenters for various

purposes in the past. The SVET group has also successfully experimented with an LED operating at a nominal wavelength of 850 nm and a bandwidth of 30 nm in their White Light Interferometry and Spectral Processing experiments. The methods of the scientists at SVET are presented in this Chapter, as these methods represent a great potential for interferometric sensors. Additionally, other more advanced methods of fiber optic strain measurement are also presented here.

4.2 White Light Interferometry-Discussion and Experimental Application

As has been discussed in Chapter Three, interferometric fiber optic sensors rely on the intensity of the reflected light and the rate of change of that reflected light to determine the change in distance, or the optical path difference, and the frequency of vibration for that measurand. For clarification, the optical path difference and the sensing gap are one and the same. The intensity of the reflected light from the sensing region, the region which is undergoing the strain applied to the structure, is measured by a photodiode to which the lead-out length of the fiber is attached. The intensity of the light striking the photodiode gives rise to an electrical potential across the photodiode, and this voltage signal is either being interpreted by a conventional oscilloscope or input into a PC-based multimeter for analysis. Typically these two measuring devices perform the same function, that is the task of signal analysis to determine the frequency of the vibration of the signal, and thus the frequency at which the structure is vibrating. The

PC-based measuring programs offer greater charting capabilities, and the ability to automatically record and update the data according to the user's preferences.

A white light interferometer relies on these same principles of measuring the intensity of light reflecting back to a photodiode. However, the wavelengths of light which are analyzed are much broader than the single wavelength measurement schemes typically used. By using more than one distinct wavelength of light for measurement, the range of measurements can be increased, becoming limited only by the bandwidth of the illuminating light source. With a single light source, it is necessary to count fringes or use automated quadrature point detection to determine the number of times that the two waves of light have shifted more than one half of a wavelength. In order to reduce complexity in the hardware and software, the methods of quadrature point detection and the bulky and expensive equipment which go along with that method are replaced by several wavelengths of light. By increasing the effective wavelength of the illuminating light source, one can increase the potential range of strain measurements without resorting to methods of quadrature point detection.

4.3 The SVET Method of White Light Interferometry

The method developed by SVET utilizes a CCD array of photodiodes to measure the intensity of the signal over a significant range of bandwidth. Using the CCD array it is possible to measure the intensity of light, after the light has reflected from the grating

spectrometer. This grating spectrometer separates the light into a distributed pattern from which the intensity over several wavelengths in the spectrum can be analyzed. The CCD array is then linked to a PC-based computer, and the signal is analyzed using the proprietary SVET software. A schematic arrangement of this measuring system appears in **Figure 4.1.**

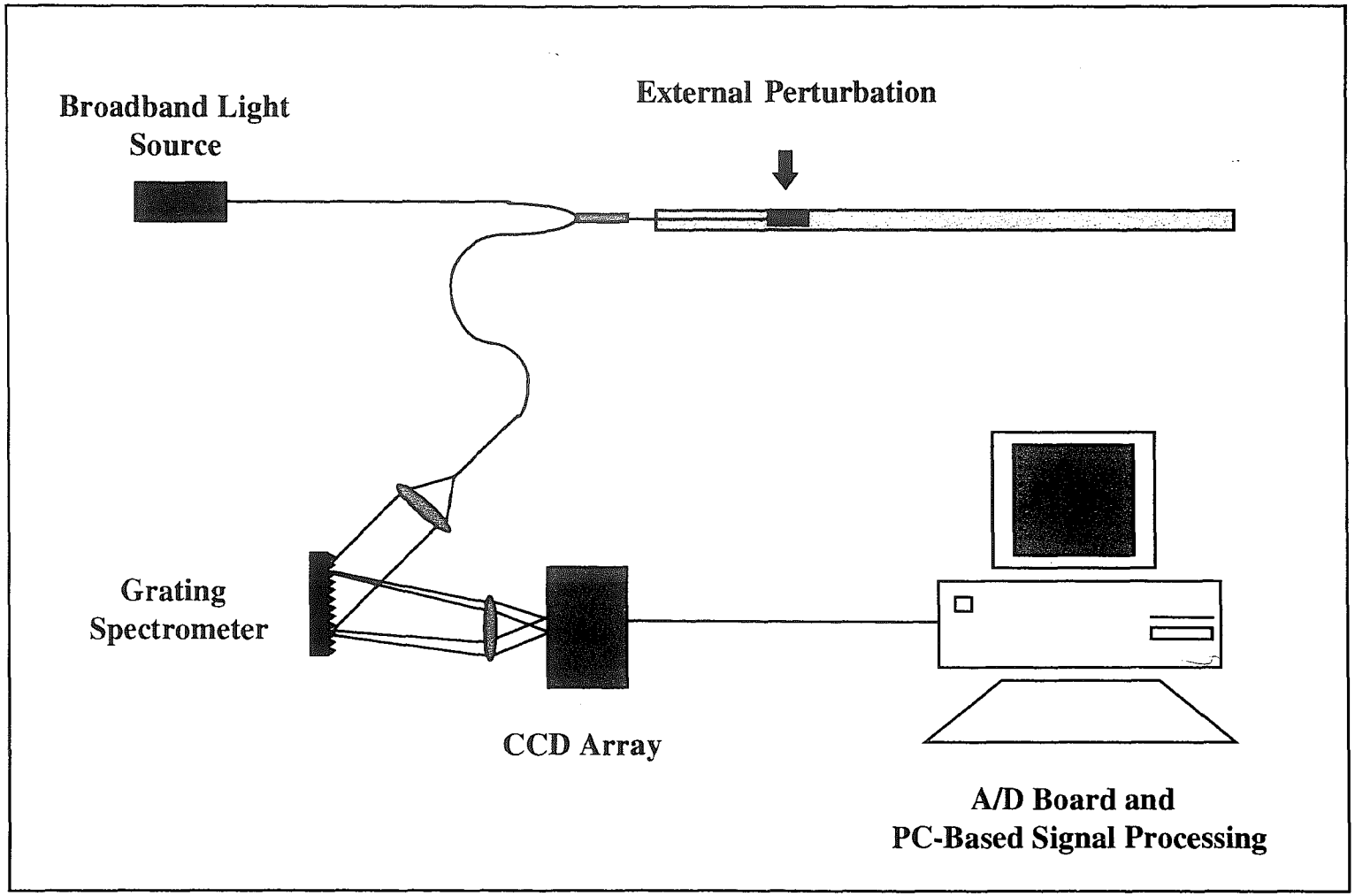

Figure 4.1. Experimental Set-Up for White Light Interferometer Using SVET Techniques

The scheme of the SVET white light interferometer and spectral signal processing method requires the illumination of the sensed region with a broadband light source, in this case a light emitting diode (LED). It utilizes a spectrometer and a CCD array photodetector to detect the distribution of the interferometer's output. It also utilizes a computer for signal processing. When using a Fabry-Perot interferometer, the spectral domain has a cosine transfer function

$$F(\nu) = S(\nu)\,[1+m\cos(\phi(\nu))] \tag{4.1}$$

$S(\nu)$ is the spectral distribution of the LED, m is the visibility of the interference pattern, $\phi(\nu)$ is equal to $2*\pi*D/c$. D, as discussed previously, is the optical path difference, c is the speed of light, and ν is the optical frequency. The challenge is to recover the phase ϕ not only for a selected frequency but as a function of the frequency ν. By inverting the cosine transfer function, SVET scientists have obtained the relation

$$\phi(\nu) = \cos^{-1}[(F(\nu)/S(\nu) - 1) / m] \tag{4.2}$$

In practice however it is often impractical to measure the visibility, m, and the spectral distribution $S(\nu)$. An alternative method to using the signal processing technique that has been developed in response to these problems is the use of an analytical signal

corresponding to the second term in the $F(v)$ expression with the module $S(v)$ and phase $\phi(v)$. This analytical term becomes

$$f(v) = S(v)\exp(i2\pi vD/c) \tag{4.3}$$

In order to obtain the relationship between the phase of the signal and the frequency, it is necessary to perform a Fourier transformation to obtain a function containing the zero harmonic which corresponds to the constant term in the first equation, $F(v)$. This new function also consists of several first harmonics corresponding to the oscillating harmonic. This function is equal to

$$G(x) = \int_{-\infty}^{\infty} S(v)[1 + m\cos(2\pi vD / c)]\exp(-i2\pi vx / c)dx \tag{4.4}$$

From $G(x)$ using the first harmonics the relation for $\phi(v)$ can be obtained. If one is to assume that the initial path imbalance of the sensing interferometer and the spectral bandwidth of the light provide adequate separation between the zeroeth and first harmonic of $G(x)$, the zeroeth harmonic can be subtracted from $G(x)$ to obtain $g(x)$ which corresponds to the oscillating term from the first equation, $F(v)$. Thus,

$$g(x) = \int_{-\infty}^{\infty} S(v)[m\cos(2\pi vD / c)]\exp(-i2\pi vx / c)dx \tag{4.5}$$

After performing the inverse Fourier transformation, $f(v)$ is obtained as

$$f(v) = \int_0^\infty g(x) \bullet \exp(i2\pi vx / c)dx \qquad (4.6)$$

The argument of the complex function $f(v)$ provides the required relation between ϕ and v and the first derivative of ϕ with respect to v provides the absolute value of the optical path difference. From the absolute value of the optical path difference, provided the initial value of the optical path difference is known, the absolute strain of the system can be determined.

The procedure of constructing the function $f(v)$ from the initial signal makes it possible to eliminate the influence of parasitic interferometers, such as those which appear in most optical connectors, and which introduce some error into a typical interferometric signal. Provided the optical path difference of the sensing interferometer is different than the optical path difference of the parasitic interferometer, the Fourier image of the parasite can be subtracted from $\boldsymbol{G(x)}$ if it is localized apart from $\boldsymbol{g(x)}$. All of these features of the SVET method of interferometric measurement and signal processing make the construction of a reliable, extremely precise measuring device possible. After the device has been calibrated once, it does not require further re-calibration, even after being turned off and on. Finally, and importantly, the method is isolated from the spectral and power fluctuations of the broadband light source.

A simpler realization of this scheme, and a less expensive one, is shown in **Figure 4.2.** This configuration uses a broadband light source for illumination of the sensing region, and utilizes two separate wavelengths of light for strain measurement and construction of the interference pattern. Using light emitting diodes (LED's) with a central frequency of 850 nm and a bandwidth of 30 nm, light is launched into the fiber and then is split at the optical coupler. This configuration also uses the grating spectrometer, but avoids the cost associated with the CCD array. In place of this array, two photodetectors, selected for their performance in this wavelength of light, are placed such that the light from the grating spectrometer is reflected onto these photodetectors, in this case simple photodiodes. These photodiodes are connected to the amplification circuitry and can then be interfaced with the PC through an A/D converter.

In this investigation, the primary goal was to measure the frequency of vibration, and of secondary consideration was the magnitude of the amplitude of vibration. That is to say that the measurement of the rate of change of the optical path difference, or the sensing gap, was our concern, not necessarily the absolute value of the optical path difference.

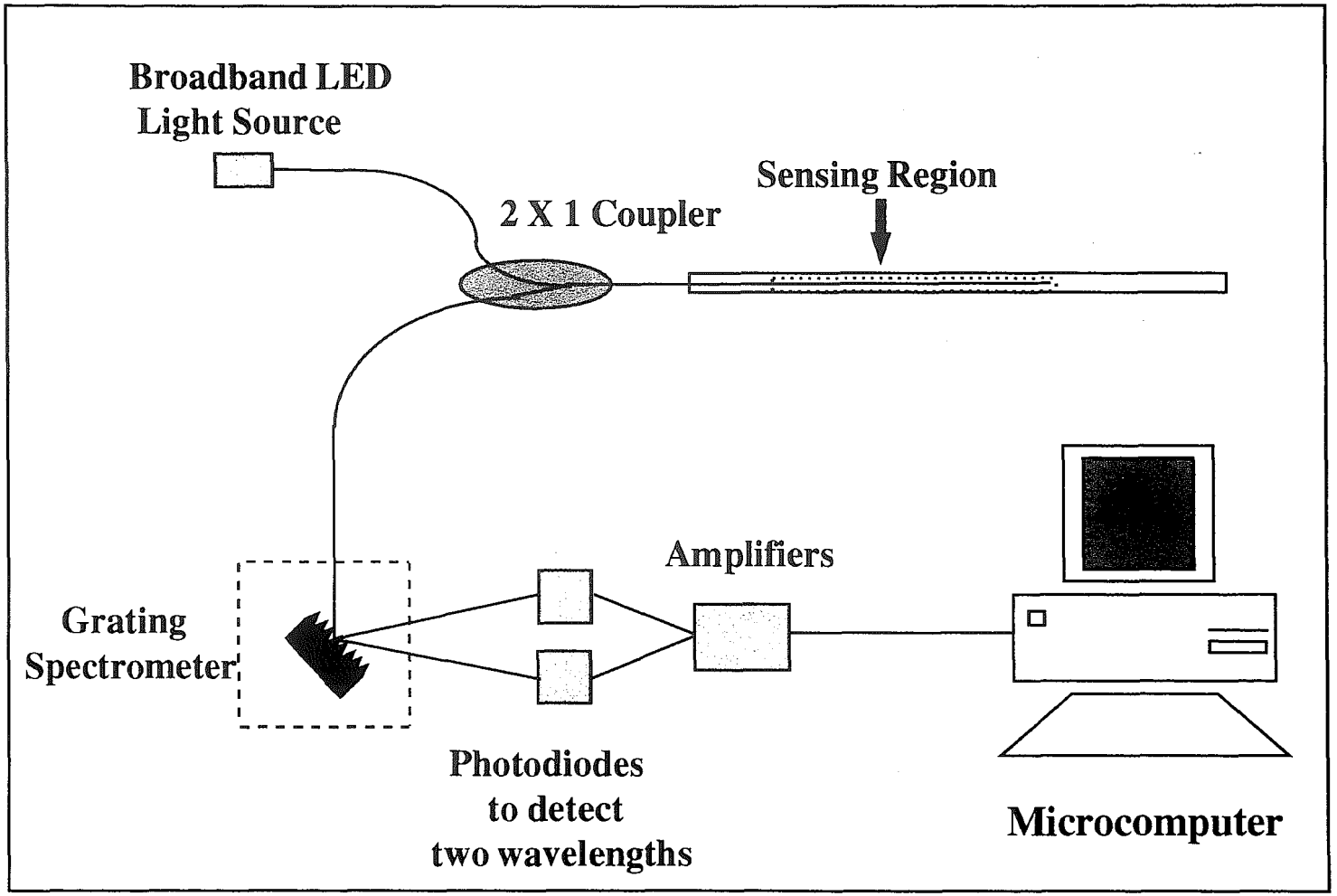

Figure 4.2. White Light Interferometer Set-Up Using Two Photodiodes Rather than A CCD Array

4.4 Bragg Grating Fiber Optic Sensors

Bragg grating sensors are relatively new developments in the field of fiber optic strain measurement. Simply put, they rely on the reflection of the light signal from several points along the fiber. From the change in these reflections, or the reflective signature of the sensor, the strains which are induced in the sensor can be determined. A schematic of a simple Bragg sensor is shown in **Figure 4.3.** The method which is applied to this type of signal analysis is often referred to as Optical Time Domain Reflectometry, or OTDR (Claus, 1993).

As has been mentioned, these sensors operate by introducing a change in the refractive index of the transmitting fiber optic cable. The introduction of this change in refractive index results in a coupling of the forward and backward propagating electromagnetic waves providing that the electromagnetic field obeys the Bragg condition, all of the optical power will be coupled into the backward propagating wave. That is, all of the energy will be entirely reflected. The most common form of the Bragg condition is given by

$$2n\Lambda = \lambda_b \qquad (4.7)$$

Where Λ is the pitch of the periodic index perturbation, n is the at-rest refractive index of the fiber, λ_b is the Bragg wavelength (Sirkis, 1993).

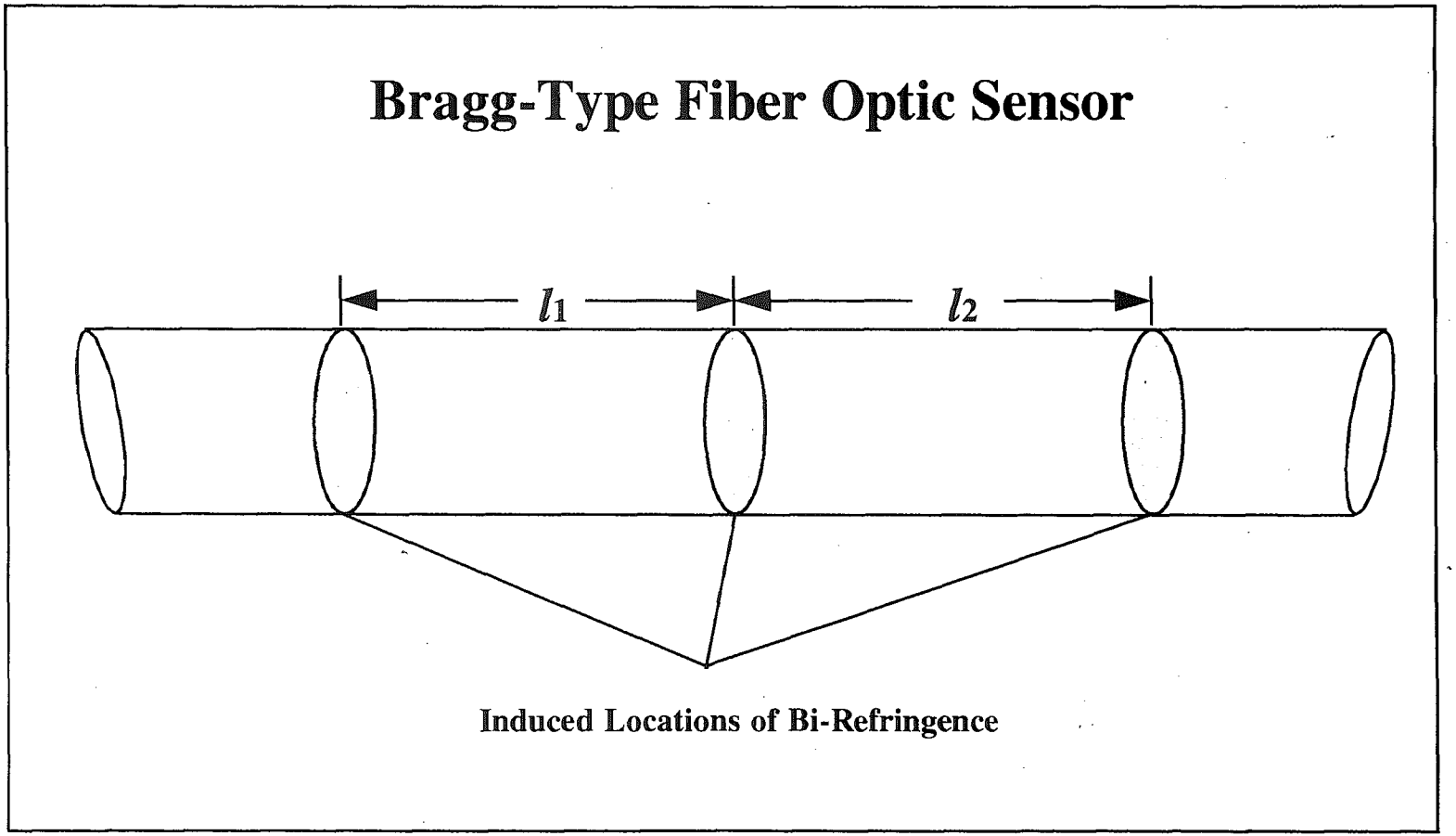

Figure 4.3. Bragg Grating-Type Sensor with Regions of Induced Bi-Refringence to Measure Strain.

Like white light interferometry, a Bragg grating sensor relies on the introduction of a broadband light source into the fiber. The reflected wavelength spectrum can be monitored on its centerline or the perturbation in the transmitted wavelength spectrum can be monitored. In order to simplify the modeling and analysis of the Bragg grating sensor, the model of a low finesse Fabry- Perot interferometer is often introduced. A Bragg sensor of this type can utilize hi-birefringence (hi-bi) fibers which have had the Bragg pitch impressed upon them, that is regions of stress have been induced in the fiber during manufacture, or it can use single mode fibers which have undergone similar modification. This modification results in a stress induced bi-refringence which produces a pair of possible reflected waves. The constructive interference of these waves can be monitored and the induced changes in the Bragg sensor due to loading can be determined.

4.5 Conventional Applications of Advanced Fiber Optic Techniques

As we have discussed, the advanced techniques for fiber optic strain measurement and frequency sensing have permitted researchers to determine more precisely certain operating parameters which are important to the operation of a component or system. Bragg grating sensors have been used to perform non-destructive evaluation on composite panels, and have been used to monitor the service lifetime of composite parts in critical applications, for example aircraft structures. High temperature sapphire fibers have been developed for use in applications where temperatures approach 1200°C, and have been

implemented in metal matrix composite structures, MMC's, to measure the loading and strain states (Claus, 1993).

By incorporating multiplexed sensors in a sensor array, the potential for fiber optic sensors to monitor critical variables at numerous locations can be realized. Simply put, a multiplexed signal minimizes the number of optical connectors in the system. It also permits the use of the minimum number of light sources and photodetectors. A multiplexed array is shown in **Figure 4.4.** Though the advantages of this arrangement are its simplicity and minimum number of components and cost, the reliability of the system must be considered to be less than that of a conventional system with an equivalent number of sensors. This is due to the fact that a single failure in any of the components of the system result in a complete failure of that system. Therefore, it can be said that the components selected for such an array must be of the highest quality and reliability, and that the location and installation of the multiplexed network must be carefully considered to ensure this reliability.

4.6 White Light Interferometry for Smart Structures

This investigation was primarily concerned with the behavior and sensing of smart structures, and it is believed that white light interferometry for future work will be valuable. As we have mentioned, there are distinct advantages to using white light interferometry for strain measurement. The potential to measure significantly larger

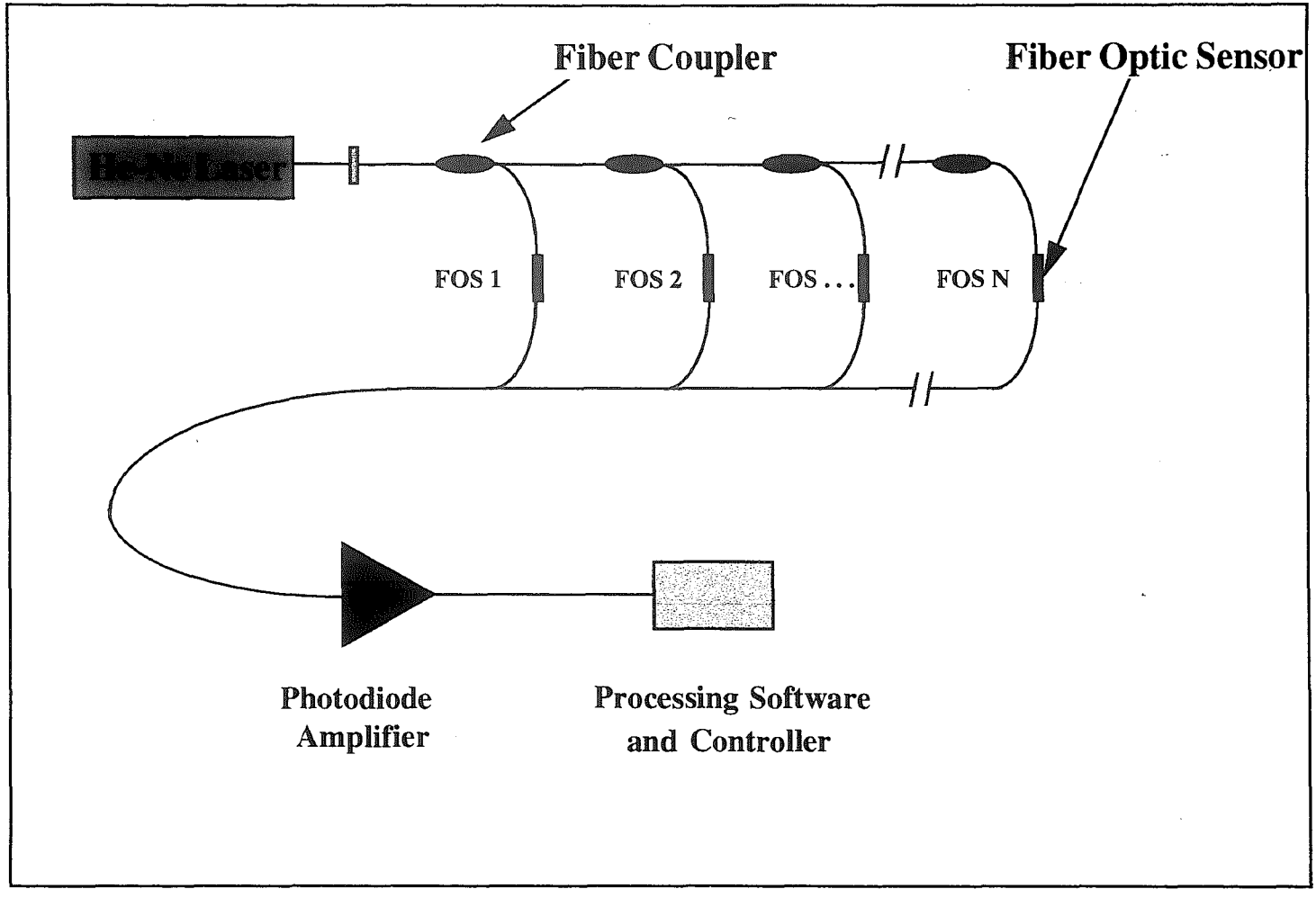

Figure 4.4. Multiplexed array of Fiber Optic Sensors

strains occurring in the material is but one. The fact that the signal from the interferometer can be interpreted, and the results are invariant, without regards to the fluctuations in the spectral bandwidth or the output power of the device are another. The ease with which the signal from the interferometer can be interfaced with the controller, and the user-friendly nature of the available software, all point to fiber optic white light interferometry as the next step in a logical progression to measure more accurately, and more reliably, the strains and frequencies of vibration in intelligent structures.

Because the system can be integrated into a self-contained unit that is able to control a smart structure, the potential incorporation of a white-light interferometric strain sensor into a smart structure's design, utilizing a neural network controller or other "intelligent" controller to optimize the control outputs, represents a significant step towards a feasible control scheme. The conventional neural network controller capable of taking into account the information from the structure, making a "decision" with regards to the optimum output signals that should be sent to the structure, and then sending that signal to the voltage field amplifier has shown in this investigation to be effective in controlling the vibration of the structure.

During portions of the present investigation, the control of the smart structure was treated in a manual fashion. That is, the PC-based control algorithm took as its inputs the frequency of vibration from the fiber optic sensor. It also took the magnitude of the voltage change from the photodiode and converted it to a normalized change in voltage.

Using this normalized voltage and using the frequency obtained through a Fourier transform, the controller would output to the screen the voltage field that should be applied to the smart structure, and this field would be applied by the experimenter manually. Further discussion of the experimental methods, and a description of the potential controllers for smart structures, as well as a discussion of the controller used for this experiment, follow in Chapter Five.

Chapter Five

Lengthwise and Pointwise Fiber Optic Sensors for ER Smart Structures

During the present investigation several types of fiber optic devices were investigated for use as strain and vibration sensors. Though the ultimate result of the work was an extrinsic Fabry-Perot sensor, several other types of fiber optic sensors were evaluated for the purposes of measuring the frequency of vibration, as well as the absolute strain experienced by a smart structure. With these various iterations of sensor types, strain was measured both integrated along the length of the structure, as well as at specified point locations. The sensor types studied included several configurations of polarimetric fibers, embedded within the smart structure and also externally attached, as well as other types of interferometers.

The work of Han et al. (1995) focused on the initial use of Michelson and Mach-Zehnder type interferometers for use in smart structure sensing. These interferometers were found to have very poor levels of reliability and were difficult to use. When applied to the surface externally, they proved susceptible to damage from improper handling, with the mirrored ends of the fibers being exposed. The first truly successful sensors which were interfaced with the neural network controller were of the polarimetric type. A thorough description of the experimental apparatus is presented in this section, followed by a more detailed examination of all of the fiber optic sensors used during the present

investigation. Developmental issues and the complications which arose during testing are also presented in this chapter.

5.1 Experimental Apparatus and Set-Up

As mentioned previously, the principal focus of the investigation was on smart structures which utilized electrorheological materials to effect adaptive control of overall structural mechanical properties. These smart structures were analyzed both experimentally as well as analytically, and the results were compared. For simplicity of construction of the experimental prototypes, these smart structures were modeled as flat beams and plates, in order to facilitate construction and testing. A simple schematic of these plate and beam structures appears in **Figures 5.1 and 5.2.**

During the investigation and development of fiber optic strain sensors, all experimentation was carried out with electrorheological material-filled composite beams, rather than the ER plates. This was simply due to economic considerations, as the composite beams could be fabricated for less than $10, excluding fluid costs, while the plate structures required processing at an outside laboratory, and the assistance of an electrical technician. Thus, all developmental sensing work was done on beams, and over the course of the investigation approximately 20 beams were fabricated for testing polarimetric and interferometric sensors.

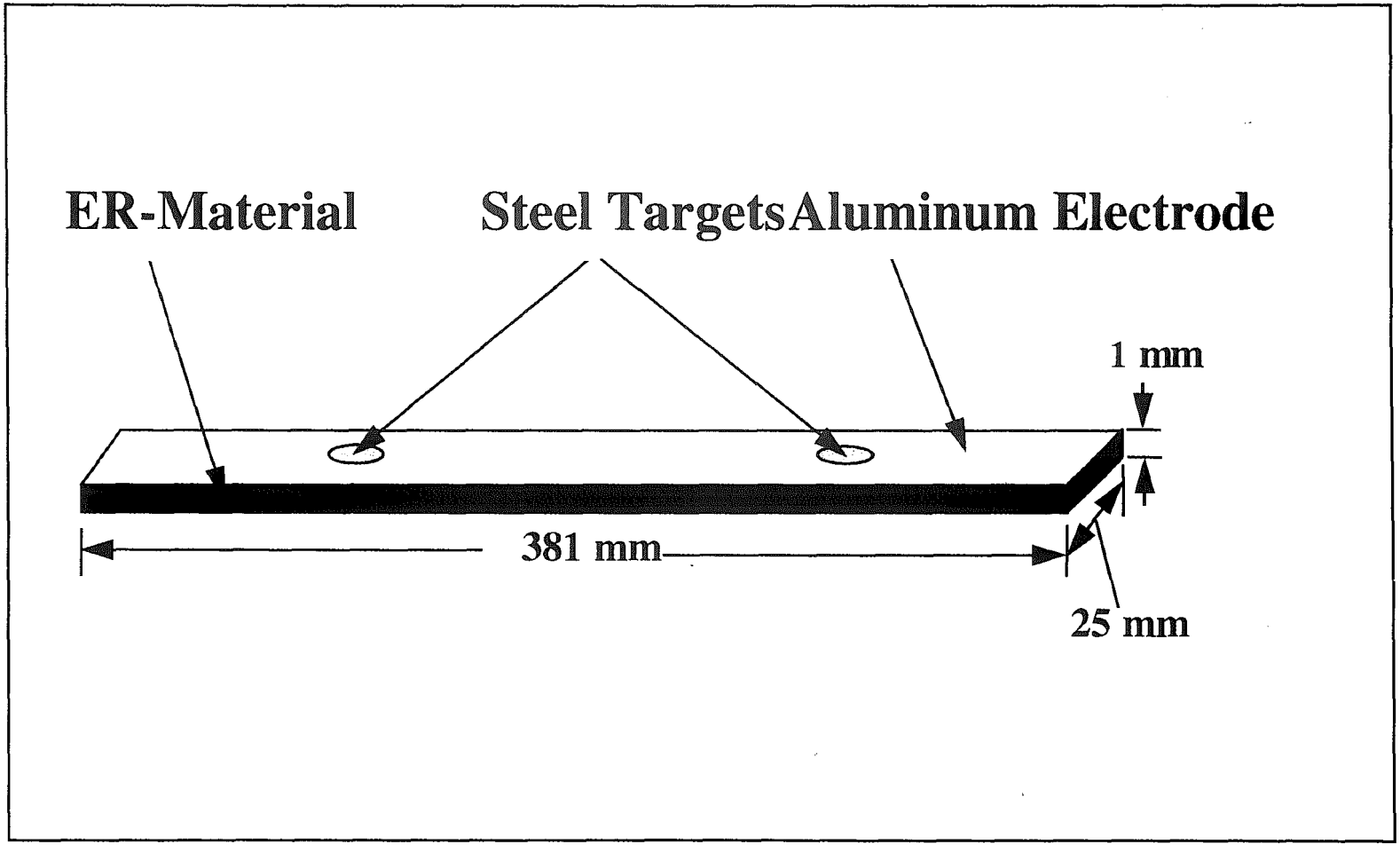

Figure 5.1. Composite ER-Filled Beams Used For Testing

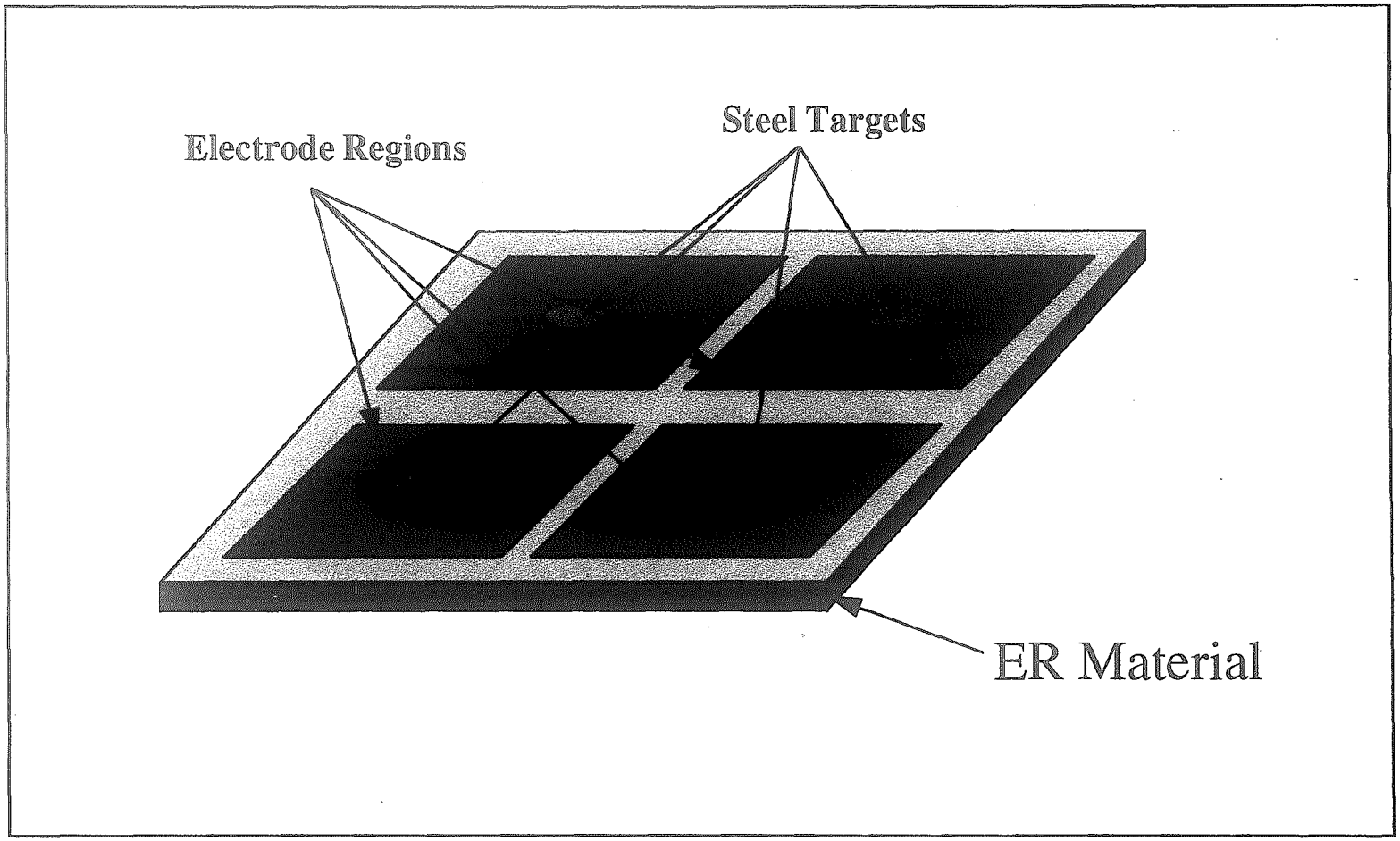

Figure 5.2. Schematic of ER-Fluid filled plates used for testing.

The beams were constructed of 6061-T6 aluminum beam sections, approximately 1 mm in thickness, 25 mm wide, and 381 mm in length. These two sections were separated along the edges by an elastomeric membrane layer. This elastomeric layer was either 1 mm in thickness or 0.5 mm in thickness. This elastomeric layer was attached to the thin beam sections using Ashland Oil's Pliobond elastomeric adhesive. The Pliobond proved the most effective method of sealing the edges of the beam, as its strength in shear did not restrict the motion of the plates, and it proved an effective method of attaching the elastomeric layer to the beams of aluminum. Concern arose about the properties of the elastomeric layer, that it might contribute to the stiffness of the beam and artificially high stiffnesses would be obtained. True, it must contribute to the stiffness of the beams, however, its contribution will generally be the same from beam to beam. Thus, the qualitative results from one experiment could be qualitatively applied to another.

Prior to bonding, the elastomeric layer was cut in two pieces, to form a frame around the edges of the beam, and all surfaces of the aluminum plates, which would serve as the electrodes, were cleaned of contaminants. The frame shape eliminated the past problems with sealing the beams at the junctions of the elastomeric layers, for example at a corner joint. Additionally, at areas which would present pockets for air to be trapped during filling, the corners were mitered to form a 45 degree angle between the edges of the material. The elastomeric layer was bonded to the surface of one beam, using pressure to ensure an adequate bond, and allowed to cure. After curing, excess Pliobond was removed from the interior surfaces of the beam, to maximize the electrode area and

increase the potential controllable range of the structure. The beams were then aligned, and with adhesive applied to the remaining exposed surface of the elastomer, were pressed together. At this stage, it is very important to note that excess adhesive would not be removable, and would reduce the effective electrode area of the beam. Thus, the adhesive was applied in a thin film using a small spreading edge. This ensured that the maximum electrode area could be attained. Also, while bonding at this stage, pins or blanking plates were inserted into the region which would serve as the fill and vent ports for the beam. These ensured that no blockage of these ports would take place. Again, if blockage took place, the only choice the experimenter would have is to forcibly re-open the ports, and any debris which was blocking the ports would be lodged inside the beam, reducing the electrode area or having other adverse effects.

After the adhesive had sufficiently cured, the tubing pieces which would serve as the transfer tube and the vent tube were applied to the structure. These tubes were attached at the fill and vent ports, respectively, and were simple fabrications of polyurethane tubing. These tubes were attached to the beams using CopperBond adhesive produced the by the Noble Corporation, as the tubes were subject to more stress and had less surface area for bonding than the joint between the elastomeric layer and the aluminum beam sections. Though this adhesive was more rigid than the adhesive used for bonding the aluminum and elastomeric layers together, it was considered that the location of the filling tubes, outside of the clamped area, would not present a significant contribution to the stiffness of the beam area being tested.

Just prior to bonding, the polyurethane tubing was heat-formed to a flat shape which followed the dimensions of the beams. This was done for two reasons; 1) To permit a greater surface area for the bond between the tubing and the adhesive, and 2) To reduce the amount of adhesive required for joining the two parts together, by eliminating the domed area which would form under the surfaces of the tubing had the tube not been deformed. Again, a blanking apparatus was inserted into the ports in order to prevent any adhesive from blocking those ports.

Once the adhesive for the filling and vent tubes had cured, steel targets 25 mm in diameter were attached to the surface of the beam to effect forced actuation of the structure. These steel targets were actuated by a non-contacting electromagnetic actuator initially. In later experiments the non-contacting actuator was replaced with a contacting actuator. This actuator was an MB Mini-Shaker Table. The motion of the shaker was coupled to the motion of the beam through a machined plastic union. Both the steel targets and the plastic union were attached using Pliobond adhesive. The leads for the electrodes were attached to the structure at this point as well, using GRAFO 223 colloidal graphite solution. This solution was used to ensure that adequate contact had been established between the electrodes and the leads from the amplifier.

Once the beam had been constructed, the electrorheological fluid was mixed and evacuated and prepared for injection into the beams. The fluid was shaken using a Miracle brand mechanical mixer, for approximately 20 to 30 minutes. After mixing, the

fluid was placed in an evacuation chamber and the chamber was sealed. For approximately 90 minutes a vacuum was drawn on the chamber to draw any air out of the fluid that might have been ingested during mixing. During this time, the beam was positioned vertically and clamped in order to fill the beam from the bottom to the top. This would eliminate the tendency for air to be trapped in the beam during filling. After having mixed and evacuated the fluid, the material was drawn into a syringe of appropriate capacity. This syringe was selected for its ability to mate with the polyurethane tubing attached to the beam.

Having attached the syringe to the tubing, the ER fluid was slowly injected into the beam. Care was taken to check for overfilling of the beam, as this would reduce the effective electrical field which would be applied to the beam due to swelling of the beam. Overfilling also would present a very real risk of beam bursting and fluid loss, particularly during an experiment. The potential loss of expensive fluid and time invested in fabricating a beam was to be avoided at all costs. Prior to filling, the volume of the fluid required for the beam was calculated to further minimize the risk of overfilling. During the final stage of filling, the fluid would appear in the vent tube, and this would signal that the experimenter should inject no more fluid into the beam. At this point the syringe was held in position, and the vent tube was clamped and filled with CopperBond to prevent any fluid leakage from the end of the beam. Once the CopperBond in the vent tube had solidified, the beam was turned upside-down and the fill port was again clamped. The syringe was then removed and filled with CopperBond. After the fill port

had been sealed, the beam was considered ready for application of the appropriate polarimetric or interferometric fiber optic sensor and testing.

The experimental set-up, including the attached fiber optic sensor, was then placed on the vibration-free table, and placed in machined clamps. The clamps were machined so as to permit a uniform clamping force to be applied to the beam. These clamps were such that the thickness of the elastomeric layer and the two aluminum plates was the gap between the clamps, less a 0.125 mm distance to ensure that the clamps were tight. The fiber optic cable was aligned with the laser and the photodiode. A Trek 609-C high-voltage amplifier was then connected to the beam leads. In order to obtain a reliable means for verifying the vibration of the beam, a proximity probe was placed above an actuation target which was not being used. The system was powered up and all systems were checked for operation in the nominal range. At this stage the fiber optic sensor was tested, either in polarimetric or interferometric configuration. The development of both the polarimetric fiber optic strain sensor, in integrating and pointwise configuration, as well as the interferometric sensor, is described in the following sections.

5.2 Polarimetric Strain and Vibration Sensors - An Integrated Approach

The primary objectives of the study were to develop a sensor which was capable of determining the frequency of vibration of a smart structure, to develop a sensor which was able to measure the localized strain of the structure, and to interface this sensor with

a controller capable of exploiting the controllable nature of the structures. The use of a polarimetric sensor for strain and vibration measurement was the first step towards achieving that goal, and through the use of the sensor in various experimental configurations, it was possible to adapt the polarimetric configuration to attain these goals.

The fiber optic sensor illustrated in **Figure 5.3** shows the configuration of the sensor as it was initially attached to the beams. **Figure 5.4** illustrates the arrangement of the polarizers and quarter wave plates as used in the polarimetric fiber optic sensor configuration. The high birefringence (hi-bi) fibers were bonded along the length of the beam, and the light was launched into the fiber through the polarizing and quarter wave plates. This separated the light into two modes, orthogonal to each other, traveling along the fiber's fast and slow axes. At the output end of the fiber, the signals were recombined through the same procedure, and targeted on the photodetector.

By analyzing the changing signal of the photodetector, it was possible to obtain the frequency of vibration and the strain within the structure. The sensing length of fiber was tested in two configurations, either bonded within the beam or bonded to the outside of the structure. Both configurations performed satisfactorily from a technical standpoint, and when comparing the signals from the sensor within the beam to the sensor bonded to the outside surface of the beam, there was no noticeable difference between the two

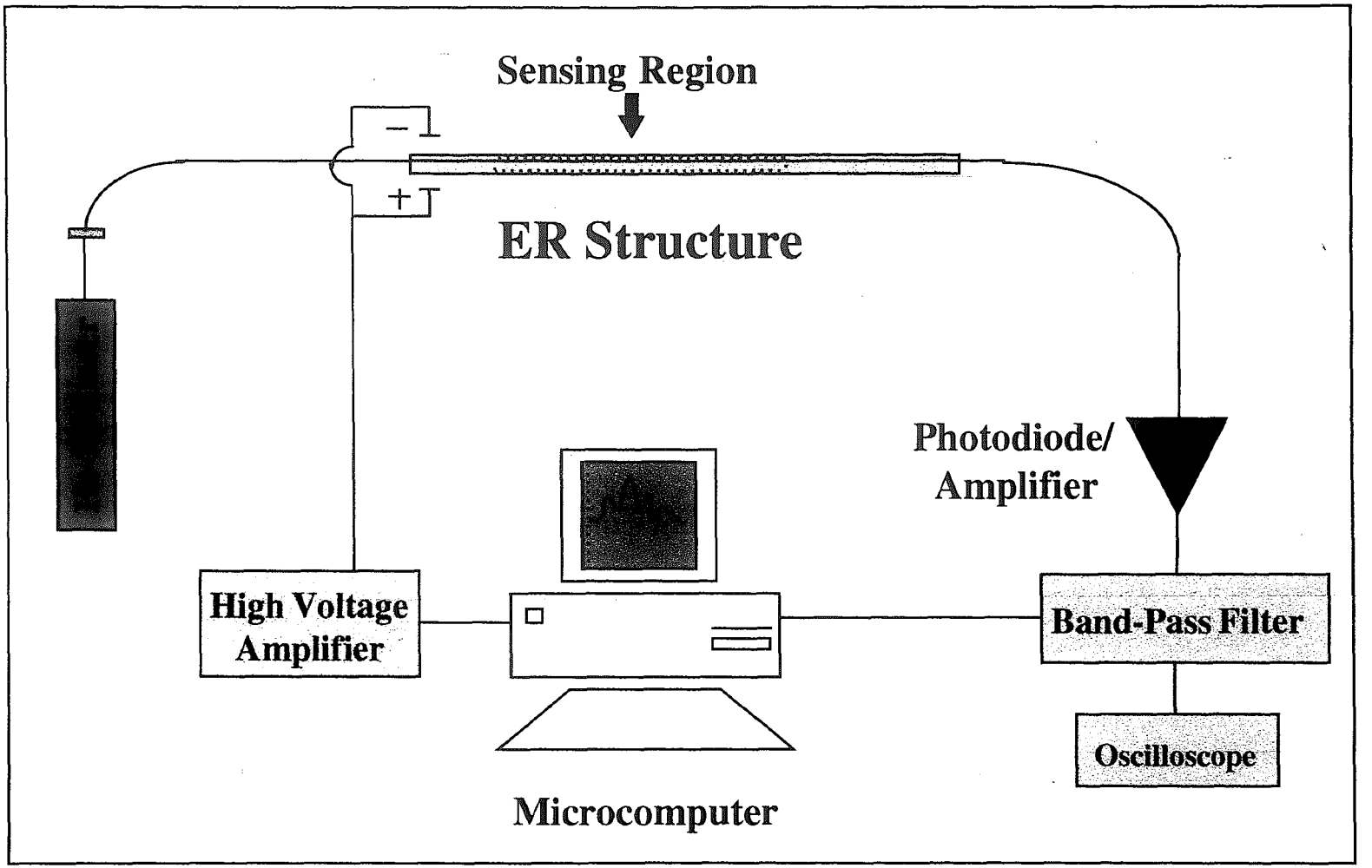

Figure 5.3. Lengthwise polarimetric fiber optic sensor

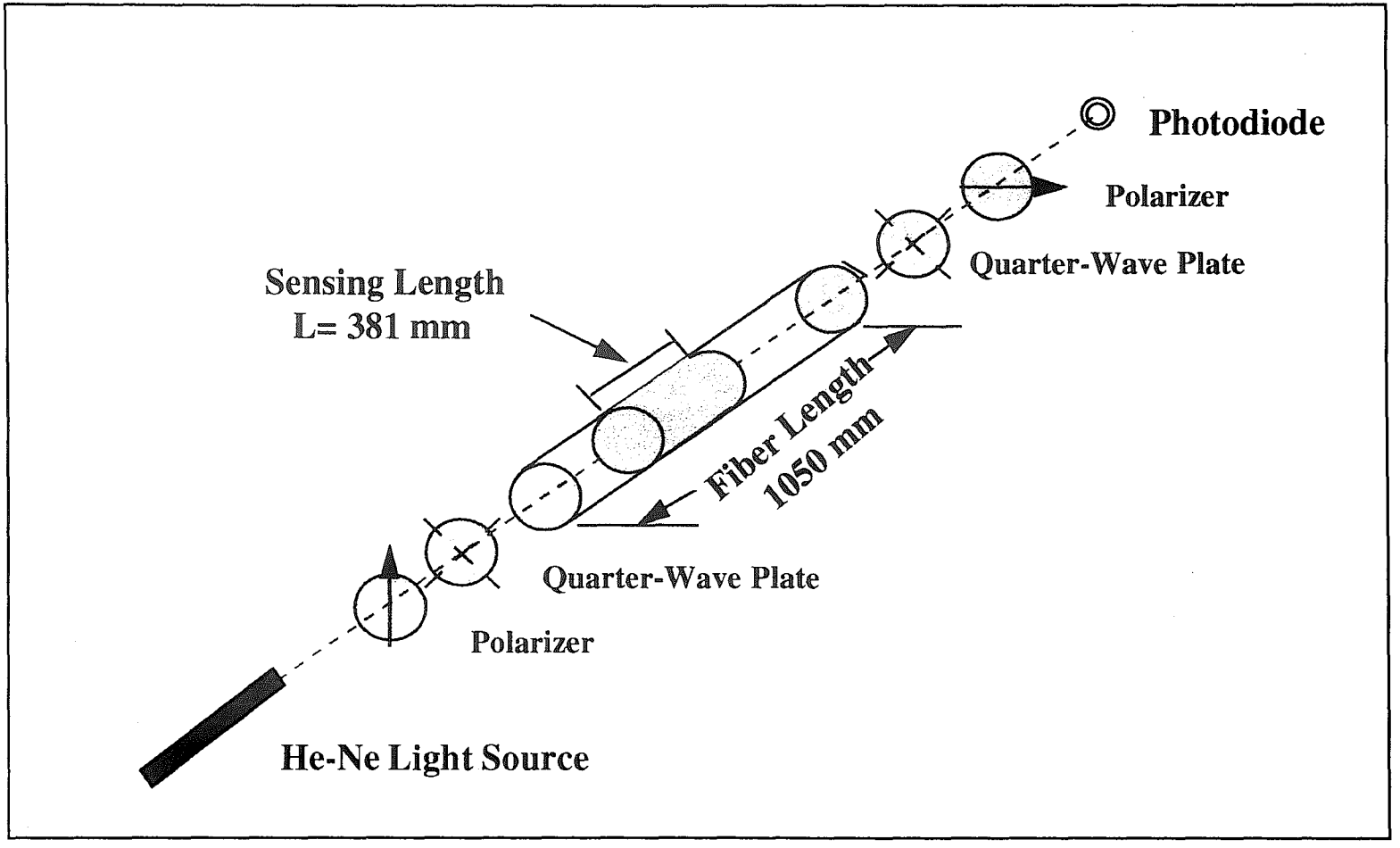

Figure 5.4. Layout of the Polarimetric Fiber Optic Vibration and Strain Sensor used in this Investigation

signals. However, the logistics of introducing the fiber into the beam, and drawing it out the other end of the beam, proved troublesome. Beams that were produced with fibers running inside the beams proved very unstable and leaked their ER-fluid contents readily. These beams gave inconsistent results from experiment to experiment. These inconsistent results can possibly be attributed to capillary action at the fiber entrance and exit points, exacerbated by the vibration of the beam effectively "pumping" fluid through whatever opening might have existed. This theory would also account for the increased tendency of these beams to arc, as a result of fluid aeration, more readily than their counterparts fabricated with externally applied fibers.

The attachment of the fiber along the length of the beam permitted an overall strain reading to be obtained from the sensing cavity. That is, the total strain occurring throughout the bonded length of fiber, as a result of the strain on the surface of the entire beam, was measured. This reading was considered to be analogous to the strain on the surface of the beam being tested, and that losses at the interface between the fiber and the beam are negligible. However, it becomes more difficult to determine the strain of the beam at a specified *point,* such as at a location 100 mm from the clamped end of the beam, using the lengthwise polarimetric sensor. Only through an extensive modeling effort, to determine the correlation between surface strains and modal shapes, could the value of strain at a point be extrapolated.

The work of Yalcintas attempted to model the behavior of these fluid composite beams, using various analytical methods. The thrust of the modeling effort was in the area of beam behavior prediction, based on a linear viscoelastic assumption for the shear behavior of the ER fluid. Using both fourth order and sixth order differential forms of beam equations, it was found that the resulting theory predicted the beam behavior well for low frequencies, while its performance compared to experiments at higher frequencies deteriorated. The work of Yalcintas led to the development of an expanded model for the prediction of adaptive beam and plate behavior(Yalcintas et al., 1994) This expanded model was developed for the forced flexural vibrations of simply supported beams, and was later modified to include clamped-clamped end conditions. From the model, the natural frequencies, mode shapes, structural loss factors, and transverse displacements could be determined as functions of the applied electrical field and excitation frequency.

In general, the model was able to predict trends in the data and the qualitative behavior of the beams that were tested. Problems arose, however, in that the inconsistent behavior of the beams was never able to exactly match the predicted quantitative behavior from the model. This is primarily due to two reasons, fluid rheology and beam construction techniques. The assumption in the model that the shear behavior of the electrorheological fluid is linear viscoelastic is a simplification for modeling purposes(Yalcintas, 1995). In fact, the shear behavior of the fluid is non-linear, and becomes nearly exponential at higher values of applied electric field. Additionally, when preparing the fluid for use in the composite beam, the exact ratio of carrier oil to

polarized particles could never be assured. During beam preparation the fluid was thoroughly mixed for an extended period of time. This mixing procedure introduced air bubbles into the fluid which needed to be removed from the fluid prior to beam assembly to eliminate fluid arcing within the device. The de-aeration procedure, typically encompassing one and a half to two hours, permitted adequate time for the fluid to settle, and for the carrier oil to particle ratio to become non-homogeneous.

It was believed that the reduction of the amount of air within the fluid was significantly more important than the problems that would be encountered due to an imperfect mixing of the particles and carrier oils. The thorough evacuation of the air within the beam ensured that several experimental runs could be performed on the beam, and that the beam would be able to sustain an electrical field and would not arc. In the event that the beam did arc, a new beam would be required, the construction and filling procedure repeated, and the experiments would be performed again. Conversely, if the fluid mixture was not uniform, a minor performance degradation was likely, but nothing worse was likely to occur. The beam would perform and would exhibit the same general tendencies when subjected to forced vibration and electrical fields, but the beam would be useful for several experimental sessions.

Thus, correlation of the data from the model has proven difficult, due to the nature of the fluids as well as the construction techniques that could be used for experimental beam fabrication. Though the model would be capable of providing the pointwise

displacement, by extrapolating the behavior of the beam from the lengthwise sensor, a sensor capable of making pointwise measurements, of both vibrational frequency and strain, would provide the same information without the potential ambiguity which might be introduced by the extrapolation of the data from the model. The information from this pointwise sensor would also be used to directly control the smart structure through the on-line controller. The ability to use actual experimental data, rather than extrapolated or predicted data, is most certainly the preferred method of control. This reduces the potential for error and allows accurate real-time monitoring of the structure.

Initially, the point-wise sensors were of the polarimetric type, fabricated from the same high-birefringence fibers that the lengthwise integrating sensors had utilized. However, later experiments, and the subject of this investigation, would focus on the use of interferometric sensors.

5.3 Polarimetric Strain and Vibration Sensors - Pointwise Approach

The method to fabricate a pointwise strain sensor using a polarimetric approach is not new; various techniques have been used to accomplish the task. Here, the technique of wrapping the length of fiber in a "bow-tie" shape was used. This method involves wrapping the fiber many times, in order to effectively create multiple "sensing lengths", and bonding this fabrication to the surface of the beam. This is necessary in order to obtain a significantly large phase shift at the photodetector. Too short a sensing length

effects very little change in light intensity at the photodiode, often the change is too small to be separated from signal noise even with complex electronics. Thus, the artificial method of introducing multiple sensing lengths, which results in a phase shift significant enough to be picked up at the photodetector, was used.

If we recall from our previous discussion of the polarimetric sensors, the phase change induced can be described in the form of :

$$\Delta\phi = K\,L\varepsilon \tag{5.1}$$

where K is the sensitivity factor of the polarimetric sensor, L is the sensing length, and ε is the strain in the fiber. Remembering that we desire $\Delta\phi$ to be,

$$0.1 \leq \Delta\phi \leq \pi \tag{5.2}$$

we can then determine that the sensing length for the polarimetric sensor . That sensing length can be described by the relation

$$0.1/K\varepsilon_{max} < L < \pi/K\varepsilon_{min} \tag{5.3}$$

From these relations we can determine that a polarimetric fiber wrapped multiple times and adhesively bonded to the structure, with an effective sensing length of 15 cm, would satisfy the relations for our system and provide adequate performance.

This technique was used to determine the behavior of the beam under forced vibration, while the beam was subjected to several levels of electrical field. This level of electrical field was initially chosen by the investigator to verify the satisfactory performance of the beam. The system was later configured to permit and input into the neural network controller, and the controller output the appropriate voltage to the screen. The investigator then applied this voltage manually. After successfully determining that the beam was performing nominally, the neural network controller was connected directly to the Trek high voltage amplifier to effect control of the beam automatically. The experimenter would change the forcing frequency and amplitude of vibration. The results of this fiber configuration appear in **Figure 5.5.**

5.4 Shortcomings of the Polarimetric Approach

During the course of the present investigation, more specifically during the polarimetric experimentation, it was found that the polarimetric approach had several drawbacks. These drawbacks stemmed primarily from the nature of the polarimetric approach and the equipment that must be used with the approach. In the experiments it was discovered that the excessive lead-in and lead-out lengths that were required for the

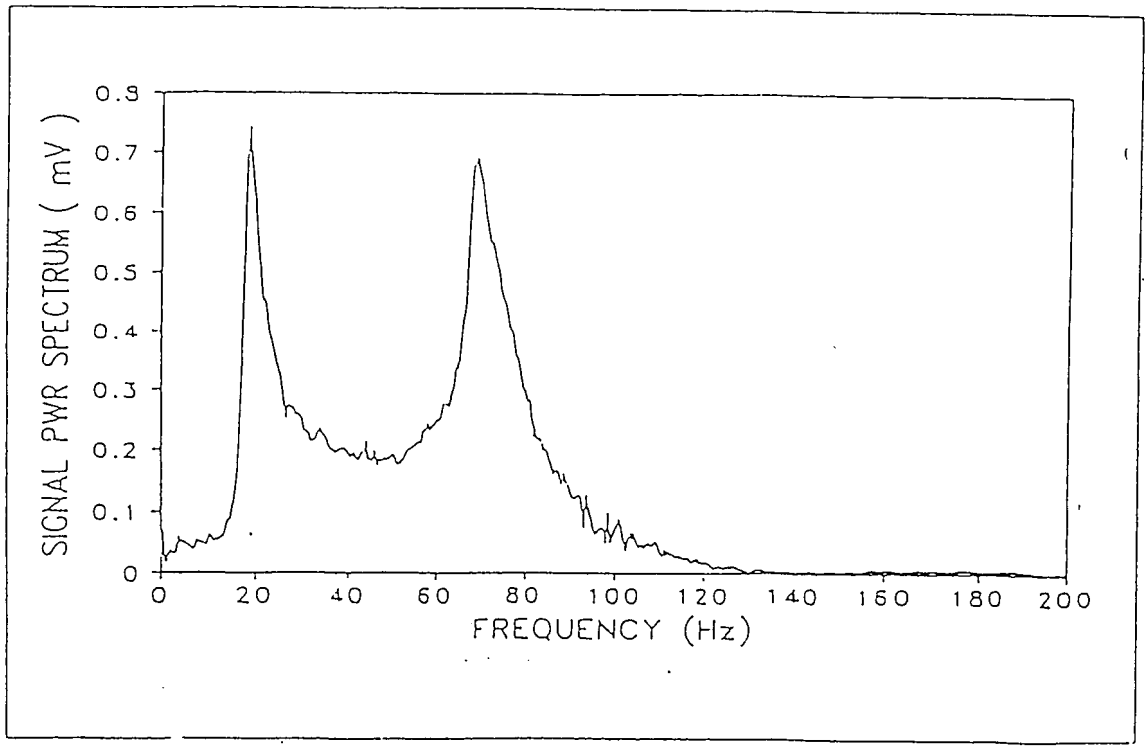

Figure 5.5 Sample results from the polarimetric fiber optic strain sensor at 20 Hz

set-up had the effect of introducing significant artificial strains into the fibers, and these effects were being read at the photodiode. Additionally, the hardware required posed problems when dealing with the issues of light management and signal alignment.

5.4.1 Artificially Induced Strains

By nature, the polarimetric fiber optic strain sensor relies on the constructive and destructive interference of the two eigen modes of the light to determine the strain occurring in the fiber, and presumably on or within the structure. Any strain within the fiber will induce a differential phase shift in the two eigen modes, and this phase shift will appear at the photodetector.

Figure 5.6 shows the lead-in and lead-out lengths on the experimental set-up used in this investigation. From this figure, it is easy to see that there is a significant length of fiber, nearly 1 meter, which is considered lead-in or lead-out. This fiber is positioned around the experimental set-up and is interfaced with the photodiode. When performing the experiments, the shortest lead-in and lead-out lengths were used to minimize the amount of fiber that was not experiencing the strain applied to the beam.

The lead-in and lead-out lengths are invariably effected by the vibration of the beam, and by any other motion which is transferred to the fiber, even though the experiments are located on a vibration free table. These lead-in and lead-out lengths

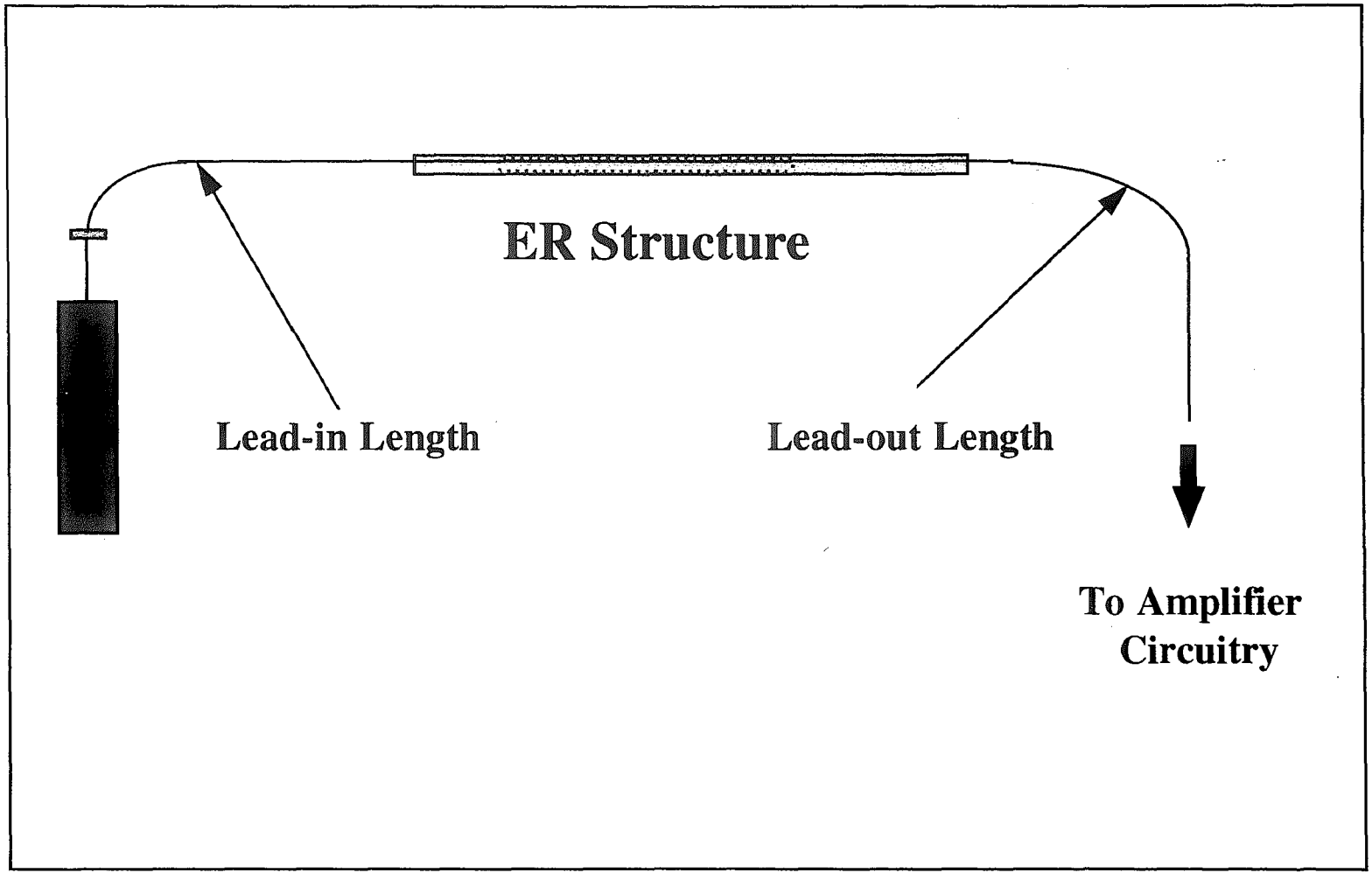

Figure 5.6. Lengthwise polarimetric fiber optic sensor showing the lead-in and lead-out lengths of the sensor which induce artificial strains in the fiber.

experience very minute strains as a result of the vibration applied to the beam itself, and these strains result in an induced phase change in the light which is traveling along the fiber. Though one would expect it to be small, due to the lightweight and therefore low inertial loadings on the fiber, nevertheless significant strains result in the fibers in both the lead-in and lead-out lengths. These strains add to the strains which are occurring in the fiber in the sensing region of the system, and are measured and processed by the photodetector and amplifier circuits.

Once it was determined that the lead-in and lead-out lengths had a measurable and significant effect on the accuracy of the system, and those lengths were made as short as possible, further experiments with the sensors were performed to determine the effectiveness of the corrections to the lead-in and lead-out lengths. It was found that there was still a significant effect from the lead-in and lead-out lengths. More interestingly, however, was the contribution to the strain from the climate control system. In the absence of forced vibration, and on the vibration free table, it was found that there was an induced strain in the fiber which was measured by the circuitry. It was discovered that this strain was due to the circulation of air within the laboratory from the climate control fan. From this point on, the experiments on polarimetric fibers were performed with this system temporarily disabled.

Although it was possible to isolate and minimize the effects of external, environmental, perturbations on the polarimetric sensors, a more reliable means of

measurement, which would ideally be immune to these minor perturbations, was pursued. It became apparent that the task of integrating these sensors into a real-world application would prove difficult and impractical, as they would likely be used in areas of climate control, random external vibrations, as well as interactions between humans and other equipment.

5.4.2 Hardware Requirements

In addition to the aforementioned problems associated with the lead-in, lead-out, and environmental considerations of polarimetric fibers, the nature of the experimental set-up for a polarimetric fiber also placed a premium on the usefulness of the sensors(Han et. al.) . The fact that the system required the use of a quarter wave plate and polarizers, to launch the light into the fiber in its orthonormal modes, complicated launching the maximum energy into the fiber. If the polarizers and quarter-wave plates were out of alignment, a significant reduction in the light power which reached the fiber would result. This reduction in the amount of light entering the fiber, coupled with the losses at the ends of the fiber, again present difficulties in obtaining a useful signal over a wide frequency range. The work on polarimetric sensors during this investigation was performed early on, and consequently did not benefit from the fiber preparation techniques endorsed by the SVET scientists. It is possible that by employing their methods it would have been possible to obtain better frequency response, however the

methods would not have had an effect on the false-signals introduced by the lead-in and lead-out lengths used for the sensor.

5.5 Fabry-Perot Interferometric Strain Sensors

As a result of the difficulties associated with the use of the polarimetric-style of fiber optic sensor, and after a literature search to determine what types of sensors were currently in use, it was decided that an interferometer would best serve the objectives of the investigation. Further, for fiber optic sensors configured as extrinsic Fabry-Perot sensors, the risk of damage during handling was significantly reduced. The interferometer can be fabricated to be less sensitive to the external strains which occur in the fibers, namely on the lead-in and lead-out lengths. In addition, the sensor could be readily configured into a pointwise sensor, and this pointwise sensor would require a significantly smaller sensing length. Since the fiber did not require the light to be conditioned with polarizing and quarter wave plates, it was possible to launch more light power into the fiber initially, which would ultimately result in less signal loss, greater operating range, and an overall improved sensor.

In **Figure 5.7** we can see the general configuration of the Fabry-Perot interferometer as applied to the measurement of strain in smart structures. This interferometer makes use of the combination of two signals, one being the reference signal, which is not exposed to the forced vibration of the beams, while the other is the

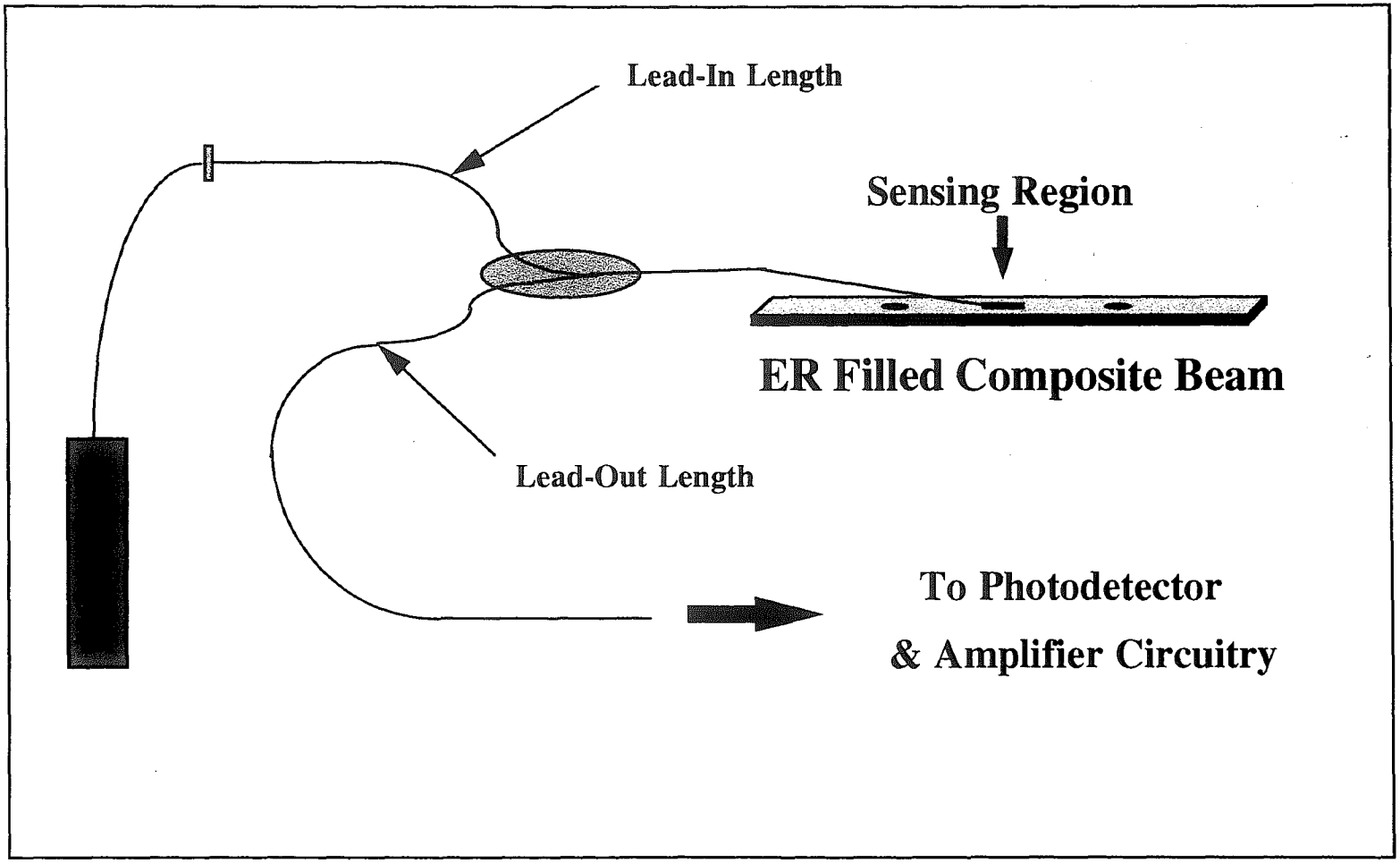

Figure 5.7. Lead-in and Lead-out lengths of the Fabry-Perot Fiber Optic Strain Sensor

measurand or the signal which is launched into the sensing region. We can see that there is effectively one lead in length, and two lead out lengths, when using a 2 x 1 coupler. The single lead-in length of fiber which is connected to the sensor contains the signal which will be subjected to the strain at the surface of the beam. The two lead-out lengths are actually an additional lead-in and a true lead-out length. The first lead-in length is the length of fiber from the laser to the optical coupler, which serves to split the light and reflect part of that light back toward the photodetector. The remainder of the light is transmitted through the coupler to the sensing region.

The true lead-out length which is connected to the photodetector carries two light signals, one being the reference signal, the other being the signal which was subjected to the strain in the sensing region. This signal will be out of phase with the reference signal if there is any strain occurring in the sensing region, and specifically in the sensing cavity. From **Figure 5.7** we can see that any environmental effects on the lead-in or lead-out lengths, which in the polarimetric sensor would have introduced significant error into the strain signal, has no effect on the signal from an interferometer. This important feature is due to the fact that both the reference and the sensing signal are subject to the same environmental perturbations.

With this in mind, a series of Fabry-Perot interferometric sensors were fabricated for use in this investigation. The principles of interferometric measurement being known, we will discuss the various detail changes that were altered in order to optimize the

performance of the sensor. Primarily, these detail changes consisted of various levels of mirroring, several different sensing gaps, and two types of mirroring material. The mirror material was changed in pursuit of more uniform heating during the evaporation process, which would permit better controllability of the mirror itself. Ultimately, commonly available aluminum foil, suitably washed of fingerprints and other oils, was chosen for the mirror material. This material proved to be softer than some other aluminum alloys which were tried, which contained too many contaminants. It also contained almost pure aluminum, and was free of alloying elements that were contained in other readily available mirroring materials. The presence of these alloying elements would form a residue which would hamper the performance of the mirror.

In order to effect a different level of mirroring, it was necessary to alter the amount of time which the fiber ends were subjected to the evaporation. Initially, a very heavy mirror, estimated at over 60% reflectivity, was applied. This resulted in a very weak signal from the interferometer, but a very strong signal from the reference source. A second mirroring sequence permitted a reflectivity of approximately 40-50%, and sensors with this level of mirroring performed somewhat better. However, their performance was still not as good as had been hoped, the sensor was not able to perform at very high frequencies. The best performance of the sensor was had from a fiber end which permitted approximately 70% of the light to be transmitted, that is it had 30% reflectivity. **Figure 5.8** illustrates the ultimate specification of the fiber optic sensor developed during this investigtaion. Sensors with less reflectivity suffered from a barely

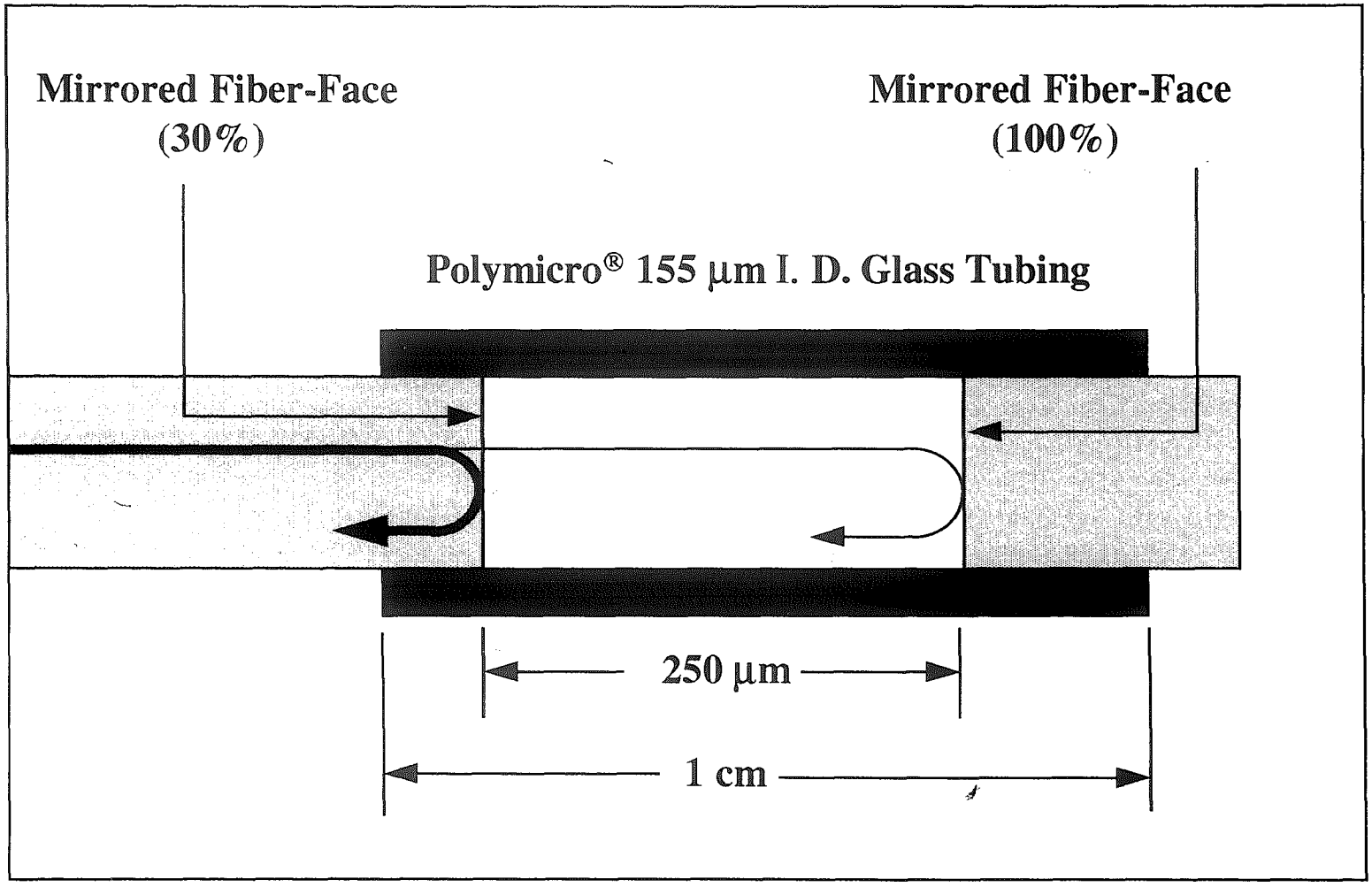

Figure 5.8. Final specification for the Fabry-Perot strain and vibration sensors used in this experiment.

visible, to the electronics, reference signal. Sensors fabricated with 30% reflectivity have proven to perform better than sensors made with other levels of mirroring. Though mention has been made of other coatings, specifically dielectric coatings, time and economic considerations prevented these coatings to be tried. There should be advantages to be had from dielectrics, however, as they do not absorb energy from the incident light source, as metallic mirroring materials might tend to do. This improvement should permit an incremental improvement in the sensing range of the fiber optic sensor.

In terms of the sensing gap which was used with the sensor, initial sensors were fabricated using a sensing gap on the order of one to two millimeters. Sensors with this sensing gap performed suitably at lower frequencies, below 100 Hz, but tended to fall off in terms of sensitivity beyond that point. Consequently, the sensing gap was made smaller, to its present distance of approximately 250 μm. This smaller sensing gap is believed to be responsible for the increased range of the sensor, through a reduction in the amount of light lost at higher frequencies due to the conical dispersion of light, discussed previously. 250 μm also represents a reasonable spacing to permit the movement of the fiber under loading while ensuring that the faces in the Fabry-Perot cavity do not touch.

From the aforementioned discussion, it can be seen that the Fabry-Perot interferometer has a significant performance advantages over a polarimetric fiber optic sensor. In the following chapters, results from the experiments performed with this Fabry-Perot sensor will be presented and discussed. Further description of the neural

network controller will also be made, and the performances of the various sensors when incorporated into the sensing scheme shall be discussed.

Chapter Six

Advanced Smart Structures, Sensing and Controlling Issues

The simplest form of ER material-based smart structure is one having a single region of applied electrical field, with one positive and one negative electrode. Such a structure was employed as one of the test beds for fiber optic sensing and control. More complicated structures, such as composite plates and beams with numerous electrode regions, present a significantly greater challenge to the modeller, and thus it is difficult to correlate the results from testing using a fiber optic sensor and the results from any model. It becomes possible that in order to minimize the amplitude of vibration, energizing only one region is necessary. It may also be possible that all regions need to be energized with a low electrical field strength. The level and distribution of applied electrical field will depend on the location, magnitude, and number of external perturbations applied to the structure itself. So it can easily be seen that the task of modeling, as done by Yalcintas (Yalcintas, 1995) becomes much more involved.

In Chapter Five we discussed the desire to verify the results of the models for smart structures with experimental data. We will discuss the incorporation of the data from the fiber optic sensors into the neural network control algorithms used in this study. Further, the manner in which this data was used to train the neural network will be discussed. During the course of this investigation, several types of neural networks were investigated as possible candidates for the architecture of the controller. These types of

neural networks will be briefly discussed, and the ultimate configuration, a RBF-based neural network, will be described in more detail.

6.1 An Introduction to Neural Networks

Conventional neural networks are designed to approximate the learning capabilities of the human mind. One of the goals of the neural network is to minimize the time required to adapt to a decision-making situation, and to arrive at a decision which is correct, with a high level of certainty. Neural network development has shown that once a network is presented with an appropriate set of training data, it can effectively make these "correct", or appropriate, decisions. Properly trained, a neural network can make those decisions with a high degree of accuracy.

Designing a neural network is, in effect, a process of assigning an appropriate function to an operation, system, or environment. The function which is assigned to the system in question is initially defined arbitrarily, and receives as its inputs data available from the system. The number of inputs and outputs to the system can be large or small. Intermediate processing units, also known as processing layers or hidden layers, are assigned between the inputs and the outputs. At these processing units, the input variables are weighted and the function is calculated using the data from the input variables and the weight functions.

Once the general design of the network has been established by the user, the process of training can take place. Neural networks are trained through the presentation of patterns of data, sometimes with the outputs which are associated with each set of data, and sometimes without. When the data which is presented to the neural network is associated with the outputs, this is considered supervised learning. Unsupervised learning is the presentation of patterns of data without the corresponding outputs. Supervised learning is generally used when the solutions to the system in question can be readily obtained, for example the electric field which need be applied to a structure to minimize the vibration (Flanders and Burke, 1995).

One of the most common types of neural networks is the backpropagation network. This type of neural network was developed by several independent researchers, and adjusts the weights to the processing layers beginning with the output layer rather than a forward propagating network, which begins by adjusting the weights to the processing layers from the input side of the network first (Rummelhart et al., 1986; Parker, 1982; Werbos, 1974). Errors in pattern presentation trigger this adjustment of weights, beginning at the output side. A simple diagram of a neural network, of the backpropagation type, is shown in **Figure 6.1**. From this figure, it can be seen that the connections and the processing or hidden layers perform much of the computation within the network. The input layer is primarily assigned the task of taking the information from the measured parameters and presenting them to the neural network. The output layer is assigned to present the data from the neural network back to system.

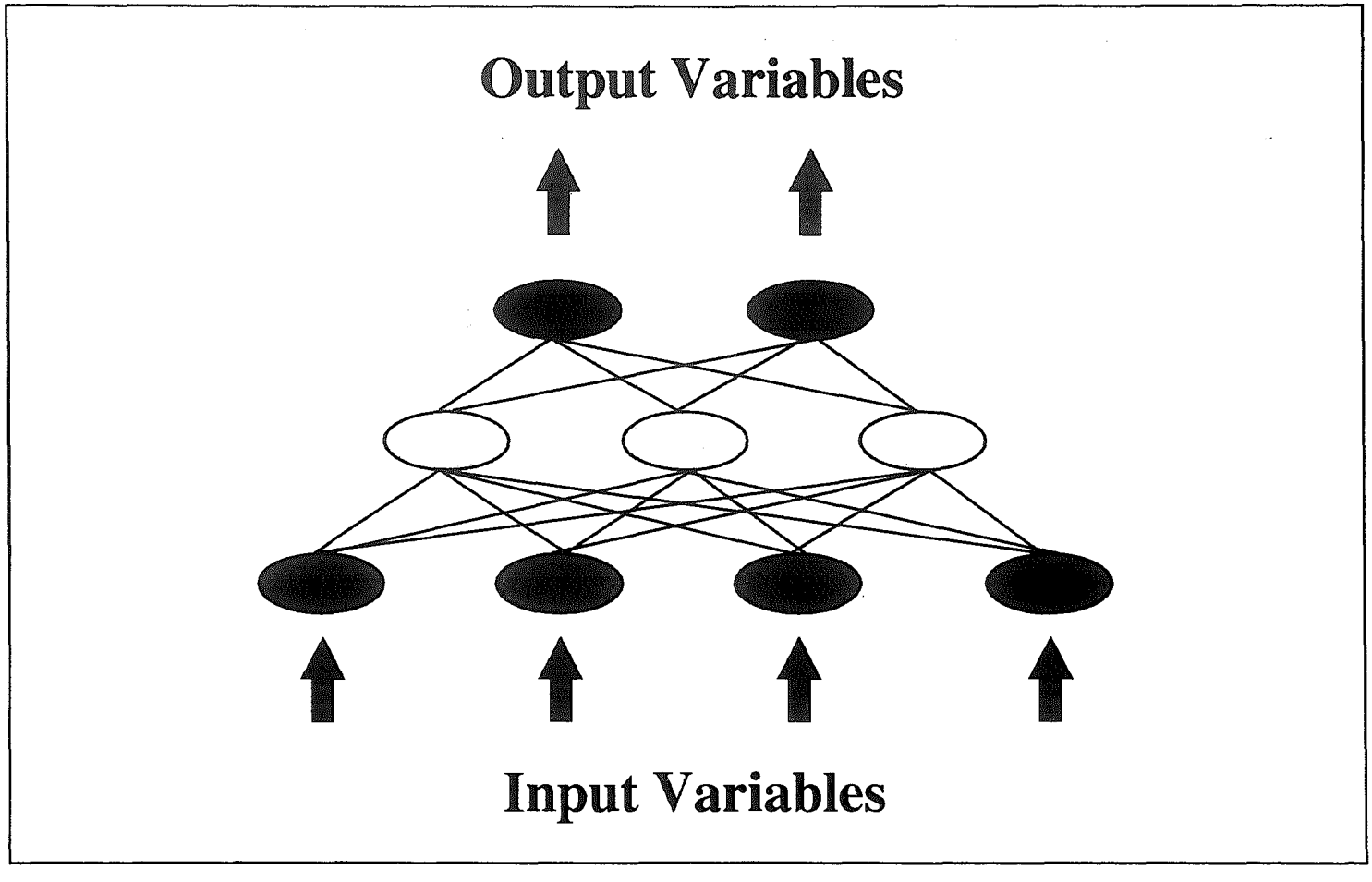

Figure 6.1. Simple Backpropagation Neural Network

Though in general applications the neural network's output can be considered to be appropriate, the backpropagation network can develop a tendency to profess knowledge outside of the areas in which it was trained. Backpropagating neural networks based on the sigmoid function will develop a system of divisions, known as hyperplanes, to provide the output of the system based on the inputs. For example, the neural network might have been trained on a set of data which is appropriate to solutions for simply-supported beams, but it will also output a solution for cases of different end conditions, for example clamped-clamped end conditions. Clearly the solutions to these problems will be different. **Figure 6.2** shows the classification space of a generic backpropagation network. In some cases it can be seen that within the classification space, but out of the experience of the network, there can be some solutions which are possible results from the neural network computations. In order to solve the problems associated with conventional neural network algorithms, the Radial Basis Function neural network architecture was developed.

6.2 Radial Basis Function Architecture of Neural Networks

Radial basis function neural networks, or RBF's, do not rely solely on the sigmoid function for their decision making, as other neural network architectures do. Radial Basis Function neural networks rely on gaussian activation functions for the hidden layers (Flanders and Burke, 1995). The RBF network is established in a manner different from a backpropagation network as well, which would be defined by the users. The inputs are

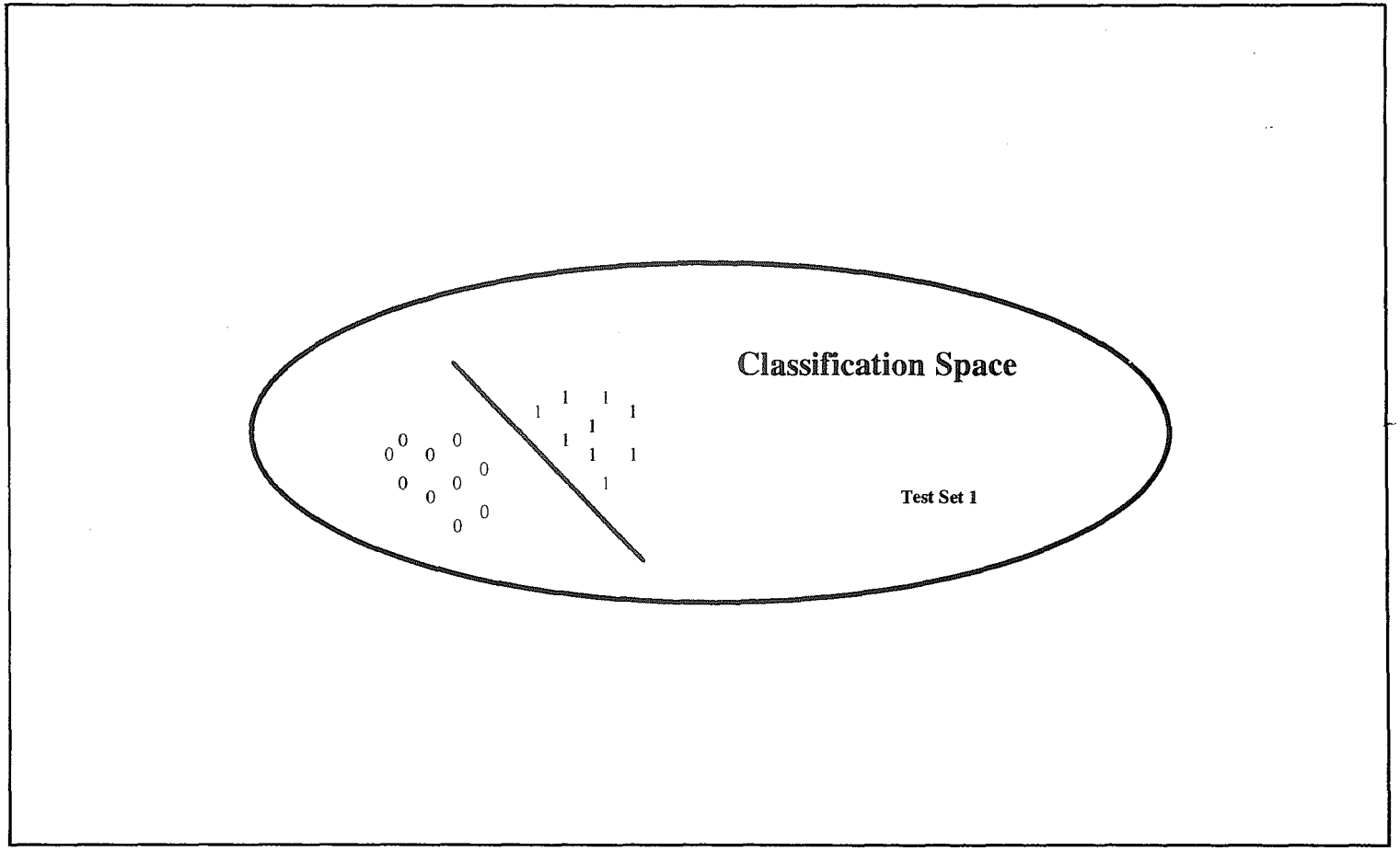

Figure 6.2. Classification space of a backpropagation neural network

grouped by a K-means method to minimize the error between the inputs and a set of vectors. The K-means method applies to the number of basis functions which are chosen to partition the input space.

After the basic structure has been defined as described above, the training of the RBF neural network can take place. This takes place in manner similar to the training of a backpropagation network, though the RBF structure also permits adjustment to the basis function widths and the centerpoints of the basis functions. The RBF adjusts its connection weights similar to a backpropagation neural network. In contrast to the classification space, and the training set presented to the backpropagation network shown in **Figure 6.2,** the test pattern represented by Test Set 1 will result in the RBF network pronouncing "No Response", as opposed to the backpropagation network which will pronounce a decision. Radial Basis Function neural networks do not construct hyperplanes, but rather they construct boundaries outside of which the network will not attempt to make a decision, as shown in **Figure 6.3.** With a radial basis function-based neural network, the confidence levels associated with the outputs can be higher. RBF neural networks can be trained with fewer data sets, reducing the training time to obtain greater confidence and lower associated errors. On average, a radial basis function network performed with 15% less error than a backpropagation neural network, comparing both the R^2 and RMS errors (Flanders and Burke, 1995).

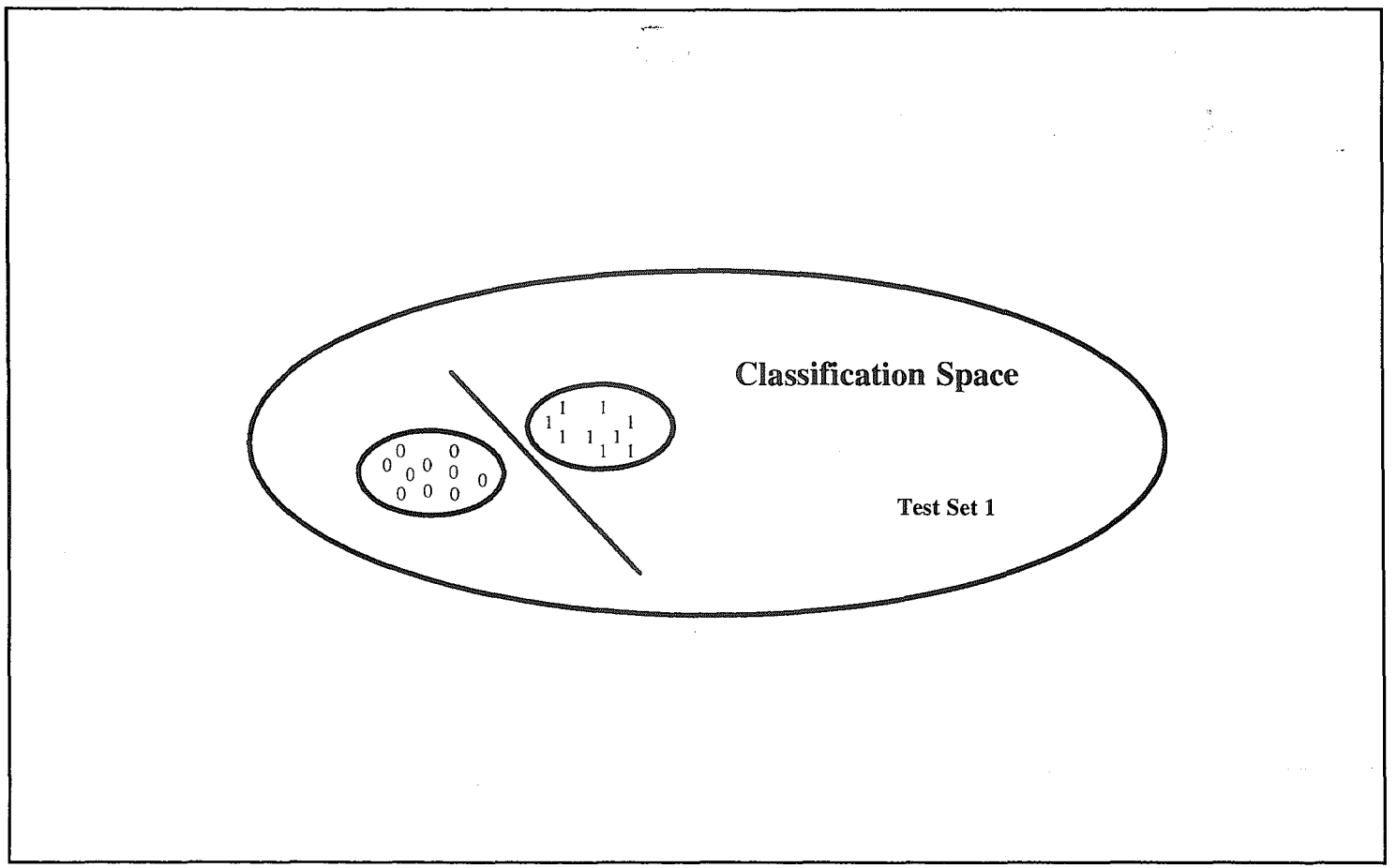

Figure 6.3. Classification space of a Radial Basis Function (RBF) neural network

6.3 Neural Networks, Fiber Optics, and Smart Structure Testing

The development of a fiber optic strain sensor, a neural network controller, and appropriate modeling capabilities were all pursed in order to develop an integrated design and control package for smart structures. The ability to accurately sense the behavior of smart structures, in deference to the inability of conventional sensing techniques to measure the same parameters, was vital to the completion of the objective. Once the data from the fiber optic strain sensor was obtained, the data could be compared against the predictions of the model. Both the data taken directly from the beam and the predictions from the model were used to trained a Radial Basis Function neural network. This controller was used to effect autonomous control over several configurations of smart structures.

Interfacing of the fiber optic strain sensor with the neural network controller and the associated amplifier circuitry took place in a manner as described previously in this report. During the course of the sensor development, from the initial use of polarimetric sensors to the ultimate use of extrinsic Fabry-Perot sensors with very small sensing gaps, several modifications were made to the basic experimental set-up to achieve better performance. This development is natural and expected, as problems with the sensors, test apparatus, and associated equipment arise. The final specification of the fiber optic sensor and the amplifiers is believed to represent the configuration which will provide the best response for this type of sensor. This specification will be described, for both the

polarimetric and the interferometric fiber sensors, in its ultimate evolution. The interim specification will be discussed briefly but will not be described in depth, it will be used as a tool to identify an area for future work.

6.4 Testing Results - Polarimetric Fiber Sensors

During the course of the investigation of potentially suitable fiber optic sensors using the polarimetric configuration, the test beams were configured as simple composite beams, with the top and bottom layers of the beam acting as the electrodes as well, as described in **Figure 5.1.** The polarimetric fiber was attached lengthwise to the outside of the beam. The fiber was not wrapped in several bows, as described previously, to permit a pointwise sensing capability. Wrapping the fiber in several bows was found to have excessive noise in the signal, particularly at higher actuation frequencies. This is believed to be due to the interactions of the loops of the fiber physically contacting each other during vibration. Consequently, the polarimetric configuration was tested in integrating form, similar to **Figure 5.3.**

In this configuration amplifiers processed the signal from the photodiode such that the amplitude of the input signal to the A/D board, A_{in}, was equal to

$$A_{in} = I_{photodiode} * K_{amplifier} \qquad (6.1)$$

where $I_{photodiode}$ was the incident current from the photodiode, and $K_{amplifier}$ was the multiplier for the processing circuitry amplifiers, either 27×10^6 or 49×10^6. Because of the noise in the signal it was desired to multiply the signal to the maximum value possible, filtering any newly introduced noise prior to inputting the signal to the PC for final processing.

The A/D board interfaced with the neural network program via an intermediate processing program which performed a Fourier Analysis on the signal to determine the frequency and amplitude of vibration. The amplitude of vibration was non-dimensionalized and input into the neural network along with the frequency of vibration. The exact value of the amplitude of vibration is unimportant in this scheme, as our controller does not assign a value to the ***absolute*** value of the strain, but compares only the ***relative*** values of the strains from the sensor. **Figure 6.4** illustrates a sample of the output from the polarimetric fiber optic strain sensor which was used with the RBF neural network controller.

The polarimetric fiber was found to operate moderately well at lower frequencies, generally less than 100 Hz. At frequencies above 100 Hz, the signal was very weak, which lead to confusion on the part of the neural network, since it was programmed to minimize the largest amplitude of vibration, at the frequency which corresponded to that largest amplitude. The sensor and the processing package did exhibit several anomalies at natural frequencies of the beam set-up, which in this case simply supported. Also,

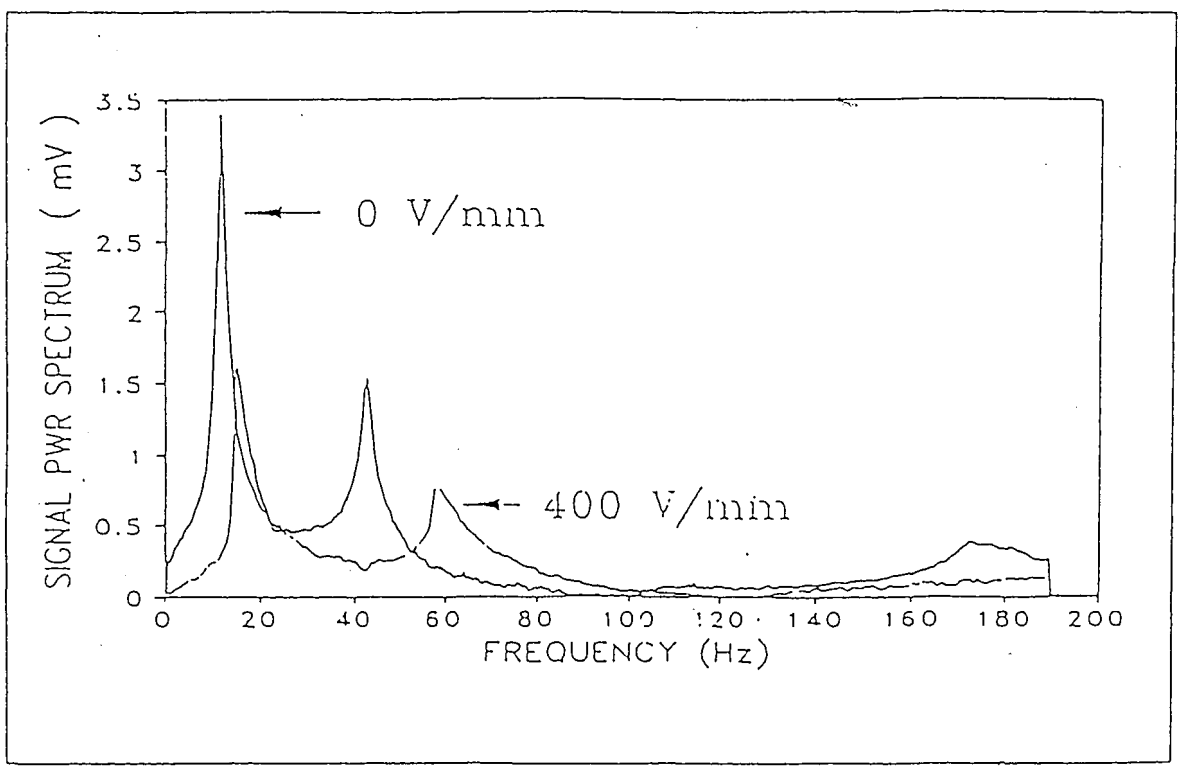

Figure 6.4 Sample output from the polarimetric sensor used in conjunction with the RBF neural network

because of the low amplitude of the output signal compared to the signals from the Fabry-Perot sensor, the processing software and neural network had a particularly difficult time differentiating between electrical noise at a frequency of 60 Hz and the signals from the beam, vibrating in the range of 55-68 Hz. Consequently, the neural network would over-react to what it believed was the signal from the fiber optic sensor, when in fact it was attempting to interpret a noisy electronic signal at 60 Hz. The aforementioned problems of lead-in and lead-out lengths making false contributions to the strain of the beam also were deemed detrimental to the ultimate objectives of this investigation.

Another drawback to the polarimetric approach was the need to filter the signal in order to clean the signal of noise introduced when the photodiode output was amplified. The signal amplifiers which were used for the polarimetric experiments were of inferior quality to those used for the Fabry-Perot experiments, and thus introduced an extra-ordinary amount of noise into the signal. It was thus necessary to filter the noise from the signal after amplification. A Krohn-Hite 3750 Band-pass filter was used to remove much of the noise incident in the signal after being amplified. As the range of vibration varied, the range of filtration was changed to ensure that the frequency of vibration fell within the frequency of filtration. In a sense this was considered compromising the validity of the experiment, as real-world applications would not afford the luxury of knowing the frequency of vibration. Additional active filtering schemes could be employed, to analyze specific ranges of vibration for the strongest signal, and then analyze that region. However, active filtering requires more electronic hardware, adding further complexity

and much higher cost. Thus, though the polarimetric fiber could perform rudimentary sensing tasks, its poor performance in higher frequency ranges and "peculiarities" at other frequencies led to the development of the extrinsic Fabry-Perot sensor.

6.5 Testing Results - Extrinsic Fabry Perot

In order to solve many of the problems that the polarimetric fiber optic sensor was unable to overcome, it was necessary to have a sensor with a significantly higher visibility, and lower noise throughout the frequency range in which the smart structure was being tested. To accomplish this would require several improvements; increases in the amount of light which is launched into the fiber, improvements in the amount of light reflected back to the photodiode, and improvements in the location and mounting of the fiber. More light launched into the fiber meant that there would be more light to process at the photodiode. More light reflected back to the photodiode meant that there is a stronger signal which can be compared to the reference signal, and thus the strain can be determined. In the case of less light reflected back to the photodiode, the reference signal is much stronger than the measurand signal, effectively nulling and destructive interference effects from the strain at the fiber optic sensor. To the photodiode and to the processing software, it appears that the reference signal is unchanged, and thus no strain is occurring in the sensing region. This is not the case as the beam does experience strain at the surface under forced vibration.

Finally, improving the mounting location of the fiber, and reducing the effects of lead-in and lead-out lengths, would improve the quality of the signal. If these effects could be eliminated, one could assume that the signal from the sensor is indicative of the strain in the region, and is not being superimposed with a strain from the lead-in and lead-out lengths.

In order to address the issues of improving the amount of light launched into the fiber, and the amount of light reflected back to the photodiode, a complete inspection of the fiber processing techniques ensued. It was found that the fiber preparation techniques were inadequate, that the ends of the fibers were neither cleaved cleanly nor perpendicularly, and that the amount of light launched into the fiber was inadequate. The techniques of Egorov and Màmaev, and their familiarity with fiber preparation, assisted to increase the amount of light and improved the quality of the ends of the fibers (Egorov and Mamaev,1995). The mirroring used on the ends of the fibers also improved to the point that a reliable mirror coating could be deposited to permit sensing very high frequencies. Their contributions to the methods used previously at Lehigh University will be described briefly.

To ensure that the fiber is properly cleaved it is necessary to use a proper cleaving device. Generally, the fiber can be cleaved using a diamond edge to scribe the outer surface of the core sharply, then the fiber is generally pulled apart. A proper cleave leaves the face of the fiber perpendicular to the axis of propagation, and free of chips or

other surface irregularities which would adversely affect the transmission of light into or out of the fiber. Previously, a carbide tipped scribe was used to perform this operation, resulting in irregular cleaves of the fiber ends. On average, one out of four cleaves was acceptable for use in an interferometer or polarimetric fiber sensor. Mamaev and Egorov championed the use of a ceramic scribing device, made by fracturing a sheet of 1 mm thick ceramic sheet. This created an edge much sharper than the carbide scribe used previously. More importantly, the edges from this fractured sheet of ceramic proved to be extremely hard, and provided cleaves suitable for fiber optic sensors nine out of every ten times, one average.

In order to align the laser with the end of the fiber optic cable, SVET had practiced the simple but effective technique of using a piece of white paper with a very small hole in it, less than 0.1 mm in diameter. This paper was placed over fiber and was used as a projector screen to view any reflections from the end of the fiber, in the event that the light was not being completely launched into the end of the fiber. In the past, the alignment of the laser was judged by the amount of light exiting the fiber end at the photodetector. When the intensity of the light at the photdetectors is very small, as is the case with interferometers and other fiber optic sensors using laboratory lasers, it is much easier to judge the intensity of the light prior to its launch into a fiber or a sensor. by minimizing the amount of light which was reflected to the surroundings, and onto the paper, one can more accurately judge the amount of light launched into the fiber (Egorov and Mamaev, 1995).

The issue of lead-in and lead-out lengths, and the effects that they would have on the fiber optic sensor's performance, can be handled by examining the extrinsic Fabry-Perot sensor and the make-up of the signal which is analyzed. **Figure 6.5** shows the general scheme and is marked with several reference locations which we will use to discuss the issue of lead-in and lead-out lengths and their influence in the extrinsic Fabry-Perot set-up.

Both the reference and the sensing signal for the Fabry-Perot sensor experience the same perturbations as they approach the input to the coupler, Location 1 in **Figure 6.5.** As the signal reaches the coupler, 50% of the launched light is reflected back into the two legs of the coupler on the input side, thus 25% of the light is launched back to the light source, and 25% of the light is reflected to the photodiode. The portion of light reflected to the photodiode will ultimately be part of the reference signal.

Now, let us consider the 50% of light which is passed through the coupler to the sensing leg of the coupler. The manufacturer of the coupler, Gould Fiber Optics, has described with the 2 x 1 coupler used for this experiment as a 2 x 2 coupler which is modified by removing one leg, in our case one leg of the sensing side has been removed. This means that of the 50% of the light which is sent to the sensing leg(s), 25% of it will be lost due to the cleaved second leg. Thus, only 25% of the light is entering the sensing region, Location 2 in **Figure 6.5.** In this sensing leg, a signal identical to the reference

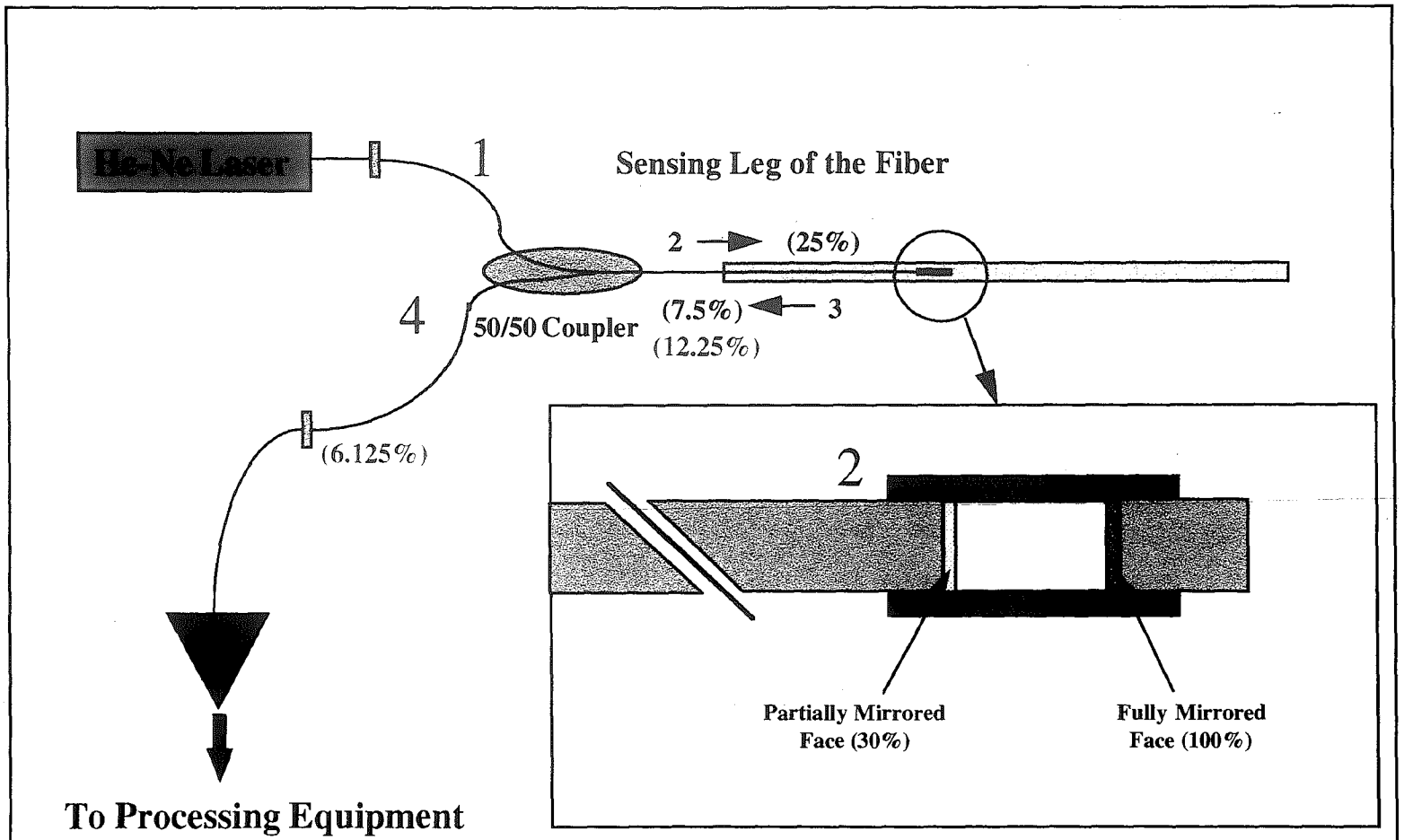

Figure 6.5. Reference Locations in a Fabry-Perot Fiber Optic Sensor

signal reflected back to the photodiode from the input side of the coupler is directed towards the sensing cavity. Some of this light reaches the sensing cavity and is reflected, the amount depending on the reflectivity of the mirror, and some of it is reflected back to the coupler, to ultimately reach the photodiode. The light which enters the sensing cavity experiences the strain which is being applied to the structure through forced vibration, and then reflects back to the coupler.

At Location 3 in **Figure 6.5,** we can see the amount of light which is vying to get through the coupler. Again, due to the reflectivity of the coupler, only 50% of the light will pass through the coupler, the rest will be reflected back and forth and will eventually be reduced to such a small amount that it can be ignored. The light which makes it through to the other side of the coupler is shown as well.

From this brief discussion, we can see that the reference signal is obtained from the initial reflection at the coupler back to the photodiode, as well as from the light which is reflected just prior to entering the sensing region. The reference signal which is reflected from just prior to the sensing region is combined with the signal from the sensing region. We can see that these two signal experience the same amount of strain, if there is indeed an induced strain in the fiber. Thus any effect that the strain has on the refractive index of one signal will affect the other signal in the same manner. Thus the induced strains and anomalies from the lead-in and lead-out lengths can be ignored.

Once these problems were rectified, the sensor was tested on several types of beams to evaluate its response. It was first mounted on the simple composite beam having only one electrode area which encompassed the entire surface of the beam. The sensor was found to be highly responsive, providing an accurate signal from 5 Hz to more than 250 Hz. It should be noted here that signals below 5 Hz were discounted. These signals were sometimes tremendously strong, even when the experiment was located on an vibration-isolating table. They were found to be caused by the normal structural vibrations of the laboratory and the building in which it was located.

With these encouraging results, it was decided to decrease the sensing gap of the sensor from approximately 1 mm to 250 μm. After fabricating a sensor with this sensing gap, the sensor was now attached to a larger beam, consisting of four electrode regions. The beams themselves were made of fiberglass-reinforced polymer, 0.4 mm in thickness. The intention of changing the beam specification was to demonstrate the applicability of the fiber optic sensor to a vibrations which were significantly different than those which were associated with the aluminum beams tested previously. This beam was held in a clamped-clamped end condition fixture, similar to the first beams which were tested with the extrinsic Fabry-Perot sensor. Its overall dimensions were 550 mm x 50 mm x 1.8 mm.

This beam permitted experimental data to be taken for the fiber optic sensor which covered a much larger range of strain than was previously possible with the smaller

aluminum beams. Additionally, the beam was monitored with a non-contacting proximity probe to obtain data that would be used for the verification of the modeling efforts by Yalcintas. After experimenting with the non-contacting magnetic actuator, which was able to provide adequate, but not very large, vibrational amplitudes, it was decided to utilize a contacting actuator. This actuator permitted much larger amplitudes of vibration to be tested, pushing the envelope of the fiber optic sensor's range.

Figures 6.6 and 6.7 illustrate the frequencies which the sensor was able to detect, plotted on the y-axis, versus the input frequency of excitation. In the ideal case, the sensed frequency and the input frequency would be equal at all points on the curve, forming a line having a slope of unity. Plotted against this ideal curve are the exact frequencies of vibration sensed by the Fabry-Perot sensor. In general, the output of the sensor agreed very closely with the applied frequency of excitation, indicating that the Fabry-Perot sensor was performing optimally. In order to effect control of the beam, a processing algortihm was written at Lehigh to interpret the signals from the photodiode and amplifier circuitry to an output signal. This output was in the form of a frequency of vibration and an amplitude of vibration. Data recorded manually from this screen output appears in Appendix A of this work.

There is some disagreement in the results from the Fabry-Perot sensor at frequencies which were multiples of 60 Hz, and at these frequencies data was recorded numerous times to filter out what is believed to be the effects of the electrical equipment

used in the experiment. Data was taken from 20 Hz to 400 Hz in increments of 20 Hz. Data was also taken at 600 Hz and 1000 Hz to check the upper limits of the sensor. Above 1000 Hz the performance of the sensor deteriorated and prediction of the applied frequency of vibration was haphazard at best, a condition most likely due to the noise induced by the amplifying circuitry, which was at its maximum amplification for higher frequencies.

Figures 6.8, **6.9**, and **6.10** illustrate sample output from the oscilloscope for applied frequencies of 20 Hz, 200 Hz, and 400 Hz, respectively. The oscilloscope was used to monitor the experiments in addition to the custom processing software, and to act as a check and to provide a raw sample of the data from the Fabry-Perot sensor prior to being processed in the PC-based software. Comparing successive peaks from these two plots of raw data, we can see that the periods of the output signals are approximately 50 milliseconds, 5 milliseconds, and 2.5 milliseconds, respectively.

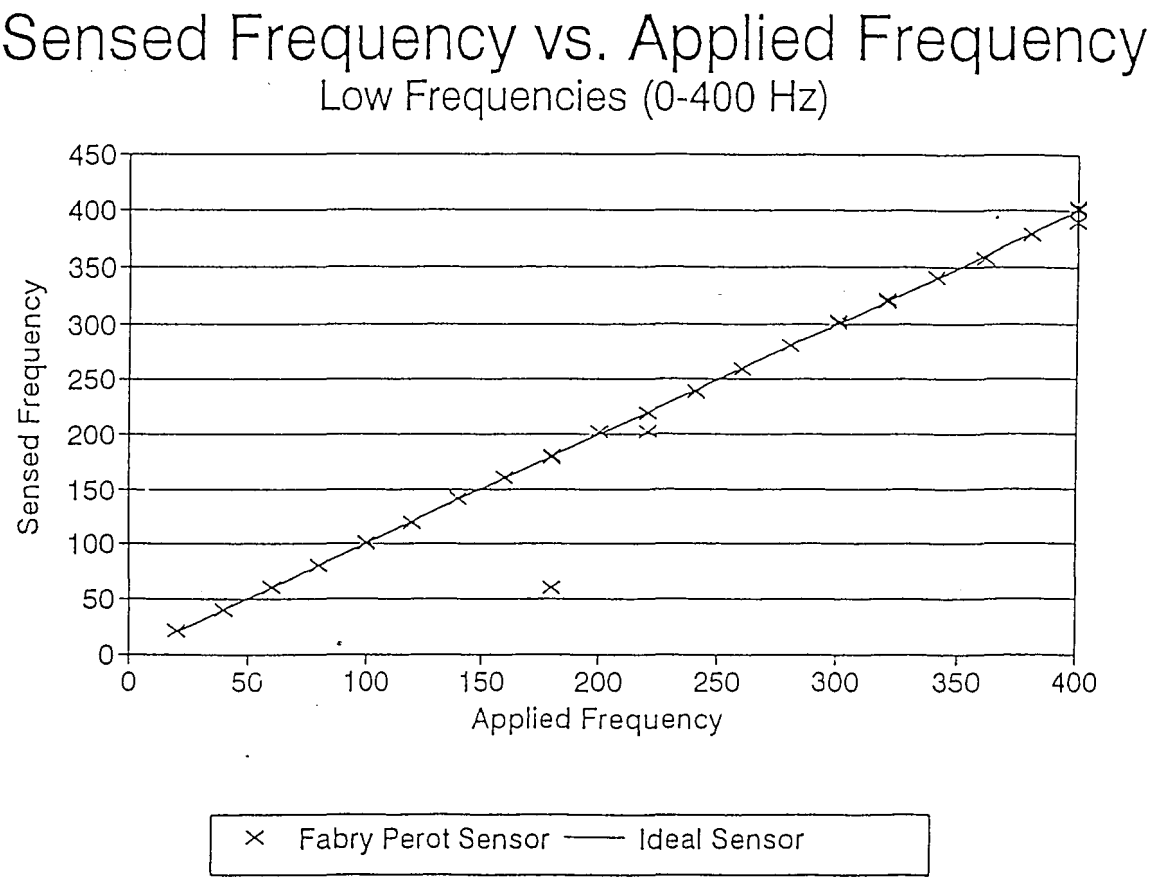

Figure 6.6. Sensed versus Applied Frequency for the Fabry Perot Sensor in the Range of 20 Hz - 400 Hz

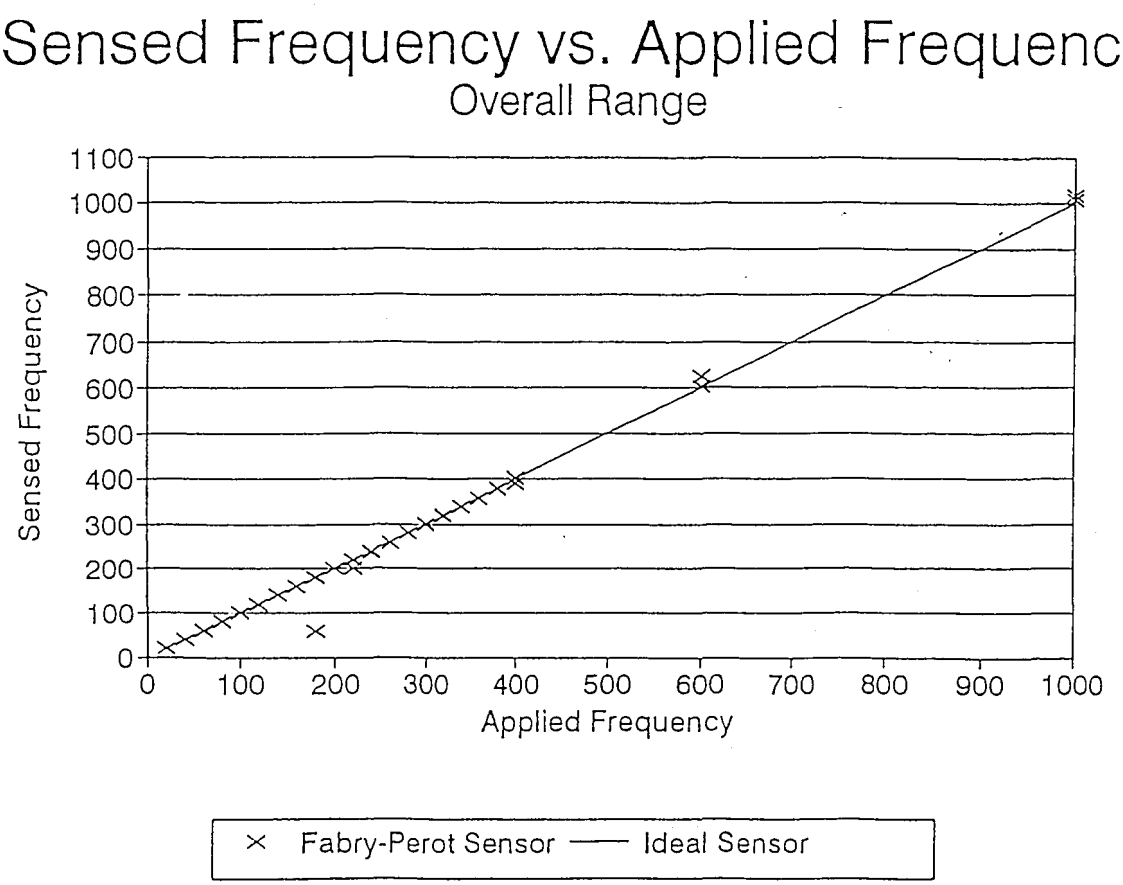

Figure 6.7. Sensed versus Applied Frequency for the Fabry Perot Sensor in the Range of 20 Hz - 1000 Hz

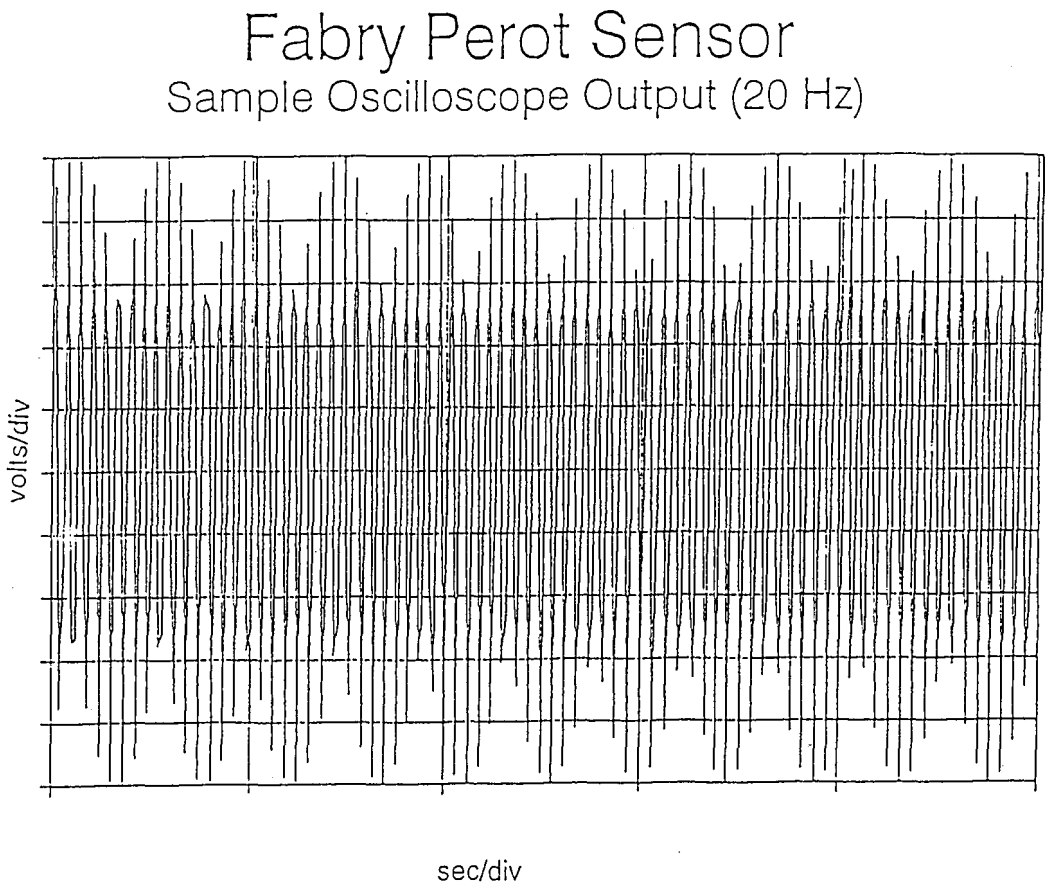

Figure 6.8. Sample Oscilloscope Output from the Fabry Perot Sensor (20 Hz)

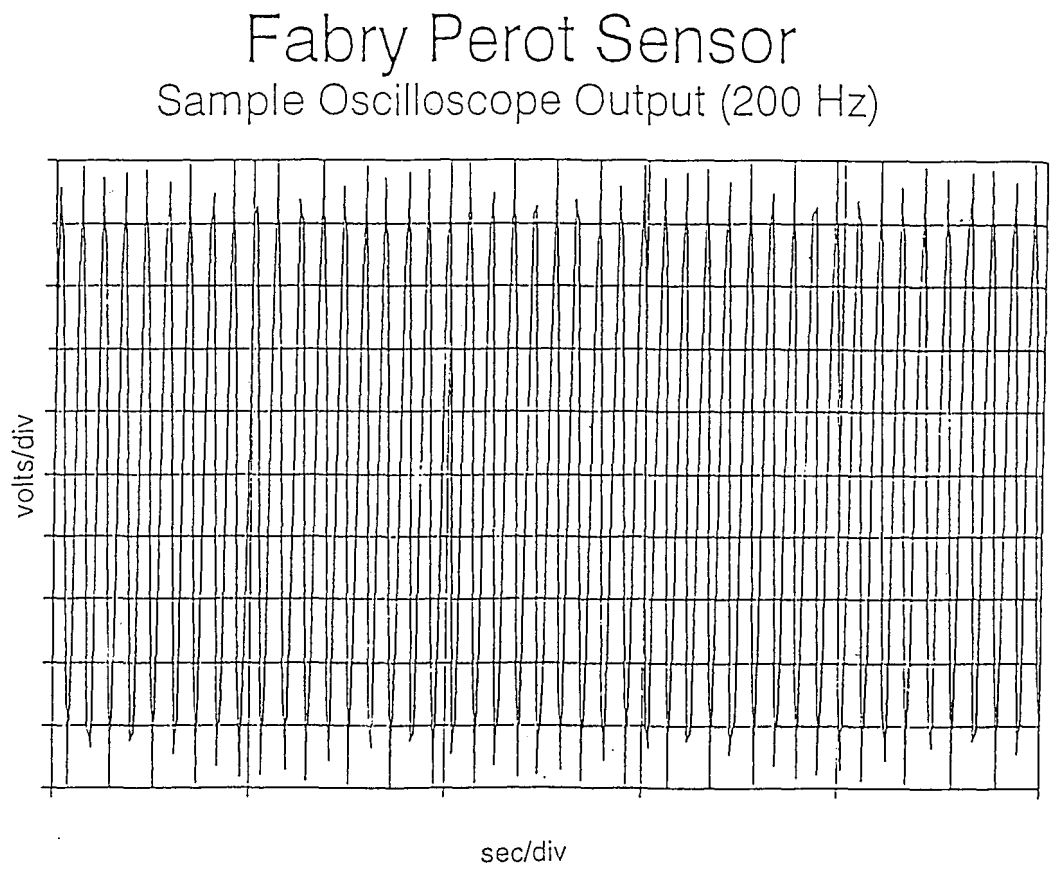

Figure 6.9. Sample Oscilloscope Output from the Fabry Perot Sensor (200 Hz)

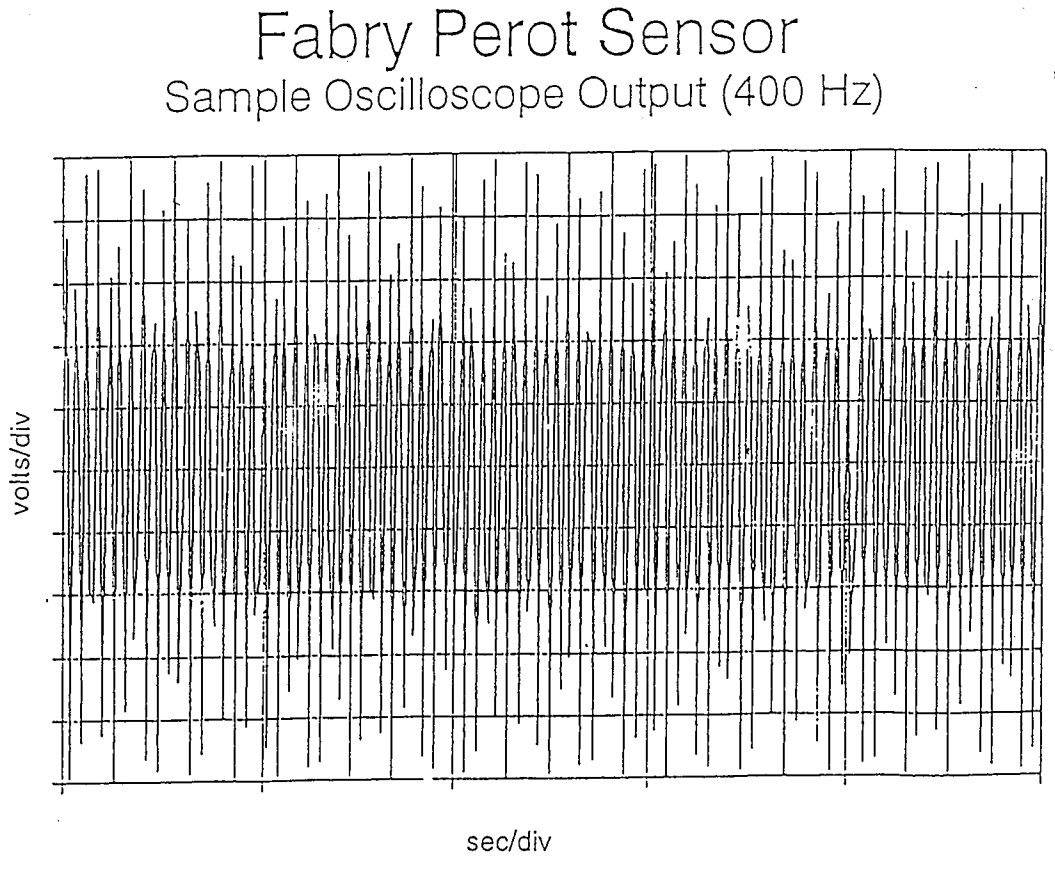

Figure 6.10: Sample Oscilloscope Output from the Fabry Perot Sensor (400 Hz)

The extrinsic Fabry-Perot sensor with a sensing gap of 250 μm was able to accurately sense frequencies of vibration up to 1000 Hz. The amplitudes of these vibrations ranged from 1 mm to 15 mm, applied at the free end of the beam. These forced vibrations occurred in a range of 10 Hz to 1000 Hz. Because it is easier to sense larger values of strain, still within the realm of one-half of one wavelength os strain, the performance of the sensor was evaluated particularly at lower amplitudes of vibration, through a wide frequency range. The performance of the sensor in these regions of lower amplitude vibration was remarkably good. The sensor exhibited no sensitivity to environmental conditions such as the presence of liquids, namely oil and water, in the sensing region. It exhibited good stability in terms of its power output, though some fluctuation was noticed, most likely due to the lightsource. The sensor was not affected by the variations in the power spectrum, as they still permitted differentiation between the reference and sensing signals.

Chapter Seven

Conclusions and Future Work

Fiber optic sensors are ideal for operating environments which preclude the selection of more common means of strain and vibration measurement. Environments of high electromagnetic interference and environments of caustic or other damaging solutions pose no threat to the fiber optic sensor. Critical applications such as those in the aerospace and petroleum industry, where a premium is placed on the safety of the sensors, can potentially use the fiber optic sensor developed here, as it is virtually incapable of igniting an explosion, is reliable when properly installed, and can be interfaced with any number of controller types.

7.1 Fiber Optic Sensors Developed During This Investigation

We have seen that a fiber optic sensor, of several configurations, can be integrated with a controller to effect autonomous adaptive control of an intelligent structure. The integration of these sensors with the controller, and the type of controller used, can vary depending upon the desired level of complexity and cost, and the specific sensing application. During the present investigation, polarimetric and interferometric fiber optic sensors were evaluated for their performance in a strain and frequency of vibration monitoring environment. Numerous developments in specification took place in the case of both the polarimetric and the interferometric sensor, and the practical performance

limit of both sensors was investigated. It was found that the polarimetric method of sensing was inferior in performance, in the pointwise sensing regime, to the extrinsic Fabry-Perot interferometric sensor. The extrinsic Fabry-Perot was more robust than the polarimetric sensor, offered a higher frequency sensing range than the polarimetric sensor.

When considering the performance of the polarimetric sensor in the lengthwise, integrated, strain sensing environment, the sensor was adversely affected by the vibrations and induced strains in the lead-in and lead-out lengths. Though a similar lengthwise approach was not attempted with the Fabry-Perot sensor, and in fact it would require re-engineering the sensor configuration itself, the lead-in and lead-out lengths of the Fabry-Perot-type sensors have no effect on the output of the sensor. This fact is helpful when considering other practical applications of Fabry-Perot interferometric strain and vibration sensors, as one can potentially envision numerous situations which would preclude short or non-existent lead-in and lead-out lengths. If the signal were affected by these lengths the applicability of the sensors developed here would be extremely limited.

7.2 Fabry-Perot Sensors for Strain and Smart Structure Monitoring

The extrinsic Fabry-Perot sensor developed during the course of this investigation readily solves the problems associated with other sensing mechanisms. It is capable of sensing very small strains on the surface of a smart structure, is not affected by the

electromagnetic interference associated with the uses of electrical and magnetic fields in smart structures. These fields typically have adverse effects on traditional means of strain and vibration measurement, and on the computer equipment. The inherent safety associated with all fiber optic sensors is another feature that the Fabry-Perot configuration has to its credit.

The extrinsic Fabry-Perot fiber optic sensor developed here is also capable of interfacing with a variety of controller configurations as well. As the output of the fiber optic sensor is a voltage signal, interfacing with an A/D board and an appropriate control program is rather straightforward. The sensors are easily multiplexed to form a network of sensors that can be embedded directly into a structure, or can be readily attached to the outside of the structure. Applications such as these include sensing strains in aircraft structures, automotive structures, pressure vessels, and numerous other structural and building applications.

The amplification of the signals from the photodetectors is also readily performed, and can in fact be modulated with rotary potentiometers, in a manner similar to that performed in this investigation. This permits situation-specific settings to be selected, and can be advantageous in situations where a system might be equipped with more than one sensor, in order to measure the strain at multiple locations. Signal conditioning can be done at the amplifier prior to being input to the A/D board, rather than requiring an algorithm to scale the inputs to the processing program and the controlling software after

the signal has been converted to digital format. Once the signals have been amplified and processed, the control algorithm can be implemented and control of the smart structure can be effected.

The extrinsic Fabry-Perot interferometer is suitable for use with smart structures because of its extremely high sensitivity, its immunity to electro-magnetic interference, its imperviousness to the carrier oils and other fluids that might be present in a smart structure operating environment. It can also perform its sensing tasks in regions where conventional strain and vibration sensors might fail, such as in highly caustic environments. There are caveats for using these sensors, as well as areas for more thorough study of Fabry-Perot sensor development to permit even broader applications. The considerations and future work shall be discussed in the next section.

7.3 Fabry-Perot Interferometer Design Considerations and Caveats

When considering the extrinsic Fabry-Perot interferometer for strain measurement applications, it is necessary to carefully examine the issues which will determine the applicability of the sensor to the sensing situation. The absolute value of the strain and the strain percentage, the nature of the working environment, and the proximity of threats to the integrity of the sensor need all be considered. They will determine the type of adhesive to be used with the structure, the material used for the capillary tubing, and most importantly the sensing gap used in the sensor. Any sensors which are placed in a

location which could potentially damage the sensor, through accidental use or in normal operation, should be avoided.

7.3.1 Considerations for Differing Amounts of Strain in a Smart Structure

When considering the amount of strain undergone by the structure, the elasticity of the structure will determine the applicability of the Fabry-Perot sensor to the strain measurement problem. If, for example, the mounting location of the sensor is composed of a material which undergoes more than 2% strain, it is unlikely that the Fabry-Perot device can be constructed with glass tubing for the capillary material, as it is unable to repeatedly sustain strain in excess of 1-2%. The capillary tubing should be made of a material which can elastically sustain strains in excess of those estimated to be taking place in the application.

In the case when the absolute value of the strain is very large, larger than the sensing gap, clearly it can be seen that the two mirrored faces in the sensing region will come into contact. In this case, it is expected that this contact will damage the sensor, requiring replacement of the sensor. To prevent this, the length of the sensing gap must be increased to a value greater that the maximum value of strain that the structure will experience. This value can be arrived at, in an admittedly painstaking manner, through trial and error, or by performing calculations. The preferred method is to calculate, through conventional means, the approximate value of strain which is expected to be

experienced. The sensing gap can be thus established, with an appropriate factor of safety, and a sensor can be constructed.

It is difficult to predict the effect that changing the length of the sensing gap will have on the sensitivity and performance of the sensor. Due to the conical dispersion of light, as described previously in **Chapter 3**, and illustrated in **Figure 3.5**, the dispersion of light in this conical fashion will greatly affect the amount of light which is reflected back to the photodetector, and thereby the sensitivity of the sensor. Additionally, changing the material of the capillary tubing, from the fused silica glass used here to another material capable of sustaining different levels of strain, will also affect the manner in which the light is reflected inside the sensing cavity, and the effect that these internal reflections will have on the light incident on the partially mirrored surface, as it is on its return path to the photodetector.

In the case of a change in the material for the capillary tubing, it is not expected that the fibers themselves will need to be changed. So long as the fibers remained oriented such that their faces are perpendicular to the axis of transmission of light, the sensor should perform in much the same fashion that it performs with the silica glass capillary tubing material.

7.3.2 Effects of the Working Environment

The application of extrinsic Fabry-Perot fiber optic sensors to harsh working environments, environments which would otherwise cause conventional sensors to fail, remain one of the fundamental strengths of all fiber optic sensors. Because the sensors are capable of functioning in caustic environments, which would otherwise rapidly deteriorate regular strain sensors, does not mean that they are correct for all applications, or that a particular specification of fiber optic sensor which works for one application will properly function in another.

Specifically, the nature of the environment will have a great effect on the type and method of attachment of the sensor to the system. Some applications may not present a threat to the fibers and capillary tubing, but rather they may dissolve the cyanoacrylate adhesive used for bonding the sensors to the smart structures in the present investigation. An alternative adhesive may need to be specified in order to ensure the integrity of the sensor and to provide it with a useful service lifetime.

7.3.3 Mechanical Threats to the Integrity of the Sensor

In the controlled laboratory environment of this investigation, it was possible to arrange the fibers, couplers, and all optical components in such a manner that they were isolated from vibrations and from pedestrian traffic. Additionally, the nature of the

experimental beams were such that they did not present a mechanical threat, by nature of multiple moving parts or mechanisms, to the fiber optic hardware or components. In a practical application, such as in a bridge or in an airplane structure, it will be necessary to consider protective measures for the fibers and the optical components. Additional jacketing of the fibers is readily available and has been commercially used in telecommunications applications, yet when transferring from the laboratory to production these considerations are sometimes overlooked. Fiber optic cables, properly jacketed, are no more fragile than conventional electrical wiring, yet there are some different considerations, such as bend radii and the alignment of the fibers and the lightsources.

Taking care to incorporate the requirements of a fiber optic system into a design, an engineer can realize the benefits of system performance sensing and damage monitoring, and with an appropriate controller, adaptive system control. These extrinsic Fabry-Perot sensors need not be confined to use in smart structures, as they perform the task of strain and vibration sensing quite well without being linked to a controller. However, with the integration of a fiber optic sensor into a smart structure it is possible to fully utilize the capabilities that the systems offer.

7.4 Direction and Scope for Future Work

The extrinsic Fabry-Perot sensors used in this investigation performed very well when incorporated with the neural network controller. They proved immune to the

problems associated with conventional strain and vibration sensors and provided a useful operating range, throughout which the performance of the sensor was highly stable. The strain sensitivity of the sensor was somewhat hampered by the fact that the wavelength of the light chosen as the lightsource a 633 nm wavelength Helium-Neon laser, and that the sensing gap was 250 μm, both of which prevented strains larger than the sensing gap from being detected.

Throughout the course of any investigation issues arise which could likely provide useful developments, but which can not be pursued due to monetary or time constraints. Several of these issues are presented here, as a roadmap for future experimenters, and to hopefully offer some hints to other engineers so that they may replicate the sensors developed here with the same if not improved performance over the sensors described, and ultimately specified as a result of the work during this investigation.

7.4.1 Lightsources and White Light Interferometry

Late in this investigation the investigator was fortunate to have the input of two scientists from SVET, of Moscow, Russia, to discuss potential developments of the fiber optic sensors which were being investigated for smart structures. These scientists' experience in developing fiber optic interferometers using white light interferometric techniques, and their input during their brief visit, indicate a very real possibility that the Fabry-Perot sensors developed here could be adapted to incorporate white light

interferometry. The incorporation of white light interferometry would permit a broadened range of strain sensing capability. In addition, the SVET processing algorithms and software is capable of determining the absolute value of the sensing gap directly from the inputs to the sensing software. The software currently used in this investigation does not permit this, though in fairness the nature of the problem does not require this knowledge. Though some basic strain calculations to determine the correlation of the experiments to the data obtained from the model were performed, these calculations were not performed regularly, nor did they need to be. The potential capability to know this information intrinsically from the software makes the SVET methods very attractive, and could open many new fields of use for these interferometric sensors as well.

The white light interferometers described in previous chapters incorporate a "super" light emitting diode with a bandwidth of 30 nm to provide a broader range of strain measurement. These light emitting diodes, often referred to a SLED's, offer increased power output over common light emitting diodes. The wavelength of some of the SLED's, in the range of 850 nm, is in the infrared spectrum. Consequently, the experimenter must be equipped with infra-red goggles to accurately set-up and align the optical equipment to perform strain measurement. These goggles are readily available from scientific supply houses. Currently, SLED's are available which are pigtailed, or pre-connected by the manufacturer, to the lead-out lengths of fiber. This configuration eliminates the need to use the micro-positioning stands and objective lenses used with the laser, and simplifies the connection of the fiber to the sensor and the photodetectors.

7.4.2 Experimental Application of Fabry-Perot Interferometers

In addition to switching the lightsources from a single wavelength source to one with a broad bandwidth, future work on the optimization of the sensor configuration for composite structure applications should also be investigated. Claus and his co-workers at Virginia Polytechnic Institute have investigated a Fabry-Perot interferometer capable of measuring the deflection of a composite panel under the influence of a shape memory material embedded in the panel (Holden, 1995). In a similar scheme to those used in this investigation, the sensors are being used to measure the deflection of the panel in an attempt to actively control the shape of the panel, using an appropriate controller. It is believed that this method might be useful to actively alter the shape of an airfoil section, improving its efficiency over a broader range of operating conditions. Though some early problems with the fibers failing during the isostatic pressing method used to fabricate the panels, researchers at Virginia Polytechnic have achieved some success with Fabry-Perot interferometry, by modifying the processing techniques for the panels (Holden, 1996).

The incorporation of Fabry-Perot interferometers into a composite panel is but one application that could be pursued. High-temperature sapphire fibers could be embedded in metallic structures to measure the strain of these structures as well. Unique applications in metal-matrix composite materials and other composite metals could provide exciting proving grounds for extrinsic Fabry-Perot white light interferometers.

7.4.3 Fabry-Perot Interferometers and Controllable Structures

An additional area which can provide suitable insight into the feasibility of Fabry-Perot interferometers as developed during this investigation is in the streamlining of the controlling schemes used for control of intelligent structures. In the present investigation, the smoothness of the controlling algorithm was compromised by the nature of the experimental beams, and the investigator's unwillingness to supply a higher than desirable electrical field to the structure, and to minimize the effect of a sudden voltage change on the high-voltage amplifiers. Thus, the controller was configured to display the recommended voltage from the neural network on the screen of the PC. In order to reset the process and control algorithm , the program requested the user press the enter key on the keyboard to reiterate and predict the next voltage field that should be applied to the structure.

A soft-amplifier which ramped the voltage up and down according to the predictions of the neural network has been specified for future use other multiple-electrode configuration ER-smart structures. This soft-amplifier circuitry is capable of gradually increasing the voltage output to the amplifier, which in turn sends the voltage to the smart structure. According to the manufacturer of the high voltage amplifier equipment, it is desirable to gradually increase the voltage supplied to the amplifier rather than provide a step-input to the voltage amplifier.

7.5 Summary of the Investigation

In this investigation it was shown that fiber optic sensors can be used to control ER-fluid-based smart structures. These sensors are not affected by the materials or the high levels of electro-magnetic interference associated with these structures. The extrinsic Fabry-Perot sensors tested here have proven that a strain and vibration sensor working in conjunction with a neural network controller is capable of effecting adaptive control of the structure.

ER based smart structures have been shown that they can be used to enhance the structural performance of many devices, permitting a much broader range of optimum operation. Significant research has been performed during the present investigation relating the strain and frequency of vibration sensing of smart structures, particularly in the area of interferometer sensor specification. Future research to transfer the technology of these sensors to practicable applications has been delineated.

References

Bamsey, I., 1993, "Formula 1 Technical Review: The State of the Art," *Racecar Engineering and Mechanics*, Volume 2, Number 6, p. 31.

Boggs, R.N., April 22, 1991, "Smart Materials Bolster Helicopter Blade Design," *Design News*, April 22, 1991, Volume 47, Number 8, p. 28.

Carlson, J.D., and Duclos, T.G., 1989, "ER Fluid Clutches and Brakes-Fluid Property and Mechanical Design Considerations," In *Electrorheological Fluids, Proceedings of the Second International Conference on Electrorheological Fluids*, , Carlson, J., Sprecher, A.F., and Conrad, H. (eds), Technomic Publishing Co. Inc., Lancaster, PA, pp. 353-367.

Claus, R. O., 1993, "Optical Fiber Sensors for Smart Skins, Materials, and Structures", Bradley Department of Electrical Engineering, Virginia Poluytechnic University, Balcksburg, VA 24061, Lecture Notes.

Conrad, H., Chen, Y., and Sprecher, A.F., "Electrorheology of Suspensions of Zeolite Particles in Silicone Oil," in *Proceedings of the Second International Conference on ER Fluids,* Eds: Carlson, J.D., Sprecher, A.F., Conrad, H., Technomic Publishing Inc., Lancaster, PA, pp. 252-264.

Coulter, J.P., 1993, "An Investigation of Electrorheological Material Based Controllable Damping Devices," In *Electrorheological Material Flows - 1993*, Singer, D.A., Kim, J.H., and Bajura, R.A. (eds.), Fluids Engineering Division Volume 164, The American Society of Mechanical Engineers, New York, NY, pp.115-128.

Ealing Electro-Optics, 1995, "The Ealing Catalog", 89 Doug Brown Way, Holliston, MA 01746.

Egorov, S. and Mamaev, A., 1995, "Lecture Notes on White Light Interferometric Techniques", SVET Ltd., P.O. Box 57, 115409, Moscow, Russia.

Flanders III, S.W., Burke, L.I., Yalcintas, M., 1995, "Alternate Neural Network Archietctures for Beam Vibration Minimization," submitted for publication.

Garner, H.D., assignee to the National Aeronautics and Space Administration, August 4, 1994, "Tactile Display Device Using an Electrorheological Fluid," *U.S. Patent Application Number* N95141123XSP.

Han, L., Voloshin, A., Coulter, J., 1993, "Vibration Sensing in Electrorheological Material Controllable Structures Using Embedded Polarimetric Fiber Optic Sensors", submitted for publication.

Han, L., Voloshin, A., Yalcintas, M., Counlter, J., 1994, "Electrorheological Adaptive Structures with Embedded Sensing and Control," Proceedings of the Smart Structres and Materials 1994: Smart Structures and Intelligent Systems, SPIE Vol. 2190, pp.2-12.

Korane, K.J., 1991, " Putting ER Fluids to Work," *Machine Design*, Volume 63, Number 9, May 9, 1991, pp. 52-60.

Leighton, D.T., 1985, *The Shear Induced Migration of Particulates in Concentrated Suspensions*, Ph. D. Dissertation, Stanford University, Stanford University, Palo Alto, California.

Lord Corporation, 1993, "Literature for Versa-Flow Controllable Fluids," Controllable Fluids Business, Lord Corporation, 405 Gregson Drive, Cary, N.C. 27511.

Newport Corporation, 1994, "The Newport Catalog 1994/1995", 1791 Deere Ave., Irvine, CA, 92714.

Omega Corporation, 1992, "Omega Complete Pressure, Strain, & Force Measurement Handbook & Encyclopedia", P.O. Box 4047, Stamford, CT, 06907-0047.

Opperman, G., Penners, G., Schulze, M., Marquardt, G., and Flindt, R., "Applications of Electroviscous Fluids as Movement Sensor Control Devices in Active Vibration Damper," in *Proceedings of the Second International Conference on ER Fluids,* Eds: Carlson, J.D., Sprecher, A.F., Conrad, H., Technomic Publishing Inc., Lancaster, PA, pp. 287-299.

Pennisi, E., 1992, "New Suspension May Smooth Maglev Ride," *Science News*, Volume 141, Number 4, January 25, p. 55.

Petek, N. , 1992. "Shock Absorber Uses Electrorheological Fluid," SAE *Automotive Engineering*, June 1992, Vol. 100, Number 6, pp.27-30.

Severson, L., 1995, "Thinking Structures", Invention, The Discovery Channel, Service Electric, October.

Sirkis, J.S., 1993, "Unified Approach to Phase-Strain Temperature Models for Smart Structure Interferometric Optical Fiber Sensors: Part 1, Development," in *Optical Engineering* 32 (4), pp.752-761 (April 1993).

Sirohi, R.S., and Kothiyal, M.P., Optical Components, Systems, and Measurement Techniques, Marcel-Dekker, Inc., New York, 1991.

Stangroom, J.E., 1989, "Tension Control Using ER Fluids - A Case Study," in *Proceedings of the Second International Conference on ER Fluids,* Eds: Carlson, J.D., Sprecher, A.F., Conrad, H., Technomic Publishing Inc., Lancaster, PA, pp. 419-425.

SVET, 1995, "SVET Literature for SPECTRPRO-1 Interferometric Fiber Optic Sensors", SVET Ltd., P.O. Box 57, 115409, Moscow, Russia.

Tolu-Honary, A., and Court, M., 1994, "Update on ER Fluids", *Hydraulics & Pneumatics*, January 1994, Volume 47, Number 1, pp. 133-138.

Wereley, N.M., 1994, "Active Damping of Flexible Rotor Blades Using ER Fluid Based Actuators," In *SPIE Proceedings of the 1994 North American Conference on Smart Structures and Materials*, Volume 2190, pp. 13-18

Yalcintas, M., 1995, *An Analytical and Experimental Investigation of Electrorheological Material Based Adaptive Structures*, Ph. D. Dissertation, Lehigh University, Bethlehem, Pennsylvania.

Yalcintas, M., Coulter, J.P., Don, D.L., 1994, "Structural Modelling and Optimal Control of Electrorheological Material Based Adaptive Beams," Journal of Smart Materials and Structures, submitted for publication.

Appendix A

Raw Experimental Data
Frequency Applied Through an MB Shaker Table
Sensed Data from Software Written at Lehigh University

Frequency Applied	Sensed Frequency (Hz)
20	20.2
40	40.1
60	61.3,59.7
80	80.2
100	100.4,101.7
120	118.7
140	141.3
160	160.6,169
180	179.1,59.9,180.7
200	202.3
220	201.9,219.1
240	239.1,239.7
260	259.7
280	280.05
300	300.7,302.7
320	319.7,322.1
340	340.7
360	357.4
380	379
400	404,390,401.7,404
600	603,626
1000	1007,1017

Vita

David J. Holden was born March 21, 1972 in Baltimore, Maryland, the son of Joanne and William Holden. After graduating from Loyola High School in Towson, Maryland, in 1990, the author entered Lehigh University, in Bethlehem, Pennsylvania. He earned his Bachelor of Science in Mechanical Engineering from Lehigh in May of 1994. David continued his studies as a research assistant at Lehigh University under the direction of Dr. John P. Coulter. In June 1996, the author earned his Master's of Science degree in Mechanical Engineering. Presently, the author plans to seek engineering challenges in industry.

END OF TITLE